

Herman Mørkved Blom
Sverre Grøtnebø Hellem

A parametric analysis of CLT wall and outrigger structural system in tall timber buildings

Master's thesis in Department of Structural Engineering
Supervisor: Haris Stamatopoulos
Co-supervisor: Osama Abdelfattah Hegeir
June 2022

Herman Mørkved Blom
Sverre Grøtnebø Hellem

A parametric analysis of CLT wall and outrigger structural system in tall timber buildings

Master's thesis in Department of Structural Engineering
Supervisor: Haris Stamatopoulos
Co-supervisor: Osama Abdelfattah Hegeir
June 2022

Norwegian University of Science and Technology
Faculty of Engineering
Department of Civil and Environmental Engineering



Norwegian University of
Science and Technology



MASTER THESIS 2022

SUBJECT AREA: Structural Engineering	DATE: 10.06.2022	NO. OF PAGES: 16+69+21
---	---------------------	---------------------------

TITLE:

A parametric analysis of CLT walls and outrigger structural systems in tall timber buildings

BY:

Herman Mørkved Blom

Sverre Grøtnebø Hellem



SUMMARY:

This Master thesis is a parametric analysis of outrigger structures in tall timber buildings. The design of Tall timber structures is often governed by the serviceability limit state (SLS). Due to the lightness and intermediate stiffness of wood timber buildings are often prone to wind-induced accelerations and lateral deformations. Semi-rigid frames developed in the Norwegian research project Woodsol were used as the basis system. By adding outriggers, the aim was to increase stiffness and fulfil the SLS criteria.

With the use of tools such as OpenSeesPy and SAP2000, the candidates were able to develop a finite element analysis routine to conduct a parametric analysis. A preliminary study was conducted to illustrate the difficulty with SLS design. The frames in the preliminary study did not have outriggers. Frames ranging from 8. to 18. floors were analyzed. A total of 291 600 analyses were performed. Results show that 28.2 % of frames fail the top floor displacement criteria. 58 % fail the interstory drift (IDR) criteria and 58.3% fail the acceleration criteria. Of these frames, only 8.7 % exceeds the ultimate limit state (ULS), thus demonstrating the difficulty designers face when designing multi-story timber buildings for SLS criteria.

In the parametric study, the influence of adding outriggers to the frames was researched. As an example, by Looking at a 10 floor reference frame with the optimal outrigger system, the top floor acceleration was reduced by 38.9%, maximum interstory drift (IDR) was reduced by 56.4 % and finally, the top floor displacement was reduced by 58.2%.

RESPONSIBLE TEACHER: Haris Stamatopoulos
SUPERVISOR(S): Haris Stamatopoulos, Osama Abdelfattah Hegeir
CARRIED OUT AT: Department of Structural Engineering, NTNU

Preface

This thesis marks the completion of the 5-year master program Civil and Environmental Engineering at the Norwegian University of Science and Technology (NTNU). The thesis is written in collaboration with the timber structure group at the Department of Structural Engineering during the spring of 2022.

The objective of the thesis is to study how outrigger structures can avail tall timber buildings to satisfy serviceability limit state requirements. Tall timber structures face challenges with wind-induced accelerations and lateral displacement. The analysis is carried out through a parametric study of semi-rigid planar frames under the influence of wind loads. The choice of topic stems from the authors' interest in programming and high-rise timber structures.

The work has given us a good understanding of structural dynamics and wind engineering for tall timber buildings. This was a topic that both candidates had limited knowledge about prior to the thesis. To perform the analysis, a routine was developed through the OpenSeesPy extension package in Python. The main emphasis of the thesis lies within the construction of the routine, which has given us valuable knowledge in FEM-analysis and object-oriented programming.

We want to use this occasion to give special thanks to supervisor Haris Stamatopoulos and co-supervisor Osama Abdelfattah Hegeir. They have made the master thesis an exciting journey and have offered us much scientific freedom, which we have appreciated exceedingly well. The work has been iterative, new ideas and suggestions for testing have constantly evolved. Help from co-supervisor Osama with setting up the analysis program and tools has proven priceless. Thank you for your fruitful collaboration.

Trondheim, June 10, 2022



Sverre Grøtnebø Hellem



Herman Mørkved Blom

Abstract

Increased urbanization and environmental factors have led to a surge in the construction of tall timber buildings. Wood is a natural material that reduces the carbon footprint of a structure, compared to more traditional materials such as concrete and steel. Although wood has beneficial environmental properties, high-rise timber buildings commonly struggle to fulfill serviceability requirements. Due to the light weight and intermediate stiffness of wood, timber buildings are prone to excessive vibrations and lateral deformations under wind loads.

The Eurocodes proposes some guidelines for acceptable top-floor displacement and interstory drift. However, these limits often vary in different projects. The ISO-standard (ISO 10137) [1] gives some guidelines for acceleration requirements. Wind-induced acceleration is a complex matter; it is a lengthy calculation. In addition, the experience of vibrations is based on human perception. This master thesis aims to investigate the serviceability limit state (SLS) issues for tall timber structures and how outriggers can improve performance. An outrigger system increases a multistory buildings overturning stiffness and strength. The authors have chosen to define "tall structures" as all structures rising above 25 meters. The study is done through a parametric analysis of planar semi-rigid timber frames. The work is theoretical and does not involve experimental work. The semi-rigid frames used in the analysis are inspired by the Norwegian research project Woodsol [2].

The research was carried out with a parametric study of semi-rigid planar frames of 8,10,12,14,16 and 18 floors. A total of 291 600 analyzes were performed. The analyze was done through the development of a routine in Python with the extension package OpenSeesPy. OpenSeesPy is a software that facilitates model and simulation procedures through incorporated modules. The placement of the outrigger, cross laminated timber core-system, bracing shape and axial stiffness was optimized.

The results have some critical takeaways. First, the optimal cross laminated timber core structure and outrigger locations were tested for both a single- and a double outrigger system in terms of acceleration. The conclusions for a single system were to place the outrigger on the floor closest to the 1/2-height of the building. The conclusion for the double outrigger system was to place the outriggers on floors closest to the 1/3 and 2/3 floor-level of the building height. A system with an external cross laminated timber core system is far better than a system with an internal cross laminated timber core structure. As a reference, a 10-story building with a single outrigger structure had a reduction in acceleration of 38.9 %, drift between floors of 56.4 %, and displacement of the top floor of 58.2 %.

Second, the stiffness and shape of the bracing system were explored. The optimal effective system axial stiffness was derived and set to $330kN/mm$. The effect of axial stiffness has been shown to diminish rapidly with small increments of axial stiffness in the members. The chevron bracing system was proven to perform better in acceleration, interstory drift, and top floor displacement with identical members compared to the other bracing systems.

Most of the workload lied within the development of the parametric analysis tool. To understand the magnitude of the work, it is essential to review the tool and its many functionalities. Due to the extent of the code, it was necessary to make it available through GitHub in the appendix.

Sammendrag

Økt urbanisering og klimafokus har ført til en økning i bygging av høyhus i tre. Tre er et naturlig materiale som kan bidra til å redusere karbonavtrykket til høyhus, sammenlignet med mer tradisjonelle materialer som betong og stål. Selv med tre sitt gunstige miljøavtrykk, er det ofte problematisk for høyhus i tre å imøtekomme kravene fra bruksgrensetilstanden. På grunn av den lave vekten og den mellomliggende stivheten til tre, er høyhus i tre ofte mer utsatt for store vibrasjoner og horisontalforskyvninger ved belastning fra vind enn tilsvarende bygg i betong og stål.

Eurokoden inneholder retningslinjer for akseptabel horisontalforskyvninger i trebygg. Disse grensene varierer ofte fra prosjekt til prosjekt. Standarden, ISO 10137 gir retningslinjer for akseptabel akselerasjon. Beregning av vind-induserte akselerasjoner er komplisert og tidkrevende. I tillegg er opplevelsen av vibrasjonene ofte basert på menneskelig oppfatning. Denne masteroppgaven ser på problemer knyttet til bruksgrensetilstand for høyhus i tre, og hvordan avstivning kan redusere problemet. Avstivningssystem ved bruk av *outriggers* kan øke styrke og stivhet i høyhus. Kandidatene har valgt å definere høyhus som alle bygg som er 25 meter eller høyere. Studien er gjennomført ved et parameterstudie av plane momentstive trerammer. De momentstive rammene, brukt i analysen, er inspirert av det norske forskningsprosjektet Woodsol.

Studien ble utført gjennom et parameterstudie av plane momentstive rammer på henholdsvis 8,10,12,14,16 og 18 etasjer. Det ble utført totalt 291 600 analyser. Analysene ble gjennomført ved hjelp av Python og en tilleggspakke i Python kalt OpenseesPy. OpenseesPy forenkler modell- og simuleringsprosedyrer gjennom integrerte moduler gitt av OpenSees. Plassering av *outrigger*, plassering av krysslaminerte tre-vegger, geometri på *outrigger* og aksialstivhet i *outriggeren* ble optimalisert i parameterstudiet.

Resultatene har flere interessante aspekter ved seg - for det første ble den optimale plasseringen av krysslaminert tre-vegger, og plassering av *outriggers* testet for både et enkelt- og et dobbelt *outrigger-system* med hensyn til akselerasjon. Konklusjonen for en bygning med et *outrigger-system* var å plassere *outriggeren* i etasjen nærmest 1/2 av høyden til bygningen. Konklusjonen for bygninger med to *outriggere* var å plassere *outriggerne* i etasjene nærmest 1/3 og 2/3 av høyden til bygningen. En ekstern kjerne av krysslaminert tre-vegger er langt bedre enn et system med en intern kjernestruktur av krysslaminert tre-vegger. Som referanse hadde en 10-etasjers bygning med en enkelt *Outrigger* en reduksjon i akselerasjonen på 38,9 %, avdriften mellom etasjene på 56,4 % og toppetasjens forskyvning på 58,2 %.

For det andre ble *outrigger* systemets stivhet og avstivningsgeometri undersøkt. Den optimale effektive aksialstivhet ble utledet og satt til $330kN/mm$. Effekten av aksialstivheten har vist seg å avta raskt med små økninger av aksialstivhet i elementene. Chevron-avstivningssystemet viste seg å yte bedre i akselerasjon og horisontalforskyvninger sammenlignet med de andre testede avstivningssystemene i denne masteroppgaven.

Mesteparten av arbeidsmengden ligger innenfor utviklingen av det parametriske analyseverktøyet. For å forstå omfanget av arbeidet er det viktig å gjennomgå verktøyet og dets mange funksjonaliteter. På grunn av omfanget av koden var det nødvendig å gjøre den tilgjengelig gjennom GitHub i vedlegget.

Table of Contents

List of Figures	x
List of Tables	xii
1 Introduction	1
1.1 Research context	1
1.2 Motivation	1
1.3 Structure	1
2 Background	3
2.1 Timber as a structural material	3
2.1.1 Sustainability	3
2.1.2 Properties	3
2.1.3 Products	4
2.2 Structural system for multistory timber buildings	5
2.2.1 Structures of CLT walls	5
2.2.2 Glulam diagonal structures	6
2.2.3 Moment-resisting frames	6
2.3 Challenges with high-rise timber structures	7
2.3.1 Acceleration	7
2.3.2 Lateral displacements and interstory drift	9
3 Problem statement	10
3.1 Requirement	10
3.1.1 Lateral displacement requirements	10
3.1.2 Acceleration requirements	10
3.2 Ultimate limit state	13
3.3 Outrigger systems	13
3.3.1 Outrigger properties	14
3.3.2 Efficiency of outrigger systems	15
3.3.3 Examples of outrigger systems	17
3.4 Research scope	18
4 Methods	19
4.1 Wind Load	20
4.1.1 Load combinations	21

4.2	Acceleration	22
4.3	Structural model	23
4.3.1	System loads	25
4.3.2	Basic model	25
4.3.3	The model with outrigger(s)	25
4.3.4	Truss stiffness	28
4.4	Implementation	29
4.5	System initialization	36
5	Results	37
5.1	Preliminary study	37
5.1.1	Serviceability limit state	39
5.1.2	Ultimate limit state	42
5.2	Outrigger system	44
5.2.1	Optimizing location for a single outrigger system	44
5.2.2	Choice of CLT core structure	46
5.2.3	Evaluation of shape	47
5.2.4	Influence of outrigger stiffness	48
5.2.5	Variable influence	50
5.2.6	Double outriggers	53
5.2.7	Ultimate limit state	59
5.2.8	Outrigger performance	63
6	Conclusion	65
7	Limitations and future work	66
7.1	Limitations	66
7.2	Future work	67
	References	68
	Appendix	70
A	Python Codes	70
B	Reference frames	71
C	Axial stiffness outrigger connection	74
D	Ultimate limit state considerations	75
E	Wind load calculation	79

F	Acceleration calculation	85
---	------------------------------------	----

List of Figures

1	Outline of thesis	2
2	Showing grain direction, and terminology for load bearing directions [14]	4
3	Moholt 50/50	5
4	Structural system of Mjøstårnet	6
5	Moment-resisting connection tested by Malo and Stamatopoulos [2]	7
6	Building topology and wind speed	8
7	Lateral displacement, due to wind	9
8	Acceptance criteria for wind-induced accelerations ISO 10137 [1]	11
9	Reduction of acceleration from ISO10137 criteria	12
10	Stress distribution	13
11	Outrigger system joint to structural core	14
12	Structural-core moment distribution	15
13	Optimal location of a singel outrigger system [7]	16
14	Optimal location of a double outrigger system [7]	16
15	Bracing shapes [30]	17
16	Hong Kong International Financial Center [33]	17
17	Bracing Hong Kong financial tower [32]	18
18	First Wisconsin center [35]	18
19	The building is divided into simplified wind zones	20
20	The final uniform wind load	21
21	Connections with rigid zone	23
22	Illustration of members	24
23	Base frame	26
24	Mirrored and diagonal bracing	27
25	Chevron bracing	27
26	Stiffness of truss	28
27	The structural environment	31
28	UML diagram	35
29	Model calculation	36
30	3D model of preliminary frame	37
31	Front and side view of preliminary frame	38
32	Top floor displacement	39
33	Interstory drift	40

34	Acceleration and frequency of preliminary frames plotted in ISO 10137 [1]	41
35	Ultimate limit state analysis for all preliminary frames	43
36	Detailed version of Figure 35	43
37	Accelerations for different placements of a single outrigger	45
38	Different core systems	46
39	Performance of external and internal vertical outrigger	47
40	Displacement and acceleration of a single outrigger	48
41	Performance of the chevron outrigger system with different axial stiffness	49
42	Result of increased stiffness in mirrored diagonal bracing system	50
43	Result of increased stiffness in diagonal bracing system	50
44	Influence of different number of bays	51
45	Influence of different bay length	52
46	Influence of different beam height	52
47	Performance of each reference frame with optimal single outrigger	53
48	System 1 (left) & System 2 (right)	54
49	System 3 (left) & System 4 (right)	54
50	Different outrigger locations for the 12 floors frame	55
51	Different outrigger locations for the 14 floors frame	56
52	Different outrigger locations for the 16 floors frame	57
53	Accelerations for the no, single and double -outrigger systems	58
54	Ultimate limit state analysis for all frames with the optimal outrigger system . . .	60
55	Detailed version of Figure 55	60
56	Shows the maximum moments from the ULS analysis	61
57	Two tests for placement of rods	62
58	Outrigger influence on acceleration and frequency	63
59	Outrigger influence on IDR and TFD	64
60	Connection concept	74
61	Connection concept; side and top view	74
62	Figure 7.4 NS-EN-1991-1-4 - WindZones	80
63	Table 4.1 NS-EN-1991-1-4	82
64	Figure 7.5 NS-EN-1991-1-4	83
65	Figure 7.23 NS-EN-1991-1-4	87
66	Figure 7.24 NS-EN-1991-1-4	88
67	Figure 7.24 NS-EN-1991-1-4	88
68	Figure 7.24 NS-EN-1991-1-4	89

List of Tables

1	Strength/density ratios for some structural materials [12]	3
2	Material properties GL30c [16]	4
3	Material properties for CLT made of C24 boards [17]	5
4	Load types	25
5	Overview of parameters chosen for the tested frames.	38
6	Variation of frames.	38
7	10 floor reference frame	44
8	Outrigger placement - SLS values	45
9	Outrigger placement - reduction	45
10	Results from testing different bracing systems	47
11	The influence of outrigger stiffness, NB* note the increment	48
12	Axial stiffness of different bracing systems	49
13	Variation of reference frames with outrigger.	51
14	Results from the double outrigger location optimization for a 12 floors frame . . .	55
15	Results from the double outrigger location optimization for a 14 floors frame . . .	56
16	Results from the double outrigger location optimization for a 16 floors frame . . .	57

Notation

B	The width of the building
D	The depth of the building
H	The height of the building
K	Stiffness of the structure
M	Mass of the structure
f_n	First modal natural frequency
δ_{Top}	The maximum lateral displacement on the top floor
δ_{IDR}	The maximum relative lateral displacement between floors
h	Floor height
f_d	Damped first modal natural frequency
ξ	The damping ratio
M'	The moment in the cross laminated timber core before implementation of outriggers
M	The cross laminated timber core moment after outriggers are applied
w_e	Wind Pressure
$q_p(z_c)$	Peak wind speed pressure
c_{pe}	Pressure coefficient
c_{pi}	Pressure coefficient
F_w	Wind force
c_s	Size factor
c_d	Dynamic factor
w_e	Wind weight
A_{ref}	Reference Area
V_b	Wind velocity
C_{Dir}	Directional factor
C_{Season}	Seasonal factor
C_{Prob}	Probability factor
V_{b0}	Basic wind speed
a	Acceleration
k_p	Peak factor for the response
$\sigma_{a,x}$	Standard deviation of the wind
v	Up-crossing frequency
T	Averaging time for the mean wind velocity
ρ	Air density
$m_{1,x}$	Along wind fundamental mass
I_v	Turbulence intensity
V_m	Mean wind velocity
R	Square root of resonant response
K_x	Non-dimensional coefficient
$\phi_{1,x}$	Fundamental along wind modal shape
k_{rb}	Beam-to-column/wall connection rotational stiffness
K_{ax}	The stiffness of the outrigger connection
K_L	Axial stiffness of outrigger
$K_{x,t}$	Axial stiffness of outrigger connection
K_{total}	Effective axial stiffness of outrigger connection
A	Area of member
E	Young modulus
L	Length
n	Number of floors
n_b	Number of bays
L_b	Span between bays
n_f	Number of frames
S	Spacing between frames
K_{rc}	Column-to-foundation connection stiffness
K_{rw}	Wall-to-foundation connection stiffness
h_b	Beam height
w_b	Beam width

Notation

h_c	Column height
w_c	Column width
h_w	Wall height
w_w	Wall width
g	Dead load
q	Live load
q_w	Wind load
t_c	Truss height
t_c	Truss width
M_n	Bending moment capacity of semi-rigid connection

Abbreviations

<i>RC</i>	Reinforced Concrete
<i>SLS</i>	Serviceability Limit State
<i>GHG</i>	Greenhouse Gas Emission
<i>CC</i>	Climate Change
<i>LCL</i>	Life Cycle Assessment
<i>TFD</i>	Top Floor Displacement
<i>IDR</i>	Interstory Drift
<i>ULS</i>	Ultimate Limit State
<i>SDOF</i>	Single Degrees of Freedom
<i>DOF</i>	Degrees of Freedom
<i>Glulam</i>	Glue laminated Timber
<i>CLT</i>	Cross Laminated Timber
<i>OR</i>	Outrigger
<i>Ult</i>	Ultimate limit state load
<i>Char</i>	Characteristic load
<i>Quasi</i>	Quasi permanent load

1 Introduction

1.1 Research context

Timber is a natural material that has been used in structures for centuries. It has been chiefly associated with small-scale structures such as cabins or single-family homes. High-rise timber structures have become more common in recent years. As the primary structural material, multistory buildings have traditionally been dominated by steel and reinforced concrete (RC). Due to the energy intensity that abides by the steel and RC design, the building industry is ushering a shift toward more eco-friendly materials, such as timber [3]. The building industry is one of the most polluting industries globally, construction of buildings is responsible for 11% of Co2 emissions globally [4]. Timber is a more environmentally friendly material than steel and RC, thus reducing the environmental footprint. Environmental motivations and increased urbanization have contributed to a substantial growth of tall timber buildings within the urban landscape of cities. Although the development of new timber-based products, such as cross laminated timber and glued laminated timber, has opted for taller designs, high-rise timber buildings are still facing complex challenges.

Wind loads tend to be the governing design action in the design of tall timber buildings. Since timber is a naturally light material with intermediate stiffness, it is more prone to wind-induced accelerations and significant lateral displacement. In other words, the serviceability limit state (SLS) brings limitations to design, especially structure height [5]. The world's tallest timber structure is currently Mjøstårnet, with 85,4 meters [6], approximately ten times smaller than the tallest skyscraper, Burj Khalifa, which is designed in a combination of steel and RC. Mjøstårnet is just within the design criteria regarding wind-induced accelerations. To overcome these challenges, designers should strive to develop new structural solutions and implement incorporated solutions from steel and RC design. In high-rise steel and concrete buildings, outriggers are commonly used to stiffen the structure [7]. By adopting solutions such as the outrigger system in timber buildings, designers can push beyond the limitations of high-rise timber design. Outriggers can pave the way for taller timber structures than ever before and are therefore a field of interest among designers. Urbanization is still increasing, which means that the demand for high-rise buildings in large cities increases [8]. To meet the demands of society, designers are constantly pushing the limits of multi-story timber buildings.

1.2 Motivation

Much of the work in the thesis is based on research from the Woodsol project. The Woodsol project was initiated in 2016 by professor Kjell Arne Malo at NTNU and aimed to develop industrialized structural solutions based on wooden frames for use in urban areas with five to ten stories of open architecture [2]. The semi-rigid timber frames developed in Woodsol are used as a basis for this thesis. This thesis aims to develop outrigger solutions for semi-rigid timber frames ranging between 8 and 18 floors. The main objective is to investigate how the implementation of outrigger structures impacts the SLS. This is done through a parametric analysis.

1.3 Structure

The content of this thesis is divided into different chapters. Figure 1 shows a schematic representation of the structure of this thesis. First, the literature review. Second, a parametric study. Third, the conclusion and remarks. The literature review introduces tall timber buildings, outrigger structures, and wind engineering. The review should give insight into the subject and provide the necessary theoretical foundation for the parametric study. The parametric study is the main part of the thesis. The development of models and tools for testing the influence of structural properties is the critical element of this part. It also contains a discussion of the results of the analysis. The third and last part, the conclusion and remarks, summarizes the main findings of the thesis. Limitations of the research and possibilities for future work are also discussed.

Literature review

The theory is presented in the background chapter. This chapter contains general information on timber as a structural material and the main structural systems of high-rise timber buildings. The main challenges of SLS in tall timber design are highlighted in the last part of the background. The problem statement explains the specific SLS requirements that designers face. To meet these SLS criteria, the use of an outrigger system is proposed as a possible solution. The theory and mechanics behind the outrigger systems are presented. The last part of this chapter contains a formulation of the research question that this master thesis aims to investigate.

Parametric study

Chapter 4 is the method chapter and explains the approach of the thesis. First, the calculations of the wind loads and the load combinations. Second, the acceleration is calculated according to the Eurocode (NS-EN 1994-1-4) [9]. Third, the structural model, system loads, and the basic model are explained. The models are processed using a set of tools developed in this thesis. An essential tool is OpenSeesPy, which is a Python extension package. The tool is used in accommodation with Python to perform the analysis. Chapter 5 contains the results. Part 5.1 contains results from a preliminary study of frames without outrigger systems. These results are used as a basis for the consecutive parts of the results. First, a system with single outrigger placement is analyzed for a given set of basis frames ranging from 8 to 12 floors. Second, there will be an analysis of outrigger systems with two outriggers. The results of the analysis are presented and discussed continuously throughout the chapter.

Research Outcome

In Chapter 6, the conclusion and main findings of the thesis are summarized. The last chapter, Chapter 7, is a discussion of limitations and future work. This chapter highlights the flaws in the research project. It discusses simplifications that are made and how the study is narrowed. This chapter also proposes some ideas for future work.

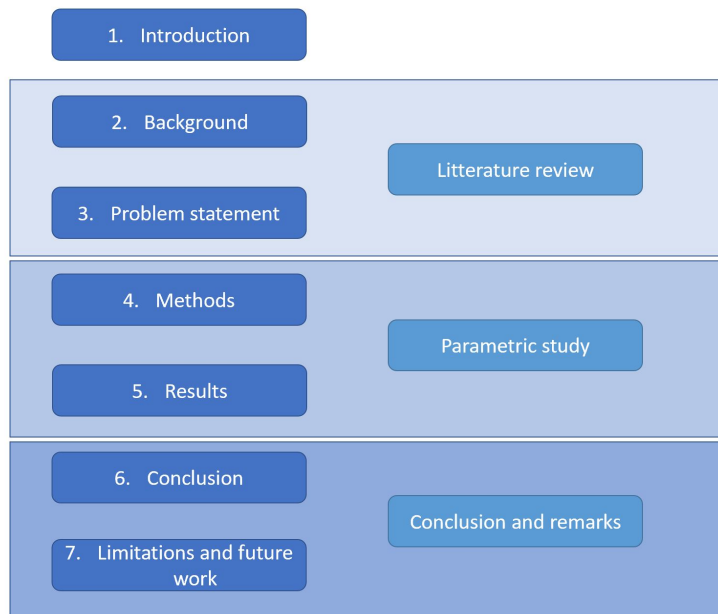


Figure 1: Outline of thesis

2 Background

This chapter contains the background theory necessary to understand the concepts in this master thesis. The first section will explain timber as a structural material. Second, the main structural systems for multistory timber buildings will be discussed. The third and last part addresses the main SLS challenges with respect to timber design.

2.1 Timber as a structural material

2.1.1 Sustainability

Increased environmental awareness is an impetus for the growing demand for timber products in the construction industry. Throughout its lifetime, timber absorbs carbon dioxide from the atmosphere through photosynthesis and emits oxygen to the atmosphere. Carbon, the by-product, is stored within the heartwood of the tree, until it is released to the atmosphere through decomposition or incinerating. In other words, timber can be considered as a natural storage unit for carbon [10]. Therefore, the use of timber as a structural material can significantly reduce the carbon footprint of new buildings, compared to the use of more traditional materials such as steel and concrete. Studies show that by substituting concrete and steel with timber, one can reduce greenhouse gas emissions (GHG) substantially. By studying climate change impact (CC) through a life cycle assessment (LCL), for four multistory buildings of 3,7,12 and 21 floors, the scientists Skullestad and Hohne concluded with potential savings in CC ranging from 34 to 84% compared to RC [11]. The CC savings were measured per floor m^2 . The study showed that the CC savings per m^2 increased with building height, thus favoring the substitution of RC with timber for taller structures. Timber structures can potentially achieve a 100% reduction compared to RC.

2.1.2 Properties

In addition to environmental motivators, timber has a good strength-to-weight ratio. Timber has approximately the same strength/weight ratio as steel and a much higher ratio than concrete [12]. Table 1 shows the values for some structural materials. The main cause for this is the low density of timber. The good strength/weight ratio is beneficial from an engineering perspective.

Strength Properties			
Material	Density kg/m^3	Strength Mpa	Strength/Density $10^{-3} MPa.m^3/kg$
Structural steel	7800	40-1000	50-130
Concrete (compression)	2400	30-120	13-50
Clear softwood (tension)	400-600	40-200	100-300
Clear softwood(compression)	400-600	30-90	70-150
Structural timber	400-600	15-40	30-80

Table 1: Strength/density ratios for some structural materials [12]

Timber consists of multiple fibers that form the grain direction, see Figure 2. Timber is strongest when loaded in the grain direction and is known to perform poorly when, for example, it is subjected to tensile stresses perpendicular to the grain. This is due to the anisotropic behavior of wood. Three orthogonal directions are defined for wood, the longitudinal, radial, and tangential direction [13]. The longitudinal direction is the strongest direction because of the orientation of the fibers. In recent years, many new timber products have been developed, such as glued laminated- and cross laminated timber.

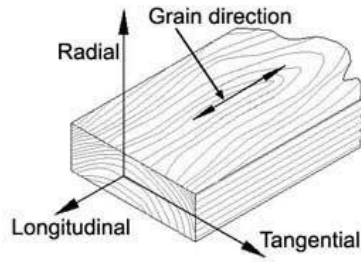


Figure 2: Showing grain direction, and terminology for load bearing directions [14]

2.1.3 Products

Glulam

Glued laminated timber (glulam) comprises a number of laminated timber lamellae, glued together. In Nordic countries, lamellae are usually made of pine or spruce, but many different species can be used as raw material. In glulam, the fibers in the laminates run parallel to the length of the piece. In the fabrication process, the lamellae are planed and sorted according to strength classes. The thicknesses of the lamellae are usually up to 45 mm, but not less than 6 mm, this varies between the species of wood [15]. Glulam is commonly divided into two types, combined glulam and homogeneous glulam. In homogeneous glulam, all lamellae are of the same strength class. To fully utilize the timber, it is common to use lamellae of higher-strength classes in the parts of the beam where the stresses are greatest, in the upper and lower parts. This is a combined glulam. Glulam has a good strength-to-weight ratio. Glulam is stronger and more rigid than solid timber of the same dimensions. In this master thesis, the class GL30c was used for the glulam members. Table 3 describes the strength and stiffness properties of GL30c [16].

Strength Properties			
Action	Symbol	Value	Unit
Bending	$f_{m,k}$	30	N/mm^2
Tension paralell	$f_{t,0,k}$	19,5	N/mm^2
Tension perpendicular	$f_{t,90,k}$	0,5	N/mm^2
Pressure paralell	$f_{c,0,k}$	24,5	N/mm^2
Pressure perpendicular	$f_{c,90,k}$	2,5	N/mm^2
Shear	$f_{v,k}$	3,5	N/mm^2
Stiffness Parameters			
Paralell	$E_{0,mean}$	10 800	N/mm^2
Perpendicular	E_{mean}	13 000	N/mm^2
Shear Modulus	G_{mean}	650	N/mm^2

Table 2: Material properties GL30c [16]

Cross Laminated Timber

Cross laminated timber (CLT) consists of at least three layers of glued boards made from wood. The layers are glued orthogonally to each other, making the material more composed in terms of mechanical properties. The boards usually have a thickness of 20 - 60 mm. The product can be easily prefabricated and glued in different kinds of shapes and forms. This offers huge opportunities for the product. In multistory buildings, it is often used in the framework as structural walls and flooring. CLT elements are preferable as structural materials because they often have a large cross section, giving them a large load bearing capacity. The increase in demand has led to the production of CLT to skyrocket in recent years. In Europe, since 2005, the manufactured volume has increased from 100,000 m^3 to 600,000 in 2015 [17]. For CLT made of graded C24 timber boards, similar to what is used in this thesis, the structural properties are the following.

Strength Properties			
Action	Symbol	Value	Unit
Bending	$f_{m,k}$	24	N/mm^2
Tension parallell	$f_{t,0,k}$	14.5	N/mm^2
Tension perpendicular	$f_{t,90,k}$	0.4	N/mm^2
Pressure parallell	$f_{c,0,k}$	21	N/mm^2
Pressure perpendicular	$f_{c,90,k}$	2,5	N/mm^2
Shear	$f_{v,k}$	4,0	N/mm^2
Stiffness Parameters			
Paralell	$E_{0,mean}$	11 000	N/mm^2
Perpendicular	E_{mean}	7 400	N/mm^2
Shear Modulus	G_{mean}	690	N/mm^2

Table 3: Material properties for CLT made of C24 boards [17]

2.2 Structural system for multistory timber buildings

In the past, multistory buildings were constructed solely with steel or concrete. Now, the list of timber structures that rise above 30 meters is getting longer. The rise and development of new and improved structural systems make it possible for designers to construct even taller buildings. These structural systems must temper the structural challenges that lie within the design of a multistory timber building.

2.2.1 Structures of CLT walls

CLT panels have been used as the main structural element in many multistory timber structures. It has been a popular structural choice for mid-rise timber structures. As mentioned above, CLT panels have a huge off-site prefabrication potential, which subsequently makes way for faster assembly on site. This reduces both construction time and cost. Since CLT panels have high load bearing capacity and stiffness, they are ideally suited to stabilize the structure [18]. Figure 3 shows the construction of a nine-story CLT-based timber building in Trondheim. In this massive timber structure, both the internal and external walls are structural elements. The CLT walls carry the shear of the lateral loads. The flooring transfers the lateral load to the walls. The use of CLT walls as structural elements restricts floor spans and the possibility of open space, thus somewhat limiting the architectural freedom [17].



Figure 3: Moholt 50/50

2.2.2 Glulam diagonal structures

Mjøstårnet, currently the worlds tallest timber building, is a great example of a multistory glulam-braced structure. Large glulam trusses, beams, and columns constitute the main load bearing system. The truss system runs along the facade, handles lateral loads, and ensures that the building has the required stiffness. Axial forces are taken by massive glulam columns. The flooring acts as a diaphragm, transferring horizontal loads to vertical elements. The glulam elements are connected through slotted in steel plates and dowels. A detailed figure of the structural system is shown in Figure 4. The dimensions of columns, beams, and trusses become quite large to account for the forces they are subjected to. For example, the largest diagonal cross section in Mjøstårnet is $625 \times 990 \text{ mm}^2$. The use of large cross sections and a stiffening system with elements running across the facade causes architectural restrictions [6].

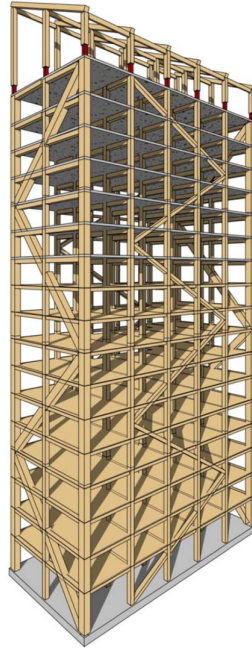


Figure 4: Structural system of Mjøstårnet

2.2.3 Moment-resisting frames

The use of moment-resisting frames in timber engineering allows for greater architectural freedom by allowing larger openings and longer spans. The system is based on semi-rigid timber moment-resisting connections. This allows for buildings without shear walls or large x-bracing [6], given that the stiffness and strength of the connections are sufficient. Longer spans can be achieved, as semi-rigid connections improve performance against human-induced vibrations of floors.

The frames consist of continuous connections between columns and semi-rigid beam-column connections. The Norwegian research project woodsol has since its start in 2016 pursued the development of industrialized solutions for moment-resisting frames. The connections consist of steel rings with threaded rods between the beam and the column. Figure 5 shows a prototype connection. This connection shows a single pair of threaded rods. The figure is taken from an experimental test carried out in a case study by Haris stamatopoulos and Kjell Arne Malo of the Norwegian research institute NTNU [2]. From experimental work, they found that a connection could provide a stiffness value on the order of 4000-4500 kNm/rad and maximal moments of 65 kNm per plane of rod. The test was carried out for a 140x450mm beam and a 140x450mm column.

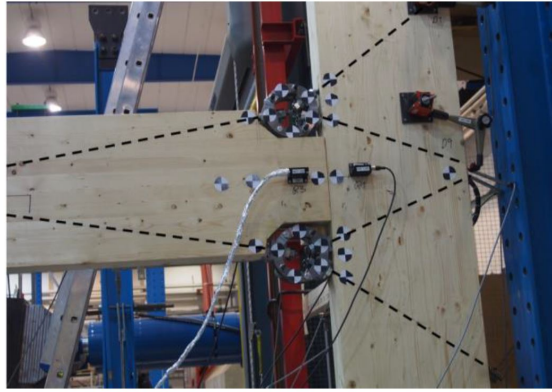


Figure 5: Moment-resisting connection tested by Malo and Stamatopoulos [2]

The frames in this master thesis have the same beam-column connection type as the one presented in Figure 5. Therefore, the experimental data from Malo and Stampodopulus are important in calculating the connection stiffness. Calculations and approximates for connections will be further addressed in Chapter 4, Methods.

2.3 Challenges with high-rise timber structures

This section aims to provide insight into the most challenging parts of multistory timber design. As mentioned above, the SLS often governs the design.

2.3.1 Acceleration

One of many challenges with high-rise timber buildings is the serviceability limit state (SLS). Mid-rise timber structures with a frequency of 1-2 Hz tend to be in resonance with wind loading, causing wind-induced accelerations to be of concern [5]. Wind-induced accelerations are caused by vibrations from fluctuating wind speed. These vibrations may cause nausea and discomfort among residents. This is a delicate field that designers have limited knowledge of. Wind-induced accelerations in tall timber structures are therefore an important topic and need further investigation. Since the experience of discomfort is dependent on human perception, it is difficult to precisely define limits. There are many ways to tackle this issue. In this thesis, the ISO10137 [1] standard is used as a basis [5].

The acceleration of a structure is a highly complex parameter. In this thesis, a simplified method from Eurocode (NS-EN 1991-1-4) [9] is used. This method is based on properties from modal analysis. The main attributes of acceleration are the building topology, the mass, the stiffness, and the damping. The typology is the height and shape of the building. Figure 6 shows an illustration of a high-rise building with dimensions. B is the width of the building, D is the depth, and H is the height of the building.

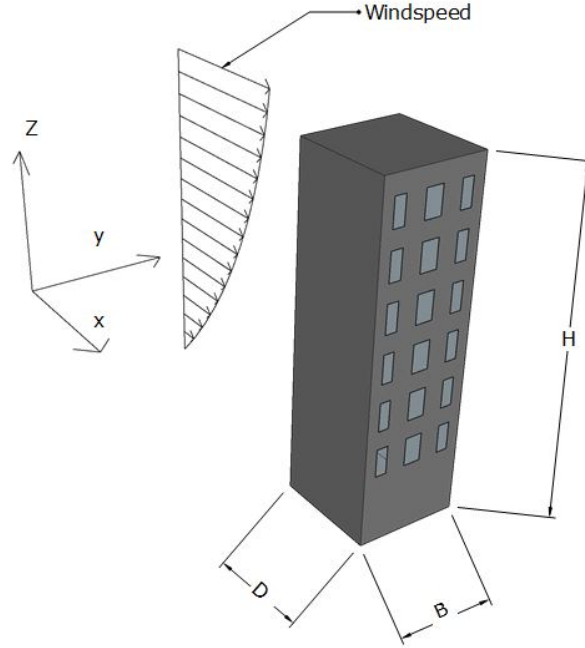


Figure 6: Building topology and wind speed

As a rough approximation, the structural system of the building can be considered as a cantilever, and in general there are three different modes of motion when subjected to wind. Bending about y -axis, bending about the x -axis, and torsion about the z -axis. Bending about the y -axis is caused by along-wind forces, since these are forces parallel to the direction of the wind. Vibrations perpendicular to the direction of wind are often referred to as vortex oscillation [19] (s. 58). This master thesis is based on a 2D in-plane analysis and only considers motion parallel to the direction of wind. The main reason for choosing a 2D analysis is based on computational consideration, this matter is further addressed in Section 4.3, Structural model.

The wind speed along the height of the building is important when looking at the distribution of the wind load. The speed of the wind increases logarithmically as the structures grow taller. This is known from the log-law expressions of wind profiles explained in Advanced Structural Wind Engineering [19] (s. 228). Figure 6 shows an illustration of the distribution of wind speed along a facade of a building.

Acceleration is strongly correlated with the frequency. The calculation method for acceleration provided by the Eurocode (NS-EN 1991-1-4) [9], is obtained by looking at the first modal eigenfrequency. For a simplified single degree of freedom system (SDOF) the frequency is given as (1). Both the mass and the stiffness are directly related to the frequency.

$$f_n = \frac{1}{2\pi} \sqrt{\frac{K}{M}} \quad (1)$$

A tall timber building will have moderate stiffness. This will result in low natural frequency and high natural period. Moderate stiffness arises from the slenderness of the tall structure. The relationship between width, in-plane length, and height determines the slenderness of the building [20]. Compared to a tall timber structure, a small timber house will have a high relative stiffness, resulting in a high natural frequency and a low natural period. This is due to the smaller height of the building.

The mass is also related to the actual force that each floor is going to experience. A greater mass will reduce acceleration because it requires more force from the wind to set the building in motion. However, a huge mass might cause other problems. This could cause problems with the bearing of

the structure. Second, if the wind manages to set the building into motion, the forces generated by the wind will increase. This could cause problems for the connections and foundations in and around the structure that must transfer the forces [21].

The measurement of the damping ratio in existing timber structures is around 2% [22]. However, an increased theoretical damping will allow the structure to absorb more energy while in resonance. This is going to have a great impact on the structure, because the greatest accelerations are going to occur while the structure is in resonance with the wind speed.

2.3.2 Lateral displacements and interstory drift

Since timber structures are often considered quite flexible, large lateral displacements may also be problematic. Large top floor displacements (TFD) and interstory drift (IDR) are common problems in tall timber structures [5]. When the building is subjected to lateral loads, it will cause lateral displacements. Figure 7 shows how the building, acting like a cantilever, will displace at the top floor. Large top floor displacements can cause damage to nonstructural elements. This can cause malfunction and affect the appearance of the structure; cracked windows and twisted facades can be a result of large lateral displacements. However, most of the time these disfigurements are related to IDR. IDR is the relative displacement between two floors. The phenomenon is often problematic if one of the adjacent floors is very stiff, or rigid, compared to the other. These disfigurements can be very costly and can potentially trigger substantial rehabilitation costs.

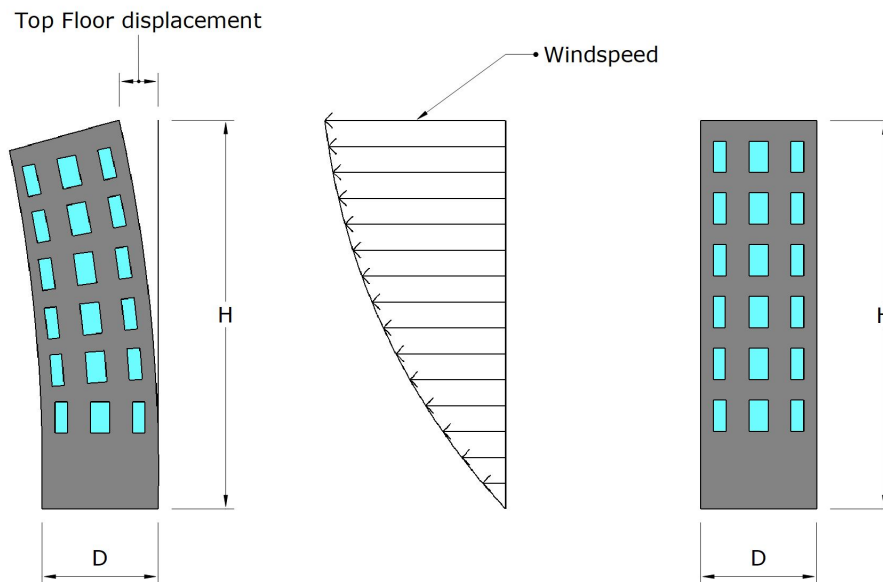


Figure 7: Lateral displacement, due to wind

3 Problem statement

This chapter explains the requirements and possible solutions for the SLS problem in tall timber structures. First, the specific requirements that needs to be fulfilled. Second, the theory behind the ultimate limit state (ULS). Third, the outrigger theory. Fourth, and finally a research scope.

3.1 Requirement

Serviceability limit state can often be challenging to define and conceptualize. This is due to the nature of peoples perception. This chapter will focus on SLS requirements for acceleration, top floor displacement and interstory drift.

3.1.1 Lateral displacement requirements

SLS criteria are often not explicitly determined by standards but are limited by maximum values defined in each project. Nevertheless, there are some rules of thumb which are helpful. According to Eurocode (NS-EN 1995-1-1) [23] the characteristic SLS requirements from Eurocode (NS-EN 1990) [24] for the deflection of a cantilever beam are within the range of $1/150$ - $1/250$ of the cantilever length. For simply supported beams, the deflection is in the range of $1/300$ - $1/500$ of the beam span. These reference values define a steady basis for acceptance criteria for top floor displacements. In this thesis, two acceptance criteria for top floor displacements have been established. These are listed below:

- $\delta_{Top} < H/300$
- $\delta_{Top} < H/500$

δ_{Top} is the maximum lateral displacement on the top floor and H is the total height of the building.

The same analogy as for top floor displacement is used when establishing limits for maximum interstory drift. A lower limit of $h/300$ and a strict limit of $h/500$ are used for the characteristic load combination (7) [5]. Eurocode (NS-EN 1998-1) [25], design of structures for earthquake resistance, also provides some values for accepted IDR. However, since this thesis does not take seismic actions into consideration, the values from Eurocode (NS-EN 1995-1-1) [23] are used [5].

- $\delta_{IDR} < h/300$
- $\delta_{IDR} < h/500$

δ_{IDR} is the maximum relative lateral displacement between floors, and h is the height of the floor.

3.1.2 Acceleration requirements

ISO 10137 describes the acceptance criteria for the maximum acceleration of a target floor for a return period of one year with respect to the maximum wind velocity. The criteria are decided on the basis of how acceleration affects the comfort of residents in a building. In D. Boggs article of 1997 the acceleration limit for nausea is given as 0.098 m/s^2 and 0.049 m/s^2 for the perception level for 50% of the population. The perception level for 2% of the population is 0.020 m/s^2 [26]. Figure 8 shows the two different acceptance criteria, with line 1 marking the criteria for offices and a more strict line 2 for residences. This is due to the greater demand for comfort in residences.

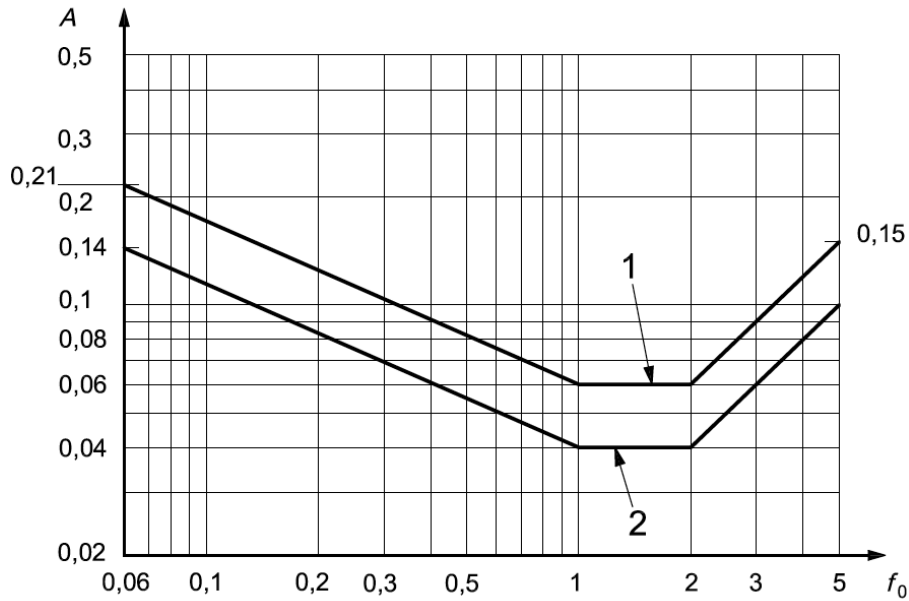


Figure 8: Acceptance criteria for wind-induced accelerations ISO 10137 [1]

There are multiple possibilities to move into more acceptable areas. These mechanisms are illustrated in Figure 9.

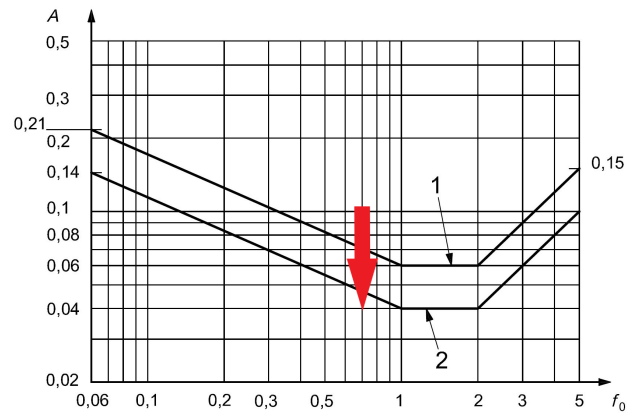
According to Equation (1), by increasing the mass of the structure the frequency will be reduced. This will move the structure into more acceptable regions on the graph, where higher accelerations are acceptable. Furthermore, with increasing mass, the building is also going to move less from the wind-induced accelerations. This will cause a movement towards the lower left part of the figure, as seen in Figure 9c [27].

The second option is to increase the stiffness. This seems counter intuitive according to Equation (1), as the frequency will increase and get a movement into more strict regions of the criteria. However, a stiffer structure will also respond less to wind-induced accelerations and results in a movement down to the right in the figure, as shown in Figure 9b [27].

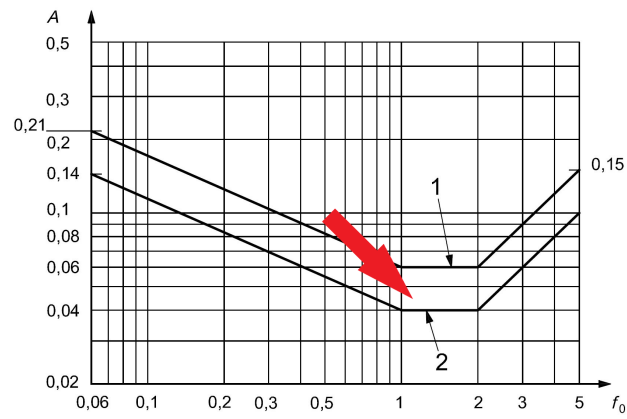
The third option is to increase the damping. This is a more theoretical concept and is not easily done in practice. By increasing the damping, the first modal frequency will approximately remain the same. As the damped frequency is given by:

$$f_d = f_n \cdot \sqrt{1 - \xi^2} \quad (2)$$

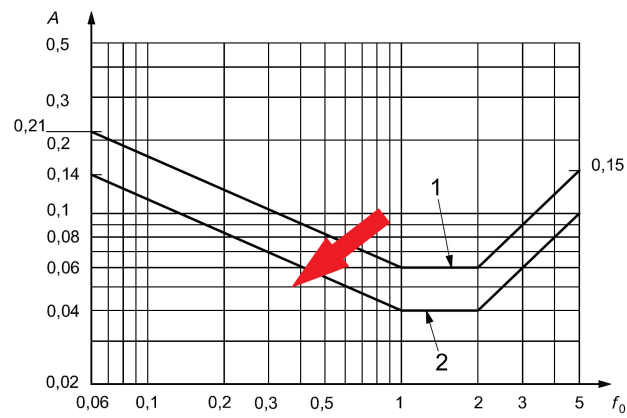
The damping ratio ξ is measured as a percentage and because the term is squared, it has to be significantly large for the frequency to change much. However, an increased damping will cause a movement straight down in the diagram. This movement is shown in Figure 9a [27].



(a) Increased damping



(b) Increased stiffness



(c) Increased mass

Figure 9: Reduction of acceleration from ISO10137 criteria

3.2 Ultimate limit state

The ultimate limit state determines the capacity of the members in the structure. Capacity is determined by the members cross section and their strength properties. The capacity determines the maximum allowable stress that the member can withstand. To obtain these stresses, the forces induced by the critical load combination must be calculated. Structural safety depends on the capacity of the individual members. It is therefore crucial to verify that the members can withstand these forces. Failure of members is not solely dependent on strength and cross-sectional properties. Stability can be governing when designing for ultimate limit state. Column buckling and lateral torsional buckling of beams are stability problems that needs to be investigated. Design of connections in timber structures is often the most complex and important component in timber design. This is due to the complex properties of wood and the compound stress transfer mechanisms [28].

Vertical loads are carried by columns and shear walls in the structure. These need to be transferred to the foundation, The distribution of stresses due to vertical loads can be seen in Figure 10. The vertical loads will cause large compression forces in the bottom columns and walls. Beams will experience moments due to the load pattern on the flooring. Bending moments are often the governing force when designing for ULS. In addition, these moments need to be carried by beam-column connections at the end points. The lateral loads are carried most efficiently by the shear walls. The slabs act as diaphragms and transfer the lateral loads from the columns and to the shear walls [28]. Figure 10 shows an illustration of the stress distribution of the lateral load. This thesis does not focus mainly on the ULS, but on the SLS. All calculations for ULS are listed in the Appendix D - ULS.

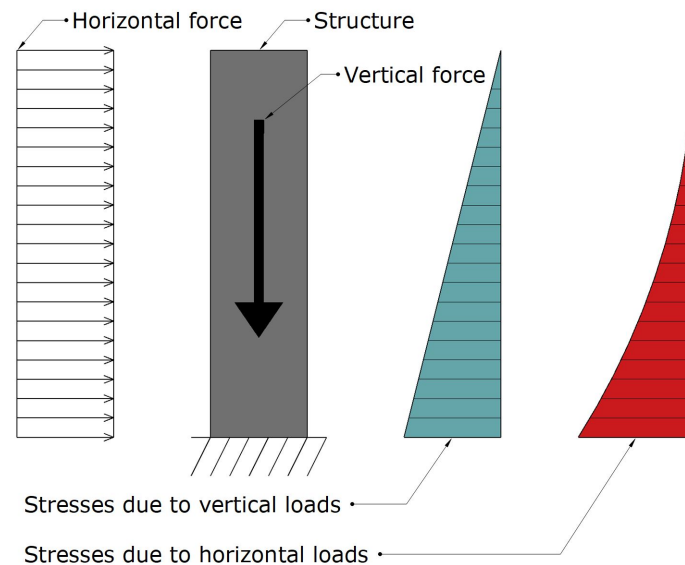


Figure 10: Stress distribution

3.3 Outrigger systems

Tall buildings are essential for urbanization and can also symbolize wealth and status. When structures grow taller, their structural core becomes insufficient against lateral loads [29]. The core structure becomes slender and offers minor stiffness against overturning moments [30]. A solution that has been applied to steel and concrete structures is outrigger systems. They are commonly used to provide sufficient resistance against lateral loading for multistory structures. This section will explain the function of an outrigger system and look at some examples.

3.3.1 Outrigger properties

An outrigger is a structural system that increase high-rise buildings' overturning stiffness and strength. The outrigger system links a perimeter system of shear walls or columns with a core structure and resembles a structural "belt" located on one or multiple floors, consisting of bracing or shear walls. The system increases flexural resistance in the structure and more efficiently distributes the shear to the core structure [7]. When the structure is stiffened through an outrigger system, the lateral displacements and acceleration will be reduced. Figure 11 illustrates the functionality of an outrigger system.

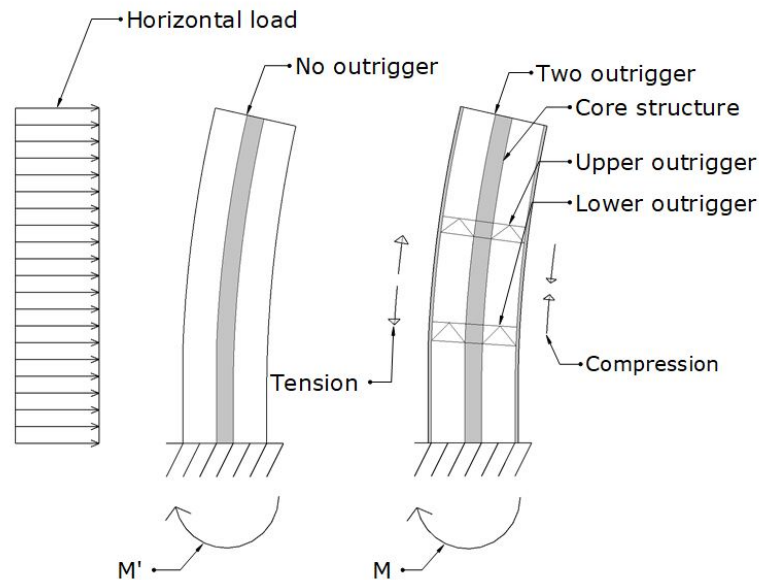


Figure 11: Outrigger system joint to structural core

As a rough approximation the structural core behaves as a cantilever when the building is subjected to vertical loads. When there is no outrigger system, most of the overturning moment will be taken by the stiffest element, in this case, the core structure. The system with outriggers activates more of the perimeter elements. The outrigger connects the distant columns with the core. This results in a couple at the level of the outrigger, which in turn reduces the bending moment of the structural core [7]. In Figure 11, M' illustrates the moment in the core before implementation of outriggers. M is the core moment after outriggers are applied. The overturning moments are now spread evenly across the building footprint, relieving the moment in the core structure [31]. Figure 12 shows a schematic illustration of how the outrigger system reduces core moments. The red color illustrates the system without outriggers, and the blue color shows the same system with outrigger.

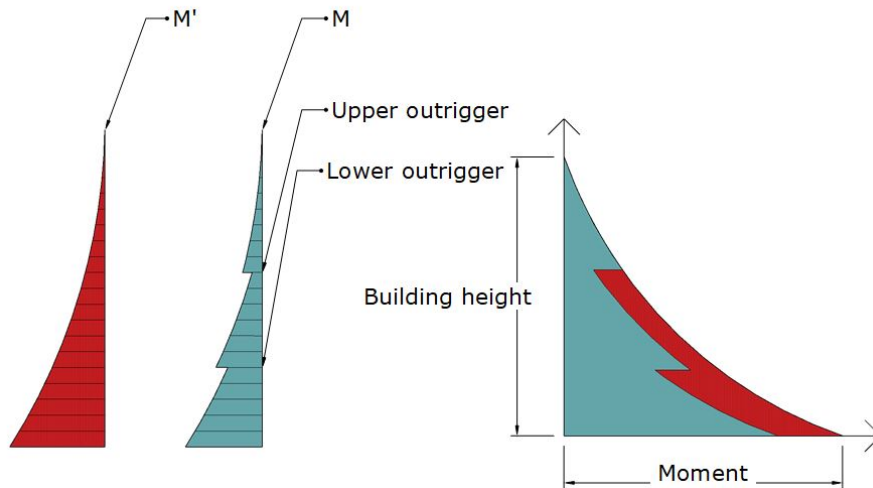


Figure 12: Structural-core moment distribution

By activating the perimeter columns, it is possible to relieve the core of moments, making it possible to reduce the dimensions [29]. The outrigger system provides an alternative loading path. Thus helping the structure to be progressive with regards to loading [28]. Since outrigger systems offer a compact stiffening system, they contribute to architectural freedom [7]. However, the use of outriggers also offers some limitations. Outrigger systems provide great stiffening in concentrated areas of a building. This can induce large forces in the surrounding members and the outriggers themselves. The flooring that acts as a diaphragm is a crucial element in the load paths that make the system work. Incorrect modeling of the stiffness of these diaphragms can result in incorrect building deformations. Placing outriggers on floors that contain mechanical installations also requires careful coordination to prevent conflicts.

3.3.2 Efficiency of outrigger systems

The placement of the outrigger system affects how a building responds to lateral loads. It is important to place the outrigger in the most optimal location possible. However, structural designers are often limited by architectural considerations. The outrigger is often placed on floors that contain mechanical installations. There are multiple studies of where the ideal placement of an outrigger is. A study by Ali Lame at MIT shows that an ideal placement for a single outrigger is approximately 0.45 of the total building height [7]. Lame performed the study by looking at where the stiffness of a single outrigger system with a structural core was at its maximum. Since both lateral deformation and acceleration correlate negatively with stiffness, it is a relevant variable. Figure 13 shows the results of the study by Lame. The non-dimensional variable α explains the relation between the rigidity of the core with respect to the column. β represents the rigidity of the core relative to the rigidity of the outrigger.

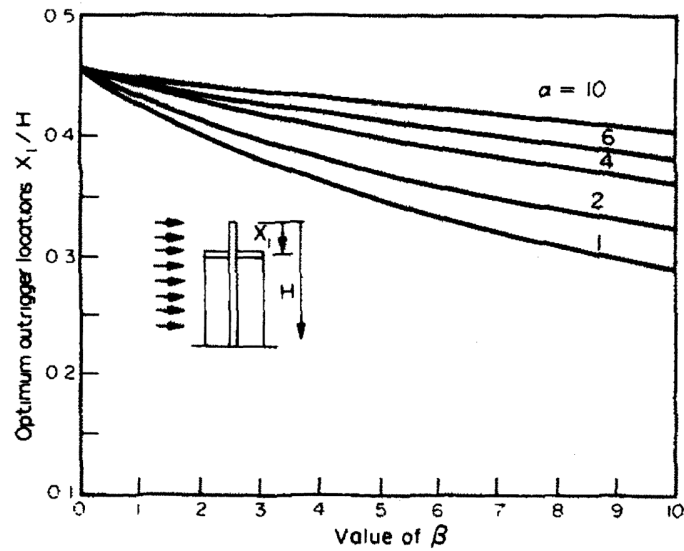


Figure 13: Optimal location of a single outrigger system [7]

Note that 0.45 of the total height represents a value where the structural core is very flexible. As the core becomes more rigid with respect to the perimeter column and the outrigger, a lower placement is more favorable. For two outriggers, the optimal placement of the outrigger is approximately 1/3 and 2/3 of total building height. Figure 14 shows the same analysis for two outriggers. For one outrigger, the increased stiffness of the core makes a lower placement more favorable [7].

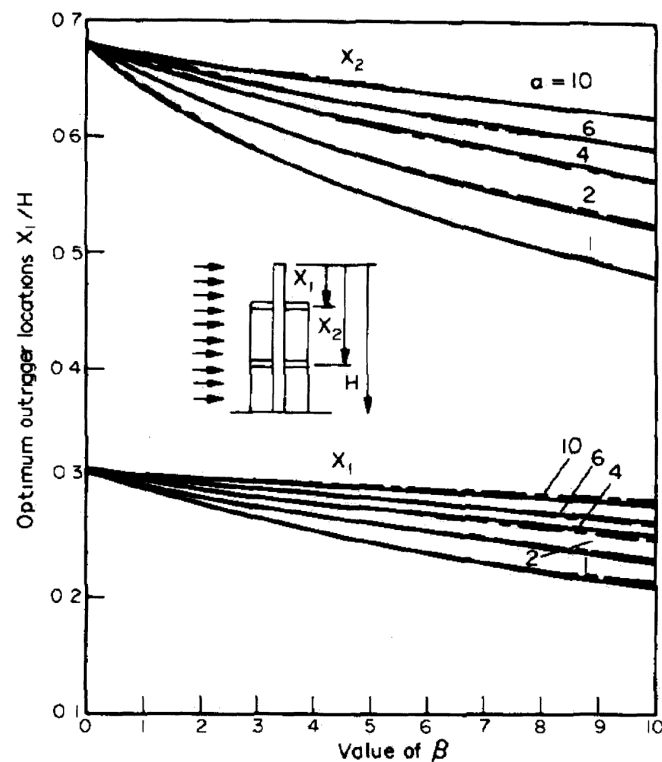


Figure 14: Optimal location of a double outrigger system [7]

The efficiency of outriggers in a structure is complex. The relation of stiffness between the core, columns, and outriggers affects the efficiency of the outrigger [7]. In this thesis the outrigger system will be bracing-based. Bracing of the outrigger can have various shapes and characteristics. Figure 15 shows different bracing shapes. Triangular shapes tend to be more stiff than regular diagonal shaped bracing [30]. When designing against wind, it is optimal to make the outrigger structure as stiff as possible to restrict the displacement of the top floor. On the other hand, this can potentially contribute to big IDR between the outrigger floor and above and underlying floors, since the difference in stiffness between floors is large. This is also problematic when designing for seismic loads [30].





	A	B	C	D
Topology				
Material	1.00	1.04	1.80	1.49
Stiffness	✓✓	✓	✓✓✓✓	✓✓✓✓
Strength	✓✓✓✓	✓✓✓	✓	✓✓

Figure 15: Bracing shapes [30]

For seismic design, the addition of very stiff outriggers can compromise the safety of the building. When subjected to seismic loads, the analogy is that the building should absorb forces uniformly and behave ductile. Stiff outriggers induce large forces and do not contribute to damping the transversal loads [30]. That is why it is common for engineers in seismic regions to balance designing for wind or seismic loads. This thesis is based on a location in Trondheim, Norway. Therefore, seismic loads will not be considered in the design.

3.3.3 Examples of outrigger systems

Hong Kong International Financial Center

The International Financial Center in Hong Kong is 415 m high with 88 floors. The structure uses a belt truss and an outrigger system. It has a total of four outriggers located throughout the building. The location of the outriggers are 6-7th, 32-33th, 53-54th and 65-66th floor [32]. The outrigger system activates the perimeter mega columns and relieves the concrete core of the overturning moment. The bracing used is a type of K-bracing, shown in Figure 17. The outriggers and belt trusses are connected with adjustable joints.



Figure 16: Hong Kong International Financial Center [33]



Figure 17: Bracing Hong Kong financial tower [32]

First Wisconsin center

The First Wisconsin Center is a 42-story building that stretches 183 meters. It contains offices and commercial banking. The truss system is a three-belt system. Two of these belts constitute the outrigger system. They are located just below the middle floor and on the top floor. The outrigger floor is used as a technical floor, mechanical equipment is stored here. Figure 18 shows the outrigger structure. The bracing system used here is a classical chevron bracing system [34].



Figure 18: First Wisconsin center [35]

3.4 Research scope

This thesis aims to analyze the effect of using outriggers in tall timber structures. Through a parametric study, the objective is to see how different variables such as location, shape, and stiffness of the outrigger influence performance. The study is limited to studying buildings with a maximum of two outrigger structures. The first part of the study is to investigate the effect of one outrigger and efficiency parameters. Next, there will be a study of structures with two outriggers. When talking about what is the best performance, the reference is top floor displacement, maximum IDR and acceleration.

The main research questions are as follows:

- What is the ideal location of outriggers?
- How does the cross laminated timber core system affect outrigger performance?
- What shape of outrigger bracing is the most efficient?
- How does outrigger stiffness affect performance?

4 Methods

In this chapter, the method of analysis and the mathematical description are presented. First, the acceleration calculation is described. Second, the wind load combinations are presented. Third, the structural model with and without the outrigger system is presented. Fourth, the implementation of the Python code. Fifth, an introduction to the initialization of the system. In the following paragraphs, an overview of the methods is provided.

The design of high-rise timber structures is governed by the dynamic behavior caused by the horizontal wind load acting along its height. To design such structures, it is critical to understand the behavior and factors that influence the wind load and the response of the structure. In this thesis, both acceleration and wind calculations are based on the simplified approach provided by the Eurocode (NS-EN 1991-1-4) [9]. The load combinations are extracted from the Eurocode (NS-EN 1990) [24].

The data required to perform a parametric study consist of the design output for various combinations of the relevant preliminary design parameters. To acquire such a collection of data, an easily adjusted parametric model is needed. The model developed in this thesis uses an integrated system of self-automated acceleration and wind calculations combined with a structural model, defined just by simple building properties as input. The model is dynamic, meaning all variables can be adjusted by the user. The routine is developed with the use of OpenSeesPy in Python.

The model is constructed as a planar 2D semi-rigid timber frame, and consists of beams, columns and walls. The column-to-column and wall-to-wall connections are modeled as continuous in all joints. The beams, columns, and walls are formulated using Timoshenko beam theory. Rotational springs are added to the beam ends to account for the beam-to-column/wall rotational connection stiffness. A reference frame is used to study the effect of different parameters. During the development of the system, the static and dynamic properties of the reference frame were validated against a model in SAP2000.

72 900 different frames with varying structural properties were constructed, and the effect of adding a single outrigger and two outriggers to the different frames was analyzed. The first modal frequencies, acceleration, interstory drift, and top floor displacement were calculated for all frames. The combinations would result in several million simulations. However, by optimizing one parameter at a time, the number of simulations was reduced to around 291 600.

Characteristics and trends of the data are investigated and polynomial expressions for some variables are proposed based on non-linear regressions. The proposed expressions show how the outrigger influences the structural properties of frequencies, acceleration, maximum interstory drift, and top floor displacement.

4.1 Wind Load

The wind pressure acting on a structure can be a complicated calculation which is dependent on numerous variables. The Eurocode provides a simplified method to obtain the wind pressure. According to Eurocode (NS-EN 1991-1-4) [9] wind loads can be calculated as:

$$w_e = q_p(z_e) * (c_{pe} + c_{pi}) \quad (3)$$

$$F_w = c_s * c_d * \sum w_e * A_{ref} \quad (4)$$

Wind speed and pressure is highly dependent on the location and topology of the structure. This is shown in Figure 19, which shows the distribution of the wind load according to Eurocode (NS-EN 1991-1-4) [9]. To simplify structural analysis, the goal is to calculate a uniform wind load on the structure. This is achieved by first calculating the base moment and shear from the wind loads provided by the Eurocode (NS-EN 1991-1-4) [9]. A uniform load is calculated to give the same base shear and bending moment as the distribution given by the Eurocode. Figure 20 shows how this results in a uniform distributed load along the building.

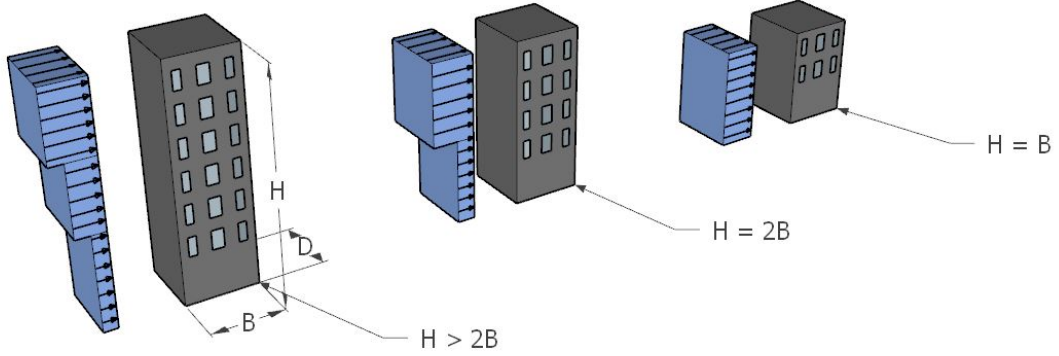


Figure 19: The building is divided into simplified wind zones

In this thesis, many of the variables in the calculations of the wind pressure have been assumed constant to reduce the computational expense of running the analysis. The return period is set to 50 years. The orthography factor and the turbulence factor are set equal to 1. The terrain category is set to 4. This implies that the structures considered are located in an area in which at least 15% of the surface is covered with buildings and their average height exceeds 15 meters. As a result, the variables: k_{r,z_0} , and z_{min} are set to 0.24, 1 and 16 respectively. The factors: C_{Dir} , C_{Season} and C_{prob} have been set equal to 1. This results in a base speed of the wind equal to the fundamental wind speed. The wind base speed is set equal to:

$$V_b = C_{Dir} \cdot C_{Season} \cdot C_{Prob} \cdot V_{b,0} \quad (5)$$

The full extent of the wind-load calculation is given in Appendix E.

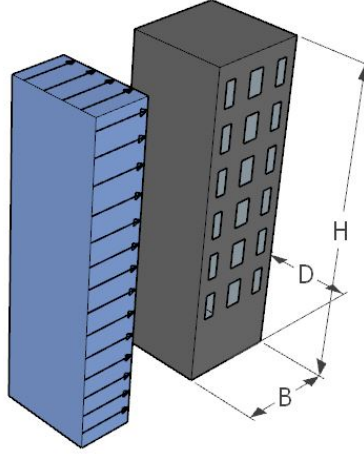


Figure 20: The final uniform wind load

4.1.1 Load combinations

The loads used in the models were based on three different load combinations found in Eurocode (NS-EN 1990) [24].

The ultimate limit state load combination is taken from §6.4.3.2 (6.10b):

$$E_d = \xi \cdot \gamma_G \cdot G_k + \gamma_{Q,i} \cdot \psi_{0,1} \cdot Q_{k,1} + \gamma_{Q,i} \cdot \psi_{0,i} \cdot Q_{k,i} \quad (6)$$

The characteristic load combination is taken from §6.5.3 (6.14b):

$$E_d = G_k + Q_{k,1} + \psi_{0,i} \cdot Q_{k,i} \quad (7)$$

The quasi permanent load combination is taken from §6.5.3 (6.16b):

$$E_d = G_k + \psi_{2,i} \cdot Q_{k,i} \quad (8)$$

where

- ξ is a reduction factor for unfavorable permanent actions G_k
- γ is a factor for favorable / unfavourable loads
- ψ is a combination factor
- G_k is a characteristic value of a permanent action
- $Q_{k,1}$ is a characteristic value of the leading variable action
- $Q_{k,2}$ is a characteristic value of the accompanying variable action

The model ultimate limit state load is defined as Equation (6), with: $\xi = 0,89$, $\gamma_G = 1,35$, $\gamma_{Q,1} = 1,5$, $\psi_{0,1} = 1,0$ and $\psi_{0,2} = 0,7$

$$\text{Ult} = 1,2 \cdot \text{Dead} + 1,5 \cdot \text{Live} + 1,0 \cdot \text{Wind} \quad (9)$$

The model characteristic load is defined as Equation (7), with: $\psi_{0,1} = 0,7$ (live)

$$\text{Char} = 1,0 \cdot \text{Dead} + 0,7 \cdot \text{Live} + 1,0 \cdot \text{Wind} \quad (10)$$

The model quasi permanent load is defined as Equation (8), with: $\psi_{2,1} = 0,3$ (live) and $\psi_{2,2} = 0,0$ (wind)

$$\text{Quasi} = 1,0 \cdot \text{Dead} + 0,3 \cdot \text{Live} + 0,0 \cdot \text{Wind} \quad (11)$$

4.2 Acceleration

Accurately predicting the acceleration of a structure is only possible by developing a full-scale finite element model. However, the magnitude of acceleration can be estimated using simplified models. The along-wind peak acceleration in m/s^2 of a structure can be estimated by the equation given in Eurocode (1991-1-4) [9], B.4(4) and reads:

$$a = k_p \cdot \sigma_{a,x} \quad (12)$$

The equation states that the acceleration depends on the k_p factor and the standard deviation of the wind $\sigma_{a,x}$. k_p is mostly depended on the wind speed. $\sigma_{a,x}$ is more related to the turbulence of the wind, and how much it deviates from the mean wind.

$$k_p = \sqrt{2 \cdot \ln(v \cdot T)} + \frac{0.6}{\sqrt{2 \cdot \ln(v \cdot T)}} \quad (13)$$

$$\sigma_{a,x} = \frac{c_f \cdot \rho \cdot D \cdot I_v(z_s) \cdot v_m^2(z_s)}{m_{1,x}} \cdot R \cdot K_x \cdot \phi_{1,x} \quad (14)$$

In addition to the wind speed, the acceleration depends on:

- The building shape and dimensions (plan and height).
- Mass and stiffness of the building
- Fundamental eigenfrequency and mode shape (Modal properties)
- Damping ratio
- Site characteristics (e.g. wind velocity)
- Wind return period

All base factors are equivalent to the factors seen in the wind calculations. However, in acceleration calculations, the factors: C_{Dir} and C_{Season} remain equal to 1, while C_{prob} now changes to 0.73. This corresponds to a 50% chance of exceeding the fundamental wind speed in half a year. $V_{b,0}$, depends on the location. The fundamental wind speed is set to $V_{b,0} = 26$ m/s. This is the characteristic wind speed in Trondheim.

A method of normalizing the modal shape of the first fundamental frequency, in order to target a specific floor acceleration, has been used. This allows one to calculate the acceleration at the floor of interest. The floor of interest is the second to top floor. This is the ground floor of the upper most apartment which is most concerned with wind-induced accelerations.

In the calculation of K_x , a simplified approach has been used. The method of fitting the polynomial: $(z/h)^\delta$ to the fundamental mode shape $\phi_1(z)$. The value of interest is the exponent: δ . The equation is presented below:

$$\phi_1(z) = \frac{z^\delta}{h} \quad (15)$$

The building mass is modeled using the quasi-load combination shown in Equation (11) in combination with the structural properties shown in Equation (16).

$$\text{Total Mass} = \text{Quasi load} \cdot \text{Spacing} \cdot \text{Number of floors} \cdot \text{Number of bays} \cdot \text{Bay length} \quad (16)$$

Z_t is set to 200 and L_t is set to 300 as recommended in the Eurocode (NS-EN 1991-1-4) [9]. The radius of the building edges is assumed to be 0. The frequency of the structure is obtained by a modal analysis of the structure in Python. The damping is assumed to be 1.9%, which is a little smaller than the normally assumed constant value of 2% [22].

This method presented by Eurocode (NS-EN 1991-1-4) [9] idealizes the building as a fixed cantilever beam. This means that the acceleration is determined by analyzing only one vibration mode. However, high-rise structures can exhibit more than one vibration mode. Thus, the acceleration provided by NS-EN 1991-1-4 may be an underestimate of the true acceleration.

4.3 Structural model

The structural model is formulated in Python, using OpenSeesPy. OpenSeesPy is a finite element module in Python consisting of inbuilt functions for creating structural elements, plotting the model, setting loads, and extracting forces. This section should give insight into the choices and construction of the model used in the analysis in a general manner.

The model is constructed as a planar 2D semi-rigid moment frame, and consists of beams, columns and walls. The column-to-column and wall-to-wall connections are modeled as continuous in all joints. In practice this is not possible for a tall structures, but it is an assumption applied in this thesis. To account for the thickness of columns and walls, the model has added a rigid zone around every column and wall that connects the wall/column to the beams through rotational springs. This rigid zone is assumed to have infinite stiffness against bending and has a length of half the column/ wall height. The beam-to-column connection and the rigid zone are shown in Figure 21. The beams, columns and walls are assumed to be two joint elements of $430/2$ in width laying next to each other. This is shown in Figure 22.

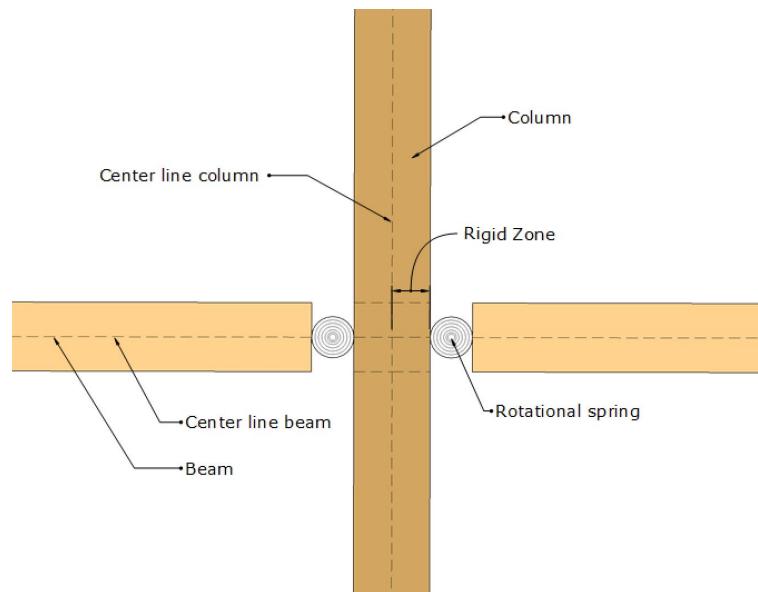


Figure 21: Connections with rigid zone

As mentioned in Section 2.3.1, the main reason for choosing a 2D analysis was computational consideration. It is much more time consuming with 3D analysis compared to the same system in 2D. This is because it takes much more elements and nodes to represent a structure in 3D compared to 2D. Therefore, collecting data for a parametric study can become computationally expensive if the models are large. To capture the influence of a parameter, various models must be developed that implement different values for the parameter, and their results must be analyzed. Thus, a model with fewer elements is preferred. When modeling a structure in a 2D environment, the structure is loaded horizontally in one single direction. Thus, only a representative cut of the structure is analyzed, and the pressure caused by the wind acting on the structure must be translated into a uniformly distributed load acting on that representative cut. This is explained in more detail in Section 4.3.1.

The columns, beams, and walls are modeled with a Timoshenko beam element. This allows the model to account for shear deformations, as well as rotational bending effects. Since the theory takes shear deformation into account, it is well suited for thick beam elements. This is advantageous in this thesis due to the massive elements. In addition, due to the low shear modulus in timber, the shear deformation cannot be neglected. Neglecting shear deformation with the use of, for instance, Euler-bernoulli beam theory is therefore considered to be insufficient.

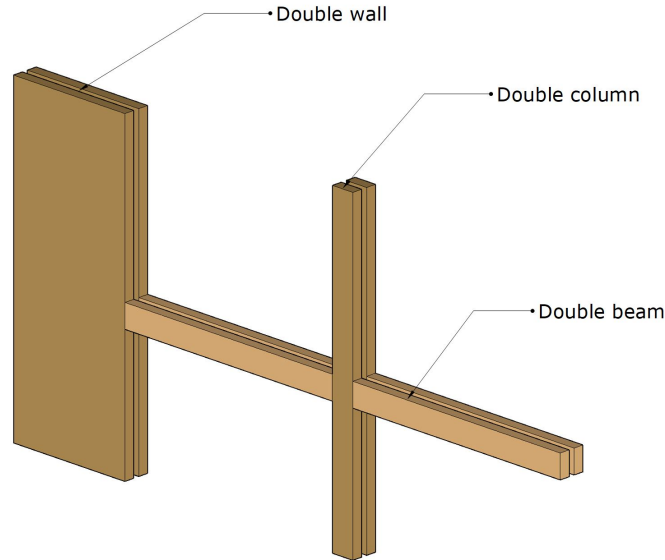


Figure 22: Illustration of members

OpenSeesPy has defined the Timoshenko beam elements with six degrees of freedom (DOF). The OpenSeesPy elements also require material inputs. Thus, in the structural model, the beams, the columns, and the rigid zones are modeled with glue laminated timber (glulam). The walls are modeled with cross laminated timber (CLT). However, for rigid zones, the shear modulus, moment of inertia, and area are assumed to be substantially larger compared to the CLT and glulam elements. Euler-bernoulli beam theory is applied for rigid zones. The beams, columns, and walls are considered massless, and the equation for the model quasi-load (11) is used to account for the mass of the structure.

The rotational beam stiffness has been modeled after a recommendation by Osama Abdelfattah Heguir. Section 2.2.3 showed that the rotational stiffness of a beam with a height of 450 mm was around 4500 [kN.m/rad]. The rotational stiffness can be scaled by the factor z^2 . This comes from the paper of Aivars [36]. Aivars composes different equations to approximate the rotational stiffness of the connection, and in all equations, the factor z^2 is represented. The assumption that only the height of the beam changes is considered a reasonable assumption. The other parameters in the equations depend on material properties, the stiffness of the rods, and more. Such parameters are kept constant in this thesis.

In combination with the proposition of a squared ratio, z^2 , and the known rotational stiffness for the beam with a height of 450 mm. A proposition for a rough estimate of the beam-to-column/wall rotational stiffness is developed. The rotational stiffness in the beam-to-column connections is thus calculated as:

$$K_{rb} = z^2 \cdot 4500 \cdot \text{kNm/rad} \cdot (\text{number of planes of rods}) , \text{ where } z = \frac{B_h}{450} \quad (17)$$

With the assumption of two joint beams laying side by side, the modeled rotational stiffness can be calculated using four planes of rods and the reference rotational stiffness value for a beam with a thickness of 430 mm. For example, a beam height of 540 mm would then result in a rotational stiffness of 26 000 [kN.m/rad].

The foundations are designed to transfer the load from the structure to the ground and prevent the structure from overturning. The influence of the foundations with all its load-bearing characteristics is a complex subject that can be highly project-specific. The load-bearing characteristics range from the material used, the size of the foundation, and the local soil properties. To simplify the scope of this thesis, all soil properties are excluded. Thus, the rotational stiffness provided by the foundations is solely dependent on the support design, the number of brackets and hold-downs. The rotational stiffness at the support in the columns is modeled with 10.000 kN.m/rad, and the

rotational stiffness in the walls is modeled with 200.000 kN.m/rad. Since a wall has a much larger dimension compared to a column, it also contributes with substantially more rotational stiffness.

4.3.1 System loads

The model is assumed to be loaded in 2D both vertically and horizontally. The horizontal loads consist of the pressure created by the wind, explained in Section 4.1, and the vertical loads are explained in this section. When modeling a structure in a 2D environment, the force exhibited on one frame is assumed to be the total force divided by one less than the number of frames. The wind force exhibited on this frame is the lateral load times the spacing for all internal frames. Only half of the force is considered on the external frames, since they only have half the spacing.

Vertical Loads

The vertical load of the structure is divided into dead and live loads. The dead load consists of the self-weight of the structure including architectural features considered to be permanent. This can be interior walls and ceilings. The live load incorporates the action of the users, as well as non-permanent loads such as snow. The live load is highly structure specific. The dead load in Table 4 are chosen based the paper by Aivars [5]. The live load is based on the recommend office live load in Eurocode (NS-EN 1991-1-1) [37].

Load type	kN/m^2
Dead Load	2
Live Load	3

Table 4: Load types

4.3.2 Basic model

The basic structural model is shown in Figure 23, and consist of a set floor height, number of floors, bay length, frame spacing, support conditions and modal damping ratio. The basic model has two external CLT walls and two internal glulam columns. The CLT walls acts like the core-structure. The walls and columns has different rotational stiffness with the base socket.

4.3.3 The model with outrigger(s)

The outrigger system is the same as the basic model with added outrigger(s). For convenience, the outrigger elements were also modeled as Timoshenko beam elements with the material properties of glulam. By only connecting the outrigger element to the main system through DOFs 1 and 2 (only in the x and y directions), the outrigger elements are assumed to be pinned at both ends. Therefore, the outrigger is given zero rotational stiffness and the outrigger element resembles a truss element. The elements are connected to the basic model using springs. The stiffness of the outrigger connection is assumed to be $K_{ax} = 1000$ kN/mm, with an elaboration in Appendix C.

The connections of the truss system need to be modeled. These connections will ultimately reduce the axial stiffness of the truss-element and result in an effective axial stiffness. This is modeled with a reduction in the area of the beam, resulting in an effective area. The concept of effective axial stiffness is shown and explained in Section 4.3.4. An outrigger system requires a core structure to work. In this system, the core structure is modeled as the CLT walls combined with the rigid zones. In this thesis, the model considers both internal and external wall systems.

The model has two options for the outrigger system (truss). The first option is shown in Figure 24. The two bracing systems consist of simple diagonal bracing elements. The second option is a chevron bracing system, this is shown in Figure 25. The first system has its outriggers connected on to the main grid, while the second system has an intersection point in the middle of the overlying

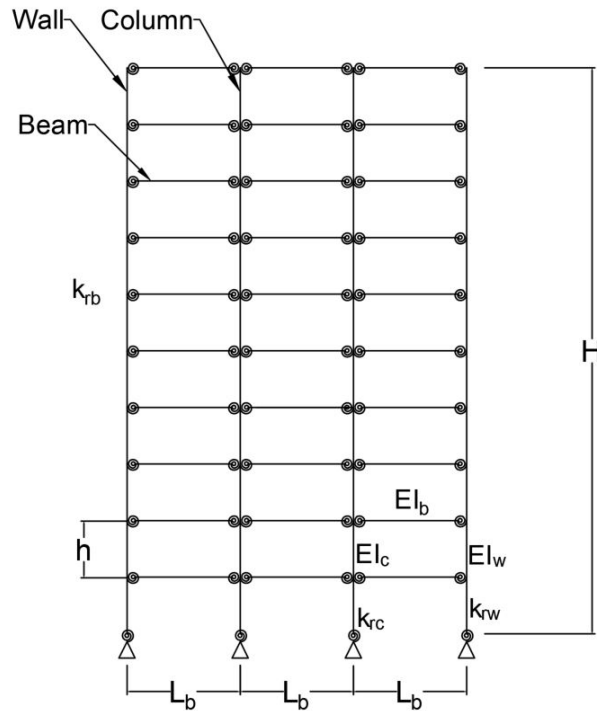


Figure 23: Base frame

beam. The connection is assumed to be on the bottom part of the beam, and therefore the beam is still modeled as continuous.

The systems shown in Figure 24 are one of the most commonly used bracing systems and comes in many shapes and forms. The diagonal bracing system is often used in an x-system with cables, where both corners are connected. It offers strong and compact connections between truss members. In this thesis both a diagonal- and a mirrored diagonal bracing system is tested. Figure 24b shows the diagonal bracing system and Figure 24a shows the mirrored diagonal bracing system. The continuous system allows for better force transferring through the members [30].

The Chevron bracing, shown in Figure 25, is commonly used in steel structures. The system is known for its architectural and practical benefits. The geometry allows for easy placement of external doors and windows, which separates the system from traditional diagonal bracing. However, there are some negative effects regarding the distribution of forces in the system. The overlying beam can be subjected to substantial shear forces when the building is subjected to large horizontal loads [30].

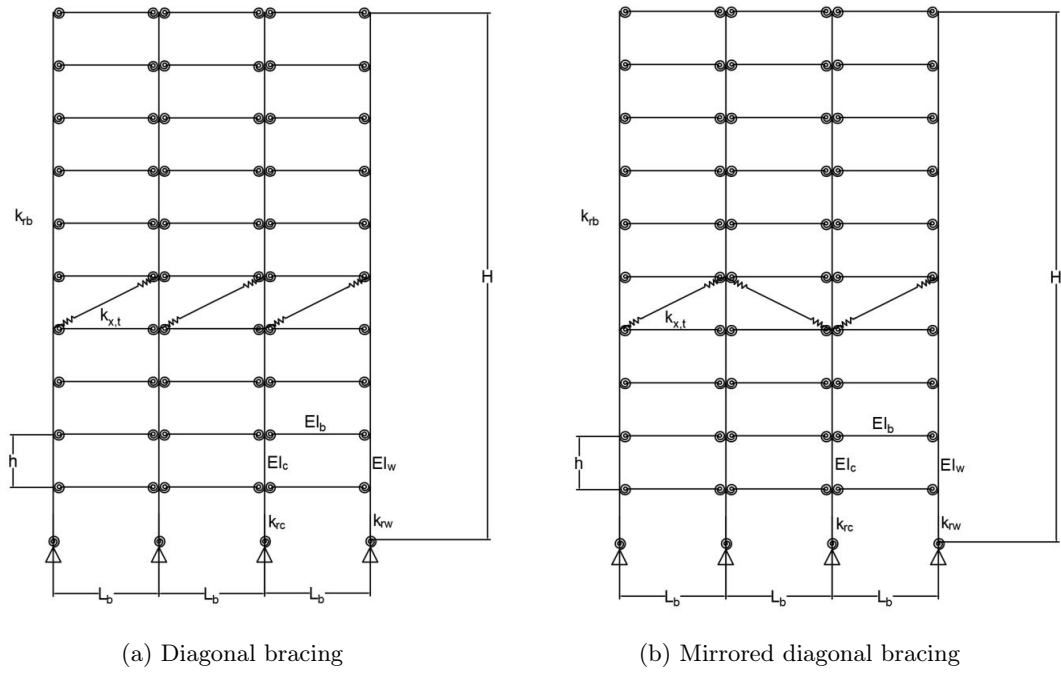


Figure 24: Mirrored and diagonal bracing

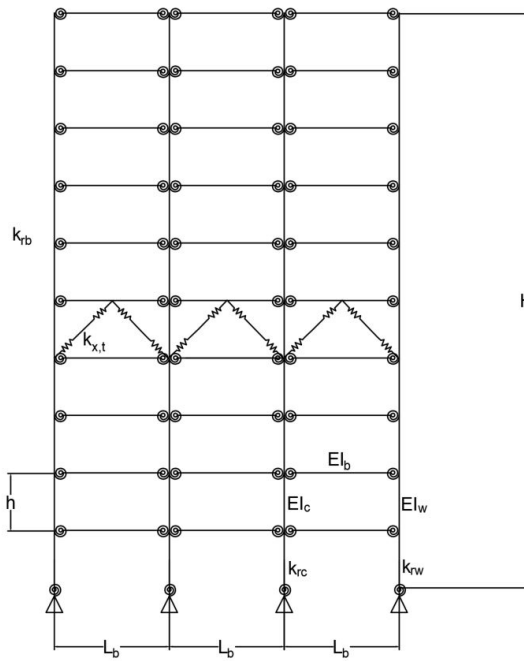


Figure 25: Chevron bracing

4.3.4 Truss stiffness

The trusses are assumed to behave as pinned in both ends, thus providing zero rotational stiffness. In this analysis the axial stiffness of the trusses is regarded as an effective stiffness. The truss-member has an axial stiffness of:

$$K_L = \frac{A \cdot E}{L} \quad (18)$$

A is the area of the cross section, L is the length of the member, and E is the Young's modulus. The effective axial stiffness should coincide with the reduction in stiffness caused by deformations in the connections. When the truss elements are subjected to forces, it causes deformation in the connections. These deformations and their magnitude depend on the type of connection and the fasteners. Figure 26 shows an illustration of how truss elements are modeled with springs.

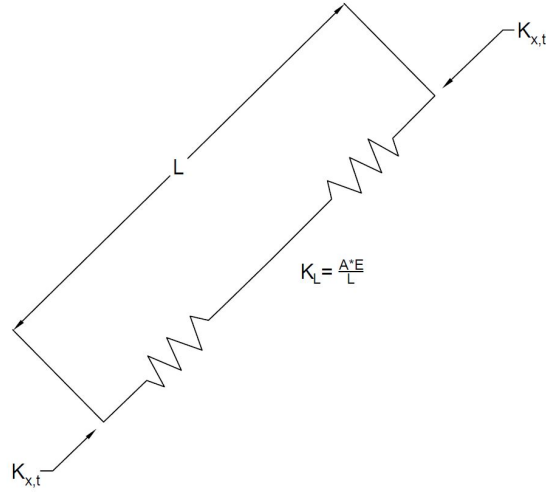


Figure 26: Stiffness of truss

Instead of using the spring stiffness $K_{x,t}$ the connections in the trusses have been modeled in OpenSeesPy with a reduction in the stiffness parameter K_L . Equation (19) shows how the springs reduce the total stiffness of the connection.

$$K_{total} = \frac{1}{\frac{1}{K_{x,t}} + \frac{1}{K_L} + \frac{1}{K_{x,t}}} = \frac{K_L \cdot K_{x,t}}{2K_L + K_{x,t}} < K_L \quad (19)$$

Equation (20) shows the approximation of using a reduced cross section to account for this reduction in stiffness.

$$K_x(A) = \frac{A' \cdot E}{L} = K_{total} \quad (20)$$

4.4 Implementation

The system is developed using Python and object-oriented programming. Object-oriented programming makes the code both more readable and more compact. The program is dynamic and uses few input parameters for both the model and the analysis. It is dynamic since it can be changed to a completely new system by changing the input parameters. All in all, the following functionalities result in around 4500 lines of code to create the system. The program consists of four main classes; the element class, the load class, the model class, and the analysis class.

The elements class is a bank that contains all structural data for the members. This includes material data such as the Young's modulus, the shear modulus, and geometric properties of the members. By creating this class, the program gains a smart way to systematize the material data and also makes the material data more accessible to other system classes. The glulam material properties as well as the CLT material properties, are found within this class. All members have a thickness of 430 mm, hence, this is set as a constant in the member class. The other properties are defined when the system is running. This is done by multiple get/set functions for more convenient access of the data.

The load class contains all the information needed about the loads applied to the system. These are the same loads as those addressed in Section 4.3.1. The class needs three input parameters: the lateral load calculated from the wind speed, the live load, and the dead load. With the three inputs, the class determines all the necessary load combinations mentioned in Section 4.1.1. Thus, the loads are easily stored for convenient access if needed in other classes. This class uses a variety of get/set functions to extract the needed information.

The model class creates the work environment. It schedules all the nodes for beams, columns, and walls to assign the correct connections and placements in the environment. Everything is determined by a few parameters:

- *The simulation type*: this is either *Linear* or *PDelta*. In this thesis, we use the linear analysis. However, if one needs to perform a buckling analysis, the simulation type needs to be *PDelta*. The variable type is String.
- *The number of bays*
- *The number of floors*
- *The floor height*
- *The spacing*
- *The bay length*
- *The Loads class*, as explained earlier.
- *The Elements class*, as explained earlier
- A Boolean value *pinned*. If set to *True* then the model is assumed to be pinned, and if pinned is set to *False* (as default), the wall and columns get their wall/column-to-foundation rotational stiffness provided in the element class.
- A Boolean value *outrigger*. If set to *True* then the model gets an internal vertical cross laminated timber core structure, and if set to *False* (as default) the model gets an external vertical cross laminated timber core structure.

The model class contains a set of class functions. All of these are shown in the UML diagram 28. The model class contains functions for first creating the main system and work environment. Second, the functionalities to plot the model and perform a modal analysis.

First, the functions to create the model environment:

- *addMainGrid()*. This function adds the main grid.

-
- *addOffsetGrid()*. This function adds *ordinary nodes* as shown in Figure 27.
 - *addDoublicantPoints()*. This function adds *hidden nodes* as shown in Figure 27.
 - *addRotationalStiffnessPointsAtBase()*. This function adds both the hidden nodes and the zero-length element at the support.
 - *setRotationalStiffness()*. This function sets the column/wall-to-foundation rotational stiffness.
 - *addColumnsAndWalls()*. This function adds both the glulam columns and CLT walls.
 - *addBeams()*. This function adds the glulam beams.
 - *addRigidZones()*. This function adds the rigid zone.
 - *addBeamConnections()*. This function sets the beam-to-column/wall rotational stiffness

Second, the functions to plot the model and the modal analysis:

- *plotModel()*. This function plots the work environment. It shows all the different beam, wall, and column elements, as well as the nodes, with geometric properties such as the length and height of the frame.
- *eigenValues(otrs)*. The input parameter *otrs* is the outrigger system (this will be addressed later in this section). If there exist no outriggers, then leave this as blank. This function starts by placing the correct nodal mass in every main grid node. Thus, it is important that this function is not used before the model is finished, because the chosen outrigger system may influence the main grid. Therefore, if the user intends to add outriggers, then this function should be called after everything is placed in the work environment. The return value is the first modal eigenvalue of the system.
- *plotModeShape()*. After the *eigenValues()*-function has been used, the *plotModeShape()*-command will plot the first three horizontal degree-of-freedom eigenvector shapes.

When creating the model class some simplifications were imposed on the system. First, to create the rigid zone, an approximation factor was used. This factor makes the rigid zone a defined amount stiffer than the connecting beam elements. The factor is tuned by doing an analysis in Python and testing the results with the equivalent system in SAP2000. After many iterations a factor of 100 seemed reasonable. Thus, the area and the moment of inertia are increased by a hundred times its ordinary value. Of course, if this factor ought to be tuned perfectly, then one need to change it every time when doing an analysis. The error when using a factor of 100 was significantly small and will not be addressed further.

Second, the nodal mass. When assigning the nodal masses, the mass is assumed to be uniformly distributed across the floors. Nodes are given mass proportional to the amount of floor that the nodes support. Thus, the nodes on the edges carry less mass compared to the internal nodes.

Third, the connections. The zero length element is a functionality to connect two nodes with a chosen number of DOFS. The outriggers are only connected to the main grid in the horizontal and the vertical degrees of freedom, giving it zero rotational stiffness. With the use of hidden nodes the beams are connected to the rigid zone with the rotational stiffness of the defined beam-to-column rotational stiffness in the element class. The beams are also connected to the rigid zone in the horizontal and the vertical degrees of freedom. The column/wall-to-foundation rotational stiffness is also added using a zero-length element and a hidden node.

Figure 27 illustrated the work environment. It highlights the main components of the model: the main grid, the hidden nodes, and ordinary nodes, as well as walls, beams, columns, outrigger (OR) elements, rigid zone and zero length elements. The main grid connects the walls and columns to the floor and outriggers. The ordinary nodes connects the beams and the rigid zones together.

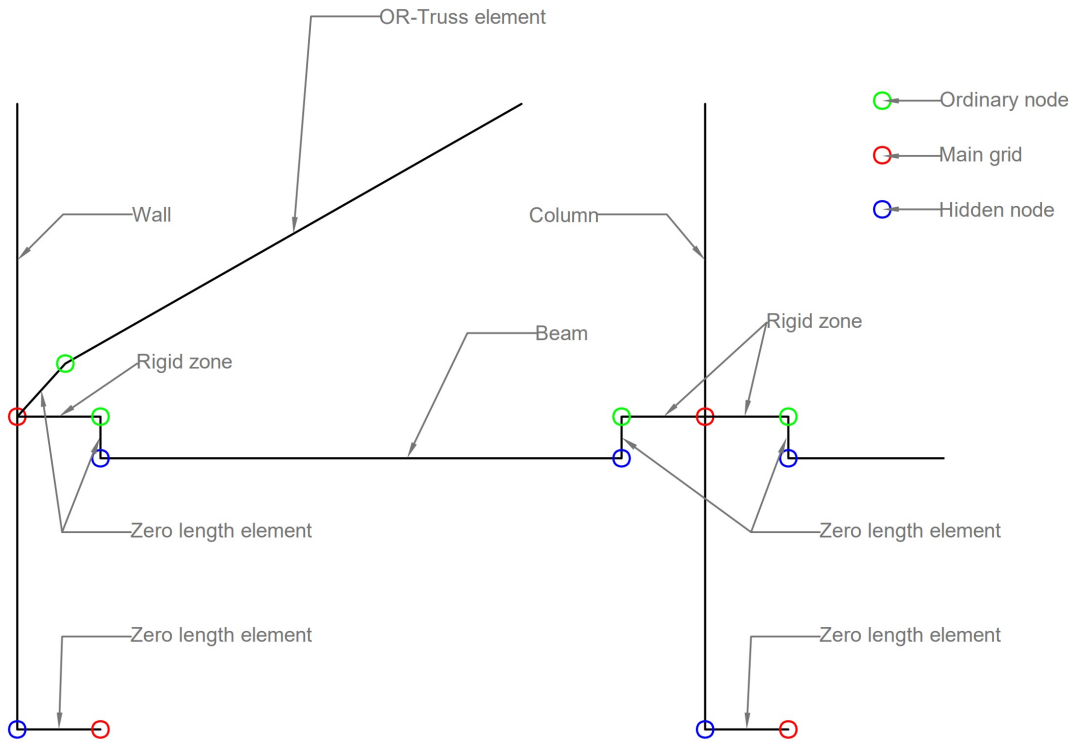


Figure 27: The structural environment

The analysis class is used to perform all structural analyzes. With the use of the class parameters, the analysis environment is created. The class has four input parameters:

- *The Model class*, as explained earlier
- *The Outrigger class*, explained later. If there exist no outrigger system, set this to *None*.
- A boolean value *uniform*. If set to *True* (as default), then the loads are applied uniformly across the members, and if set to *False*, the loads are lumped directly into the nodes.
- A boolean value *complete*. If set to *True*, then the model calculates all the forces in all members, and if set to *False* (as default), the model only calculates the forces in a predefined number of members. This will be addressed in more detail below.

The analysis uses a build-in function in OpenSeesPy to solve the system. All choices are based on the OpenSeesPy manual [38]. First, the chosen system solver. This has been set to *BandGeneral*. This command is used to construct a linear system of equation objects.

Second, a *RCM* degree-of-freedom numbering object is chosen to provide the mapping between the degrees-of-freedom at the nodes and the equation numbers. An *RCM* numberer uses the reverse Cuthill-McKee scheme to order the matrix equations.

Third, a *Plain* constraint handler is set. The plain constraint handler is chosen because it can enforce homogeneous single-point constraints and multi-point constraints constructed where the constraint matrix is equal to the identity.

Fourth, the integrator object is set to *LoadControl*. The integrator object determines the meaning of the terms in the system of equation object $Ax=B$. The change in applied loads caused by this depends on the active load pattern and the loads in the load pattern.

Fifth, the solution algorithm is chosen to be the Newton-Raphson algorithm. This algorithm determines the sequence of steps taken to solve the non-linear equation. The linear solver object

is set to 'NormDispIncr' with a tolerance criteria of 1.0e-6 and a maximum number of iterations to 1000. This means that the solver will stop if it reaches the tolerance criteria or the number of iterations reach the maximum number of iterations.

The analysis class contains a set of class functions. These are all shown in the UML diagram 28, and explained below:

- *elasticBucklingAnalysis()*. This function calculates the elastic buckling factor. First, the stiffness matrix is calculated in the initialization of the analysis object, before applying the load with the use of the *getElasticStiffnessMatrix()*-function. Now, after the loads are applied, the geometric stiffness matrix is extracted. Thus, with both the stiffness matrix and the geometric stiffness matrix, the buckling analysis can be performed. Again, to perform the buckling analysis, *simulation type* must be *PDelta* and not *Linear*.
- *getBuildingMass(plot)*. This function calculates the mass of the building. To speed up the process, it is recommended not to use this function, but rather calculate the mass directly from the use of the model quasi-load, as shown in Section 4.2. The return value is the mass of the building. The Boolean input variable *plot* shows the reaction forces if set to *True*, the default value is *False*.
- *getLateralDisplacements(wind, deadAndLive, ULS, plot)*. This function calculates the top-floor displacement, max interstory drift, and the resulting forces in the members. The Boolean input variables *wind* and *deadAndLive* determine whether or not to include the wind load (if *True*) or not (if *False*), the same goes for the dead and live load. The Boolean input variable *plot* shows the reaction forces if set to *True*, the default value is *False*. The Boolean input variable *ULS* determines if the ultimate limit state dead and live load combination is going to be used. The default value is *False*.
- *setDeadAndLiveLoad()*. This function sets the dead and live load according to the load combinations in the Load object. This is the same load combination given in in Section 4.1.1 and Equation (10).
- *setQuasiLoad()*. This function sets the quasi-load according to the load combinations in the Load object. This is the same load combination given in in Section 4.1.1 and Equation (11).
- *setWindLoad()*. This function sets the wind load according to the load combinations in the Load object.
- *setULSDeadAndLiveLoad()*. This function sets the dead and live load according to the load combinations in the Load object. This is the same load combination given in in Section 4.1.1 and Equation (9).
- *getNodeForce()*. This function displays the reaction forces.
- *getMaxIDR()*. This function returns the maximum interstory drift.
- *getTopFloorDisp()*. This function return the maximum top floor displacement.
- *getMaxIDRfloor()*. This function returns the floor of maximum interstory drift.
- *getDisplacementVector()*. This function extracts the shape of the building displacement.
- *getRelevantForces()*. This function calculates all the member forces. The forces extracted depends on the *complete*-variable in the Analysis object. If the variable is set to *True*, the forces in all the members is going to be extracted. If the variable is set to *False* only the reaction forces, and if an outrigger is present, also the forces in the outrigger and the surrounding members.
- *getForceElements()*. This function returns the member forces found with the *getRelevantForces()*-function
- *solveModel()*. This function solves the model according to the defined OpenSeesPy analysis functionalities explained above.

In addition to the four main classes, there are different outrigger classes. It implements one outrigger class for each provided outrigger system. This is because the nodes and beams are placed differently according to the chosen outrigger system. However, the three classes are structured equally, with the same class functions and the same input variables:

- *The Model class*, as explained earlier
- A Boolean value *complete*. If set to *True* then the model calculates all forces in all members, and if set to *False* (as default), the model only calculates forces in a predefined number of members. Equivalent to the Analysis object.
- A Boolean value *ULS*. If set to *True* then the reduction factor for effective stiffness is calculated using the reduction factor for ULS, and if set to *False* (as default), the reduction factor for the effective stiffness is calculated using the reduction factor for SLS.
- A Boolean value *reduction*. If set to *True* (as default) then the effective stiffness is applied, and not applied if set to *False*, .

The outrigger classes contains a set of class functions. These are all shown in the UML diagram 28, and explained below:

- *getDiagonalStiffness()*. This function returns the effective axial stiffness of the member.
- *addDoublicantPoints(nodeTag, orientation)*. This function adds ordinary points shown in Figure 27 and links the node to the main grid through the zero length element.
- *setHorizontalOutrigger(numFloor)*. This function places the outrigger in the structural environment and works differently for the different systems. The model has two options for the outrigger system (truss). The first system has its outriggers connected to the main grid, while the second system has an intersection point in the middle of the overlying beam. The connection is assumed to be on the bottom part of the beam, and therefore the beam is still modeled as continuous.
 - The first option is shown in Figure 24. The two bracing systems consist of simple diagonal bracing elements.
 - The second option is a chevron bracing system; this is shown in Figure 25. When adding the Chevron system, the beam and the outrigger are removed to attach an extra point to the main grid where the outrigger is to be connected. The beam, now divided into two elements, is modeled to work as a single continuous beam.
- *findBeamsColumns(numFloor)*. Finds the relevant members for force extraction later in the analysis object; this is the same as previously explained in the analysis object. The input variable tells the system on which floor to look for elements to extract forces. The beams, columns, and outrigger at the specified floor is added to the list later used to extract forces in the analysis object.
- *findAllBeamsColumns()*. Find all the members used for force extraction later in the analysis object, this is the same as previously explained in the analysis object.

Furthermore, the system provides a couple of extra functionalities: force extraction, member checks, wind and acceleration calculations. First, force extraction is an added functionality that displays all the necessary forces. This depends on the chosen members, either all or just the relevant forces. This is done with *forceDisplayer()*.

Second, the implementation of the member checks. This implementation consists first of a variety of system check functions. All functions use the glulam parameters provided in the function *ParametersGlulam()*, except the wall (CLT) check:

- *BendingCheck()*. This function does a variety of bending checks, after checking if the member is a column or a beam.

-
- *BucklingCheck()*. This function performs a buckling control for both the outriggers (if present) and the columns
 - *CheckWalls()*. This function performs the necessary CLT checks.
 - *ShearCheck()*. This performs an ordinary shear member check for the columns and beams.

The system check function loops through all members provided in the analysis object and controls those members according to the member type. The function returns the highest utilization and the respective utilization type, one for each member.

A function for wind calculations is provided with *WindFunction()*. An example of how to calculate the wind force is provided in Appendix E

A function for acceleration calculations is provided with *AccelFunction()*. This function also uses the *findingBestExponent()*-function to get an estimate of the exponent used in the approximation in the acceleration calculations. An example of how to calculate the acceleration is provided in Appendix F

An UML diagram of the different classes is shown in Figure 28.

DIAGRAM OF ALL THE CLASSES

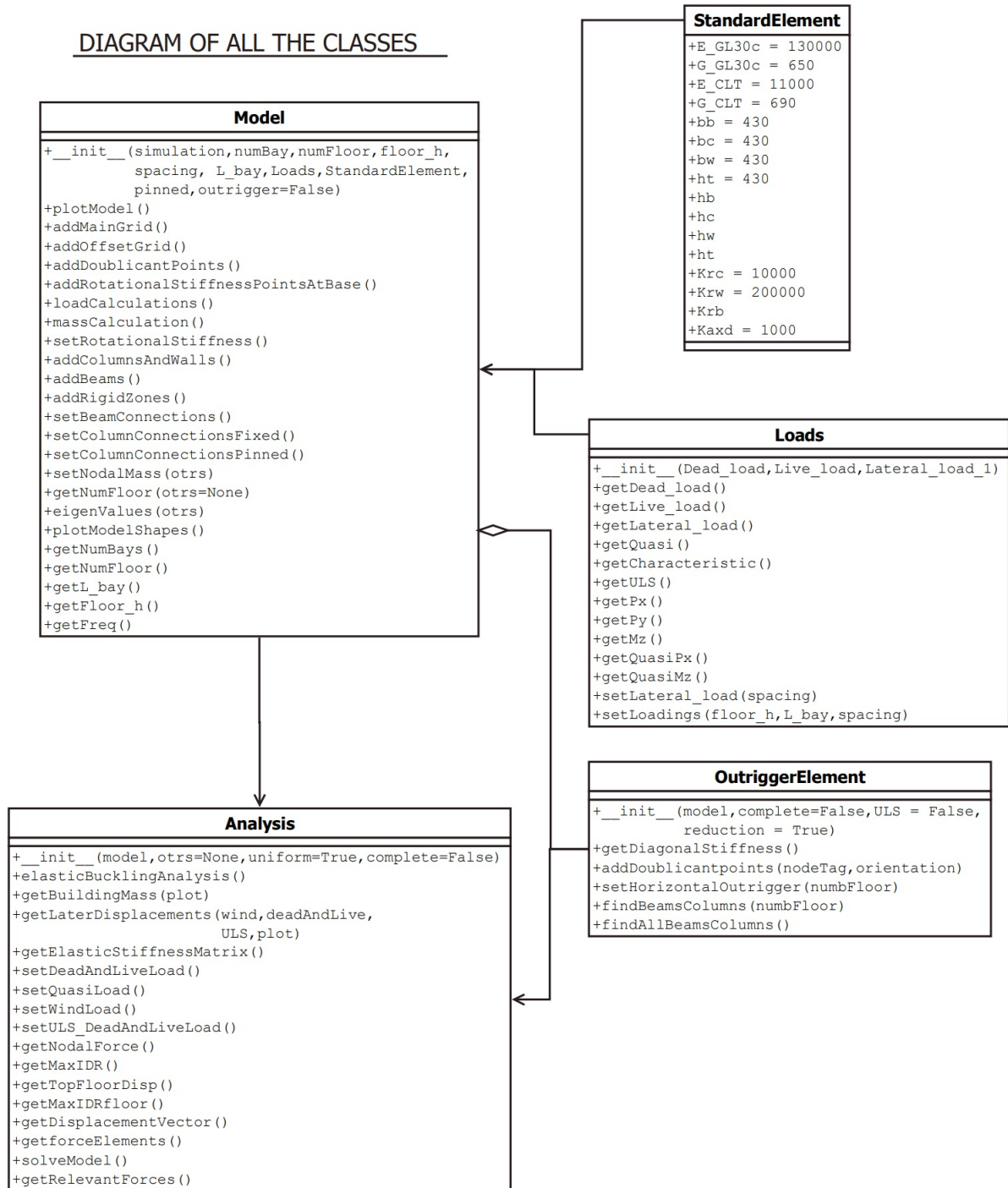


Figure 28: UML diagram

4.5 System initialization

In this section the outline of how to construct a simple model using our created finite element tool is being elaborated. The process described is the same process shown in the flow diagram 29.

The system starts by initializing all structural properties. First, it requires the values for number of bays, number of floors, floor height, length spacing, and bay length. Second, the material properties. These are material properties for glulam and CLT. Third, the model sets the rotational stiffness of the beams and the axial stiffness of the outrigger system. Lastly, the model needs information on whether there are outriggers present or not. In addition information about the location.

The system creates the model structural environment. First, it adds the nodes. These are nodes for the base system, as well as nodes for adding connection and rotational stiffness between walls and beams. Second, it adds all the structural elements; walls, columns, and beams. Third, rigid zones are created between the beams and columns. The rigid zones account for the thickness of the columns and walls. Fourth, the rotational stiffness is set in the beams, columns, and walls.

Whether the model will have an outrigger is already specified in the initialized values. The system places the outrigger elements at the specified location and sets a reduced area to account for the effective stiffness.

Now the model is complete, and the system precedes with the model analysis. This is the part where the system sets the model mass and extracts the model eigenvalues, eigenvectors, and the frequency.

The structural analysis starts after all the loads are initialized. The analysis can be performed with any set of loads and extracts all the element and nodal forces. This is later used in the system check. From the analysis, the system returns maximum inter-story drift and displacements.

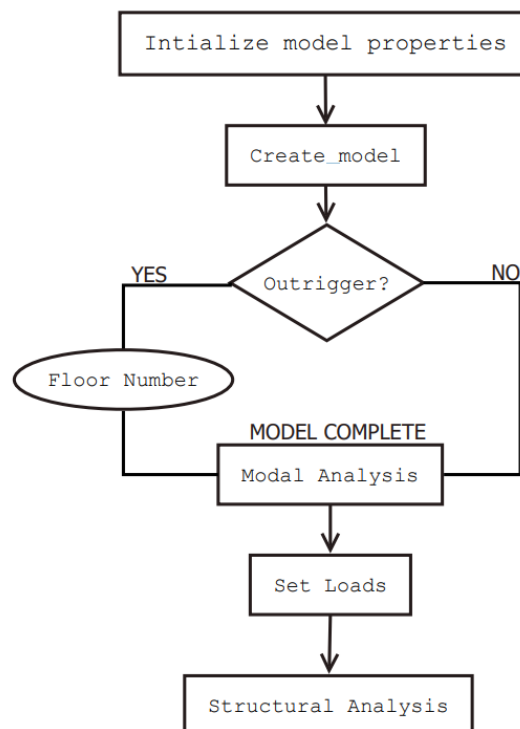


Figure 29: Model calculation

5 Results

5.1 Preliminary study

In the initial face of the parametric analysis, a preliminary study was conducted. This preliminary study should give insight into why it is necessary to increase the stiffness in tall timber structures of semi-rigid frames. With the help of PhD candidate Osama Abdelfattah Hegeir a set of reference frames was constructed. The reference frames are the starting point for further analysis. The structural system of the reference frames is the same as discussed in Section 4.3. Consisting of plane frames with external walls and internal columns. Figure 30 and Figure 31 show the structural model. All beam connections consist of 4 plane threaded rods. The connections of the beams are considered to be semi-rigid. All elements consists of double cross sections with equal width, the given widths are the total width of the cross section. The rotational stiffness given for columns and walls is the rotational stiffness at the base. Columns and walls are assumed to be continuous between floors. In total, a set of 6 reference frames was modeled, as shown in Table 5. Table 6 shows the iterations performed on the reference frames. This is to increase the data. The frames were analyzed in Python with the help of the Python package OpenSeesPy. All the reference frames with their respective variations gave a number of 291 600 analyses.

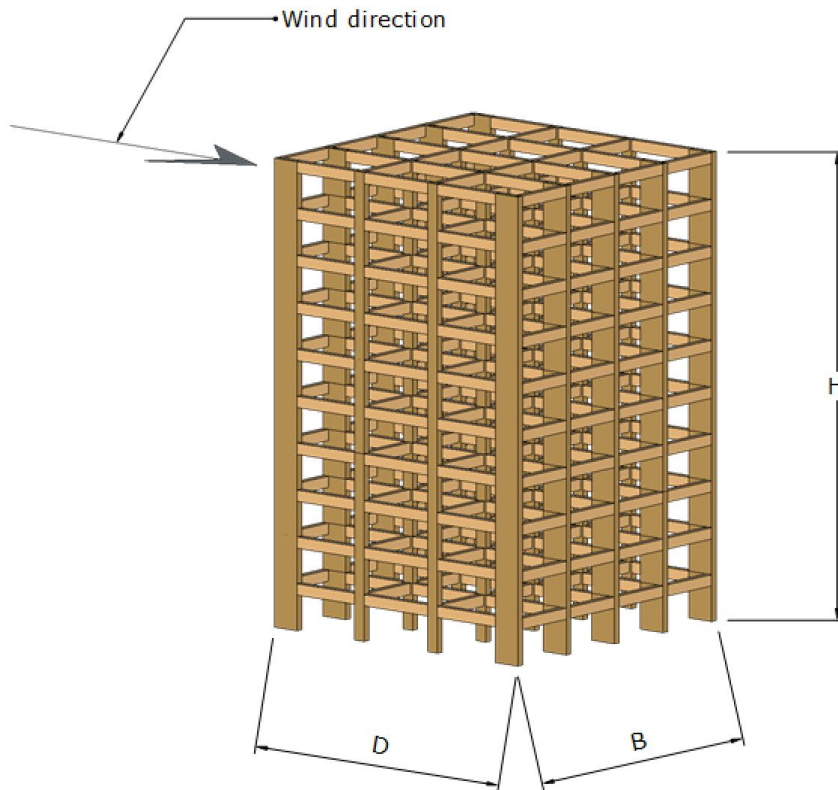


Figure 30: 3D model of preliminary frame

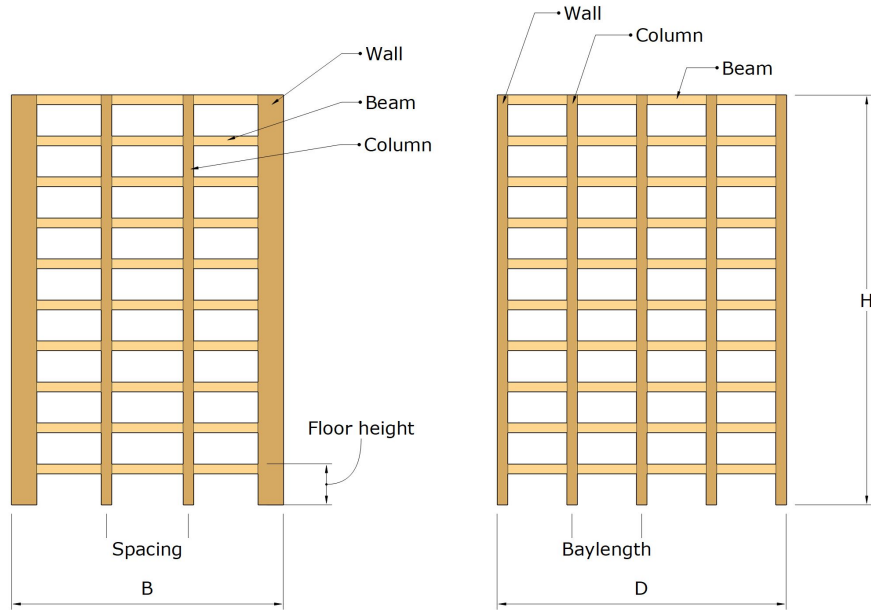


Figure 31: Front and side view of preliminary frame

Parameters	Symbol	Unit	Frames						
			8	10	12	14	16	18	
Number of floors	n	-	8	10	12	14	16	18	
Height of floors	h	mm	3500						
Number of bays	n_b	-	4						
Span between bays	L_b	mm	7000						
Number of frames	n_f	-	6						
Spacing between frames	S	mm	5000						
Beam-to-column/wall connection stiffness	K_{rb}	kNm/rad	18000	25920	35280	46080	58320	72000	
Column-to-foundation connection stiffness	K_{rc}	kNm/rad	10 000						
Wall-to-foundation connection stiffness	K_{rw}	kNm/rad	200 000						
Beam height	h_b	mm	430	540	630	720	810	900	
Beam width	w_b	mm	430						
Column height	h_c	mm ²	630		810		900		
Column width	w_c	mm	430						
Wall height	h_w	mm	3000						
Wall width	w_w	mm	430						
Dead load	g	kN/m ²	2						
Live load	q	kN/m ²	3						
Base wind speed	V_{b0}	m/s	26						
Damping ratio	ξ	-	0.019						

Table 5: Overview of parameters chosen for the tested frames.

Parameters	symbol	unit	Variations					
			$h_b - 2*90$	$h_b - 90$	h_b	$h_b + 90$	$h_b + 2*90$	
Beam height	h_b	mm	$h_b - 2*90$	$h_b - 90$	h_b	$h_b + 90$	$h_b + 2*90$	
Column height	h_c	mm	$h_c - 2*90$	$h_c - 90$	h_c	$h_c + 90$	$h_c + 2*90$	
Wall height	h_w	mm	$h_w - 1440$	$h_w - 990$	$h_w - 450$	h_w	$h_w + 450$	$h_w + 990$
Number of frames	n_f	-	$n_f - 1$			n_f	$n_f + 1$	
Number of Bays	n_b	-	$n_b - 1$			n_b	$n_b + 1$	
Bay length	L_b	mm	$L_b - 1000$			L_b	$L_b + 1000$	
Spacing	S	mm	$s - 1000$			s	$s + 1000$	

Table 6: Variation of frames.

5.1.1 Serviceability limit state

Top floor displacement

Big lateral displacements can affect the functionality of the building and destroy non structural elements as discussed in the theory 2.3.2. The acceptable top floor displacement differ from project to project. For an explanation of the criteria, see Section 3.1.1

- $\delta_{top} = H/300$
- $\delta_{top} = H/500$

The results of the analysis are presented in Figure 32. The x-axis shows the number of floors in the respective building. On the y-axis, the total building height divided by the top floor displacement is presented. The dashed black line represents the strict criterion, and the dashed red line represents the milder displacement criterion. All analyses below their respective criteria line fail the SLS for top floor displacement for this criteria.

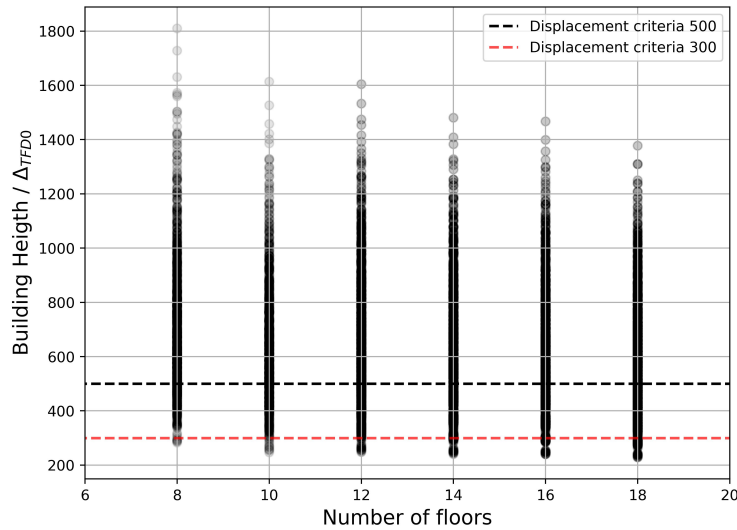


Figure 32: Top floor displacement

The results from the analysis is:

- 28.2 % of the frames fails the 500-criterion
- 2.7 % of the frames fails the 300 criterion.

The analysis shows that approximately every fourth of the reference frames, fails the strictest displacement criterion. And that practically all frames pass the mildest criterion. It is expected that the taller frames fail more frequently than the shorter ones, this can not instantaneously be concluded from this analysis. This is most likely due to the fact that when the number of floors increase, the structural dimensions of the element do as well. Increased cross sections provides the structural system with increased stiffness, thus increasing resistance against lateral loads.

IDR

Interstory drift, the relative displacement between floors, can possibly affect non structural elements in a building. When IDR becomes to large it can cause damage to windows, doors, facade as well as other non-structural elements. Due to this it is important to investigate the IDR. The same criteria as for top floor displacement was used when analyzing maximal interstory drift. h refers to the floor height.

- $\delta_{IDR} = h/500$
- $\delta_{IDR} = h/300$

The results from the analysis is presented in Figure 33. The structure of the plot is the same as for top floor displacement. However, the y-axis is now story height divided by IDR between consecutive floors.

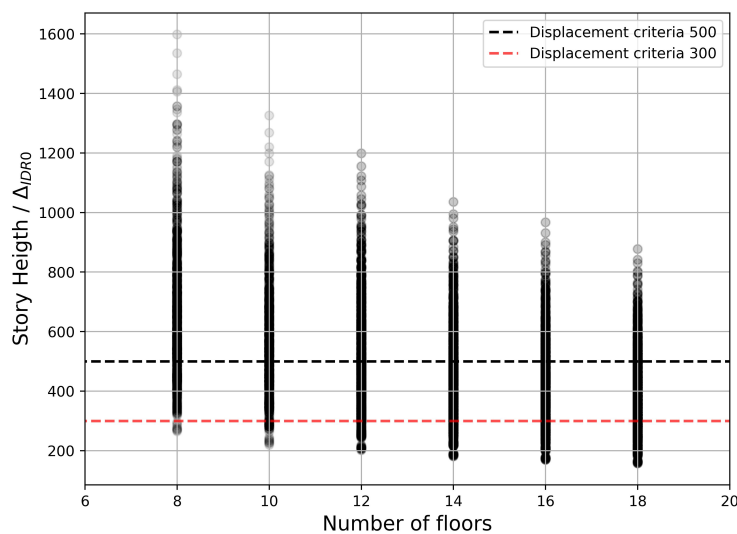


Figure 33: Interstory drift

The results from the analysis is:

- 58.02 % fails the 500-criterion
- 12.8 % fails the 300-criterion

Over half the frames fail the strictest criterion. This is significantly more than for top floor displacement. 1 out of 10 frames now fail the mildest criterion. This is an increase compared to the top floor displacement. Thus, indicating that the SLS criteria linked to IDR can be harder to meet.

Acceleration

Wind-induced accelerations are expected to cause the biggest concern out of the three SLS criteria. It is known to be a common problem in tall timber buildings. The reference frames were analyzed with respect to the ISO 10137 acceleration criterion [1]. Figure 34 shows the results of the analysis.

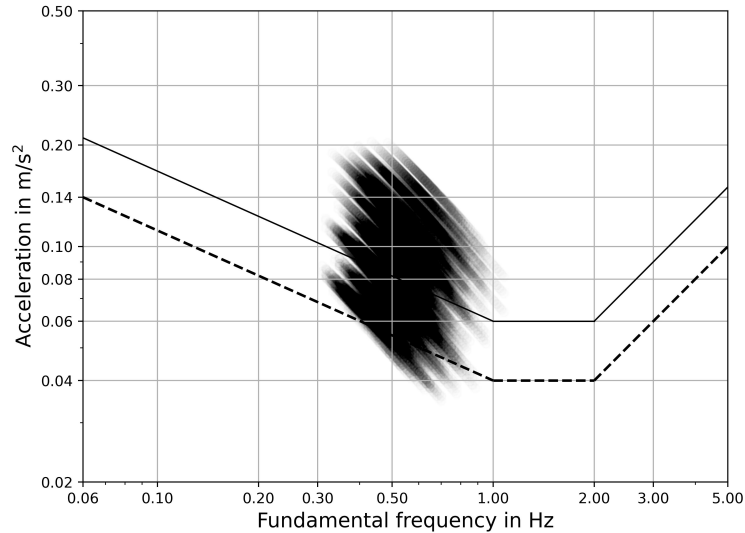


Figure 34: Acceleration and frequency of preliminary frames plotted in ISO 10137 [1]

As one can see from the plot the majority of the frames exceed both the criteria for office- and residential buildings. The upper line is the office criterion, and the lower line is the residential criterion, as shown in Figure 8 in Section 3.1.2. The statistics from the analysis is as follows:

- 4.4% of the frames are within the demands of residential criteria
- 37.3% of the frames are within the demands of office criteria but not residential
- 58.3% exceeds both criterion

The study shows that acceleration is likely to be governing for the design. Not even 1/20 of the tested frames met the residential criterion, and only 37.3 % meet the office criterion. This is an indicator that wind-induced acceleration is expected to cause concern in design of tall timber buildings. This analysis will create the basis for this thesis. Since acceleration criteria seem to be the most critical, the main focus will be on acceleration in further analysis.

5.1.2 Ultimate limit state

For completeness of the preliminary study, the ultimate limit state of the basis frames was analyzed. It is important to prove that ULS will not cause any concerns when designing frames according to the SLS criteria. Since there are a large number of possible checks, the full ULS-procedure is shown in Appendix D. The ultimate limit state load combination given in Section 4.1.1 and Equation (9) has been used in this analysis.

Check of members

The frames consists of glulam- columns, beams and truss element. The walls are made of CLT. The load bearing capacity of each element needs to be considered to evaluate the structural safety. This is done according to Eurocode (NS-EN 1995-1-1) [23] and the CLT handbook [17].

Columns

The glulam columns are mainly subjected to axial loading from the dead and live load. In addition to the lateral loading in terms of bending and shear, columns near the foundation can be subjected to substantial axial forces. It is expected that stability and stresses from axial loading will be governing.

Beams

Beams are loaded laterally from the dead and live load, this causes bending moments in the beam. The lateral loading from wind causes axial forces in the beams. The beams act as diaphragms, which transfer lateral loading to the vertical elements, thus inducing axial stresses. The beams are considered to be braced against lateral torsional buckling. The main checks for beams are assumed to be bending, bending in combination with axial forces, and shear.

Walls

The walls are located in the outermost parts of the timber framing. They transfer much of the shear forces from the wind load. It is assumed that the load bearing capacity of the crossection is substantial in both shear, axial loading and bending about strong axis. The likelihood of stability failure about the strong axis is neglectable. Thus, stability about the weak axis is the most interesting check among the ones presented in Appendix D.

Results

Figure 35 shows the results for the reference frames. The dashed line represents an utilization of 100%. This figure is divided in to each respective element. The results shows that the elements are mostly clustered below the utilization limit. It is, however, notable that some analysis for 8 floors fail in beam elements. Another take away is that for 18 floors the columns start to fail. A more detailed version of Figure 35 is shown in Figure 36. Out of all the 72 900 analysis only 8.7% exceeds the ULS limitations. This is an indicator that the chosen basis frames does not have any issues with ULS.

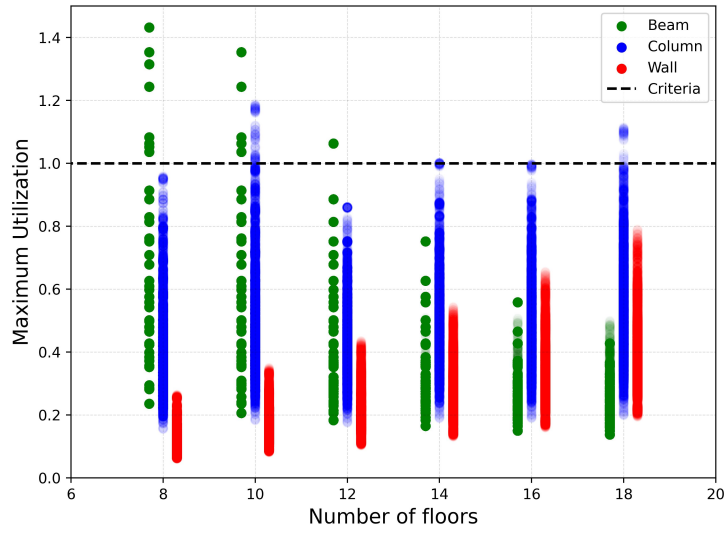


Figure 35: Ultimate limit state analysis for all preliminary frames

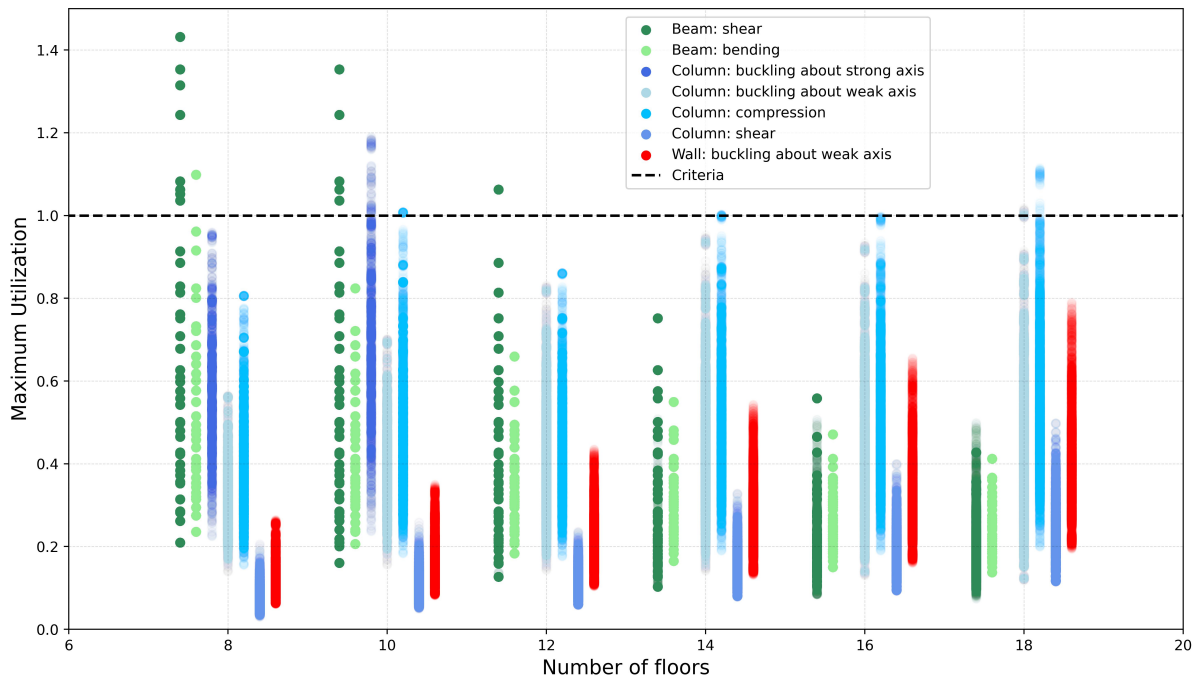


Figure 36: Detailed version of Figure 35

5.2 Outrigger system

First, a single outrigger system was studied. The reference frame will be analysed in terms of SLS requirements using the characteristic load combination in Section 4.1.1. The optimizing of outrigger placement and performance is in this paper measured mainly by the ISO 10137 criterion [1], top floor displacements and maximum interstory drift. First, the optimal location will be investigated. Second, the optimal cross laminated timber core structure. Third, the optimal outrigger shape. Fourth, the influence of the outrigger stiffness. Fifth, the variable influence. Sixth, a double outrigger system is explored. Seventh, the ultimate limit state of a single outrigger. Eighth and last, the performance of the outrigger will be presented. The parameters for the reference frame are listed in Table 7.

Parameters	symbol	Unit	Value
Number of floors	n	-	10
Number of bays	n_b	-	3
Number of frames	n_f	-	6
Bay length	l_b	mm	7000
Floor height	h	mm	3500
Spacing	S	mm	5000
Column height	h_c	mm	630
Beam height	h_b	mm	540
Wall height	h_w	mm	3000
Truss height	h_t	mm	300
Column width	w_c	mm	430
Beam width	w_b	mm	430
Wall width	w_w	mm	430
Truss width	w_t	mm	430
Rotational stiffness beams	K_{rb}	kNm/rad	26 000
Rotational stiffness columns	K_{rc}	kNm/rad	10 000
Rotational stiffness walls	K_{rw}	kNm/rad	200 000
Base wind	V_{b0}	m/s	26
Wind load	q_w	kN/m	1.00
Dead load	g	kN/m^2	2
Live load	q_s	kN/m^2	3

Table 7: 10 floor reference frame

5.2.1 Optimizing location for a single outrigger system

The placement of the outrigger (OR) system is important in terms of the distribution of forces and the stiffening of the structure. According to Ali Lame and his study, the optimal placement of an outrigger is around half of the total height of the building [7]. Ali lame studied optimal placement in terms of reduction of lateral displacement. Wind-induced accelerations and maximum interstory drift correlate with lateral displacement. The main focus when studying the optimal placement will be acceleration, maximum IDR and top floor displacement (TFD).

For this study an outrigger system with chevron bracing was used, as shown in Figure 25. In the reference frame the single outrigger can be placed in a total of 10 different floors, the first floor is excluded from the study. Firstly, the performance in terms of ISO-criterion is measured. Figure 37 shows all possible placements in addition to the structure without the outrigger. Thus, yielding ten data points.

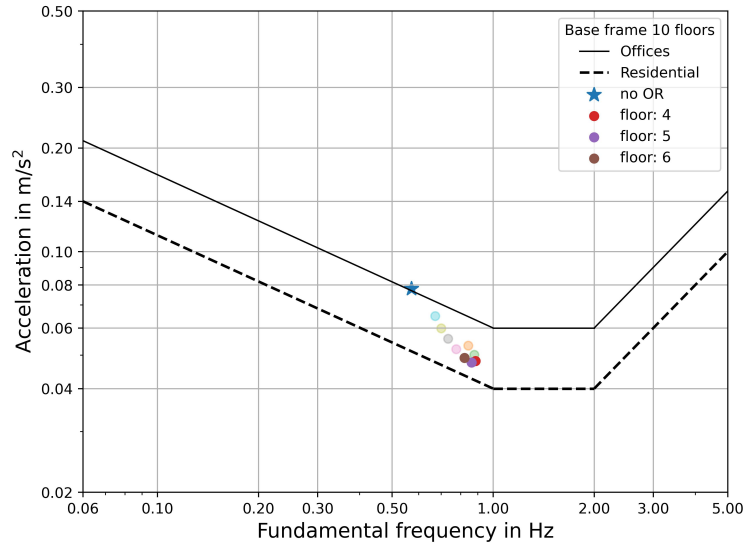


Figure 37: Accelerations for different placements of a single outrigger

Floor	Acceleration	Max IDR	Top floor displacement
Unit	m/s^2	mm	mm
No OR	0.078	6.22	54.338
2	0.0533	3.0	24.95
3	0.0502	2.71	23.14
4	0.0481	3.2	22.73
5	0.0477	3.69	23.49
6	0.0491	4.13	25.21
7	0.0521	4.51	27.61
8	0.0558	4.82	30.41
9	0.0599	5.06	33.26
10	0.065	5.25	35.99

Table 8: Outrigger placement - SLS values

Floor	Acceleration reduction	IDR Reduction	Top floor displacement reduction
2	31.64%	51.77%	54.13%
3	35.72%	56.43%	57.45%
4	38.36%	48.55%	58.21%
5	38.9%	40.68%	56.81%
6	37.03%	33.6%	53.65%
7	33.27%	27.49%	49.23%
8	28.45%	22.51%	44.09%
9	23.24%	18.65%	38.86%
10	16.6%4	15.59%	33.83%

Table 9: Outrigger placement - reduction

From Table 9 - in terms of acceleration reduction, the fifth floor is the optimal choice. If lateral displacement is governing, the preferred choice would be the fourth floor. Lastly, by taking the maximum IDR into consideration, it is clear that placing the outrigger on the third floor would be optimal. From the analysis, it is apparent that all maximum IDR occurred between the ground floor and the first floor. In other words, the conclusion is not unanimous. In the next chapter, the shape will be analyzed based on an assumption that acceleration criterion is governing, hence placing the outrigger in floor number five. This is also in line with the theory discussed in Section 3.3.2, where the optimal location is set to be on the middle floor of the structure.

5.2.2 Choice of CLT core structure

An outrigger system needs a core structure, as explained in Section 3.3. In this thesis, the core structure is modeled as CLT walls. This section will focus on the difference between placing the CLT-walls in the outermost part or internally in the building, and how it affects the SLS-criteria in terms of acceleration. If the walls are placed internally, then the system places columns in the exterior parts of the building. Likewise, the placement can be done opposite, with the walls in the external parts. Figure 38 shows the two different systems for the reference frame.

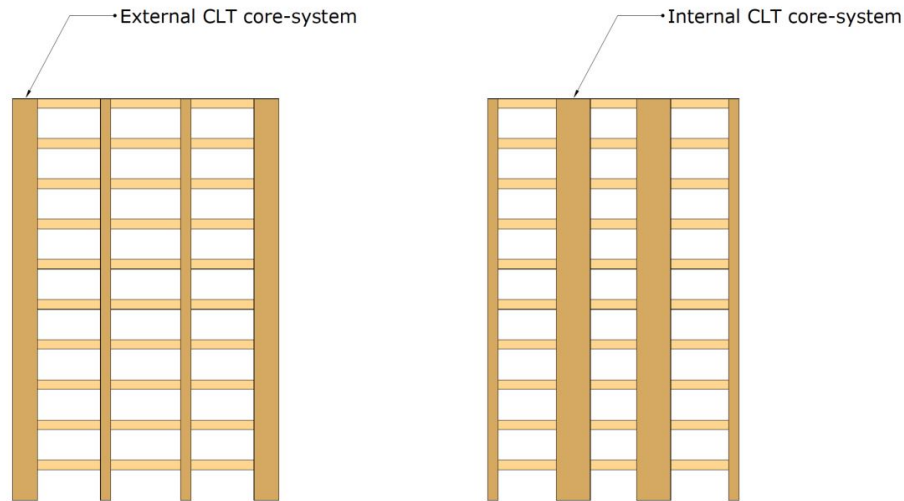


Figure 38: Different core systems

Figure 39 shows the difference in performance between the external and internal placement of CLT walls. The performance of the system with an external core (shown in purple) is clearly better than that of the system with an internal core (shown in red). With an external core, the system is much better at absorbing the external force exerted on the structure due to the lever arm created by the distance between the two cores. The lever arm for the internal core is much smaller and, therefore, performs worse than the external core system.

However, one thing to consider is how the system is created. An internal core may be easier to adapt to a structure and, therefore, might be the best option for an architect. This is not something that is considered in this thesis. Thus, the system with the external core is considered the best system and will be used in the consecutive parts.

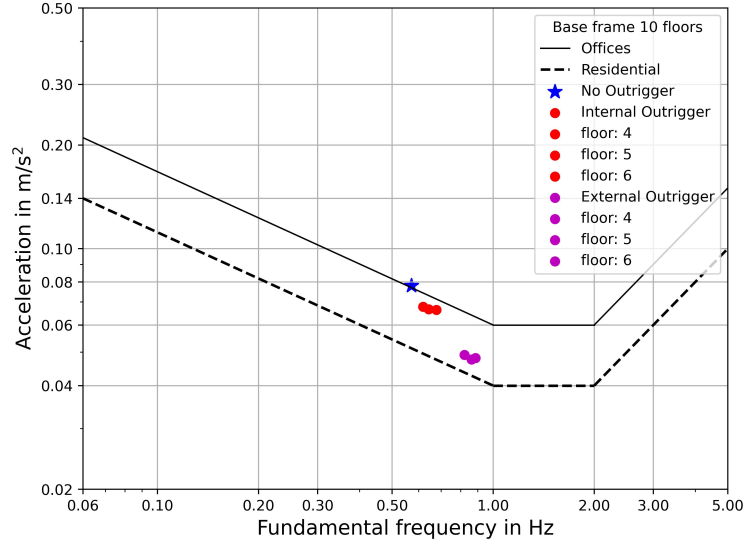


Figure 39: Performance of external and internal vertical outrigger

5.2.3 Evaluation of shape

In this section the shape of the outrigger will be investigated. The systems will be evaluated in terms of SLS requirements such as top floor displacement, maximum interstorey drift and acceleration. The systems are based on the reference frame, with the outrigger placed on the fifth floor and with an external CLT core, based on the findings from the previous sections. Three different variations of shapes have been evaluated. These are already described in Section 4.3.3 and shown in Figure 24 and Figure 25. Each system will be compared to the system without an outrigger, shown in Figure 23. The results are presented in Table 10.

No Outrigger				
Parameter	symbol	Unit	Value	reduction
Acceleration	a	m/s^2	0.0772	-
Max IDR	δ_{IDR}	mm	6.12	-
Top floor displacement	δ_{top}	mm	53.343	-
Chevron				
Acceleration	a	m/s^2	0.0473	37.5 %
Max IDR	δ_{IDR}	mm	3.65	39.0 %
Top floor displacement	δ_{top}	mm	23.162	54.5 %
Diagonal				
Acceleration	a	m/s^2	0.05066	34.4 %
Max IDR	δ_{IDR}	mm	3.98	35.0 %
Top floor displacement	δ_{top}	mm	27.301	48.8 %
Mirrored diagonal				
Acceleration	a	m/s^2	0.0507	34.3 %
Max IDR	δ_{IDR}	mm	3.89	36.4 %
Top floor displacement	δ_{top}	mm	26.192	50.9 %

Table 10: Results from testing different bracing systems

The findings are quite clear. The chevron bracing system is more efficient than the diagonal-based bracing systems. It outperforms the other systems in terms of acceleration, top floor displacement, and interstorey drift. It is important to note that all maximum IDR for the frames occur between

ground level and the 1st floor, while the maximum IDR occurs between floor 1 and 2 for all the reference frames with no outrigger.

Figure 40 shows all three systems with their lateral displacement. The systems move in unison from the base to the start of the outrigger floor. However, after the floor with the outrigger, all three systems have different output angles. This results in the lowest total displacement for the chevron bracing system.

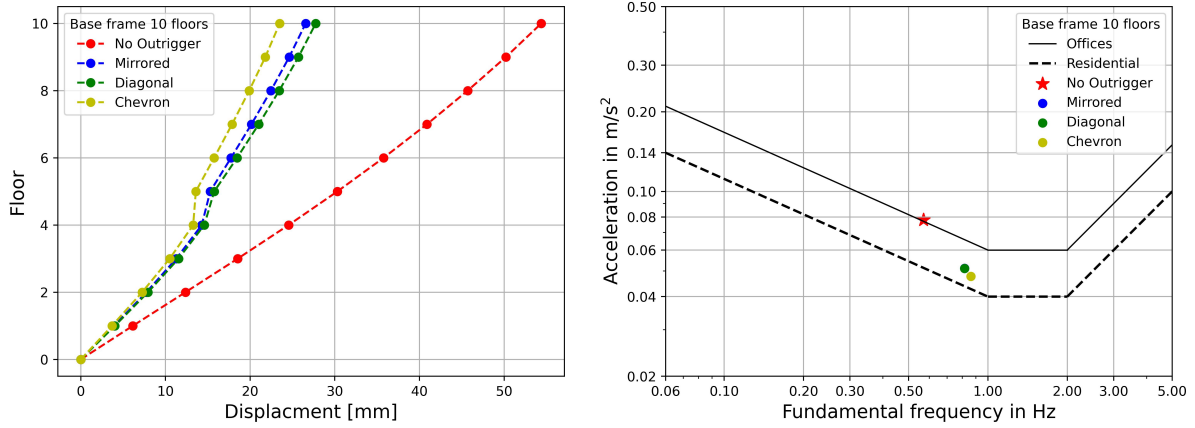


Figure 40: Displacement and acceleration of a single outrigger

5.2.4 Influence of outrigger stiffness

In this section the influence of the effective axial stiffness, addressed in Section 4.3.4 of the outrigger system, will be tested. The influence of axial stiffness is tested using the optimal outrigger parameters found in previous sections.

In Figure 41 the influence of an increase in axial stiffness is presented in the outrigger. The figure shows how small amounts of axial stiffness will improve the system by a great amount when the axial stiffness is low. However, the performance decreases rapidly with increasing axial stiffness. This is true for all reference frames. This is also shown in Table 11. The influence of the outrigger stiffness is quickly stabilizing, and additional increments of the stiffness will not reduce the acceleration nor the top floor displacement significantly. The six reference frames tested are listed in Appendix B.

K_x [kN/mm]	D. K_x [%]	Area [mm^2]	TFD [mm]	D.TFD [%]	ACC [m/s^2]	D.ACC [%]
0.0	0	0	38.62	0	0.06633	0
11.29	inf	3000	29.21	-24.35	0.05663	-14.62
33.88	200.0	9000	21.78	-25.46	0.04776	-15.67
67.76	100.0	18000	17.58	-19.26	0.04207	-11.9
101.64	50.0	27000	15.66	-10.9*	0.03926	-6.69
203.28	100.0	54000	13.35	-14.79	0.03563	-9.25
304.92	50.0	81000	12.46	-6.64	0.03416	-4.12
406.57	33.33	108000	11.99	-3.76	0.03336	-2.33
508.21	25.0	135000	11.7	-2.43	0.03286	-1.5
609.85	20.0	162000	11.5	-1.69	0.03252	-1.05
711.49	16.67	189000	11.36	-1.24	0.03227	-0.77

Table 11: The influence of outrigger stiffness, NB* note the increment

Figure 41 might also give some insight into how the chevron bracing system had the best performance earlier. The three different shapes discussed in Section 5.2.3 have very different effective axial stiffness. Using Equation (18) from Section 4.3.4 and comparing the three systems in Table 12 it is clear that the chevron bracing system is stiffer with the same sized cross section. This is due to the different lengths of the trusses. Both the diagonal and the mirrored diagonal bracings have longer members.

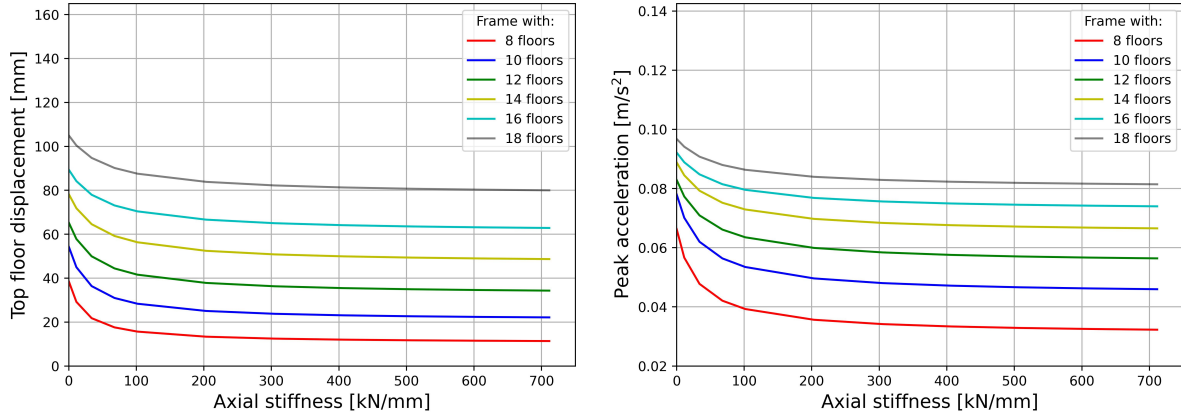


Figure 41: Performance of the chevron outrigger system with different axial stiffness

Bracing System	Unit	Value	Member Size [b x h]
Chevron	kN/mm	338	$430 \times 300 \text{ mm}^2$
Diagonal	kN/mm	192	$430 \times 300 \text{ mm}^2$
Mirrored Diagonal	kN/mm	192	$430 \times 300 \text{ mm}^2$

Table 12: Axial stiffness of different bracing systems

The increased axial stiffness of the different bracing systems was then tested. Both Figure 42 and 43 show the increased performance of the Mirrored Diagonal and the Diagonal bracing respectively, with increasing effective axial stiffness. The increased effective axial stiffness is created by varying the height of the member, along with the reduction of the axial stiffness from the connections. Thus, yielding the effective axial stiffness shown in the figures.

It is clear from both figures that the three systems can perform equally well, with enough axial stiffness in the members. Hence, from this discovery the bracing systems will from now on be referred to as an effective axial stiffness, rather than the actual bracing system.

The effective axial stiffness is set to $K_x = 338 \text{ [kN/mm]}$.

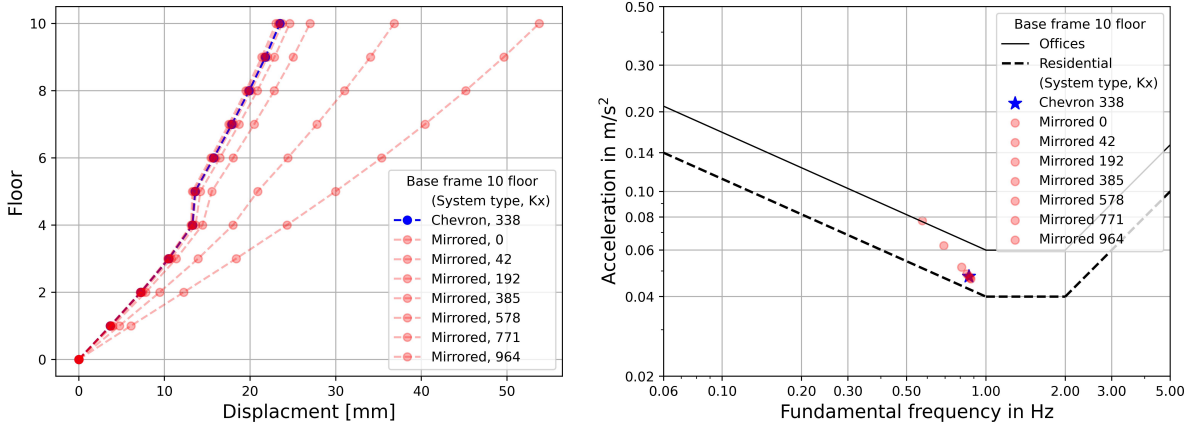


Figure 42: Result of increased stiffness in mirrored diagonal bracing system

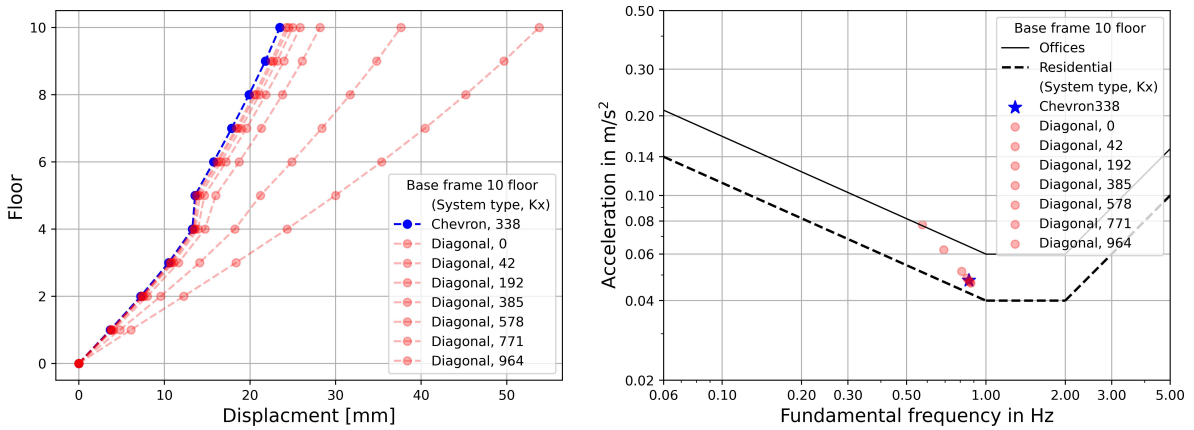


Figure 43: Result of increased stiffness in diagonal bracing system

5.2.5 Variable influence

In this section, the influence of different structural variables was tested. The results are based on the ten story reference frame, with varying geometrical properties shown in Table 13. The following figures shows the relationship between varying the beam height, bay length and number of bays. Tested variables are held at the base value when testing for the other test variables. While the varying variables are always iterated through. For example when testing the beam height the bay length and number of bays are held at their base values L_b and n_b . While the column and wall heights, as well as the truss effective stiffness is varied according to the table.

<i>Tested variables</i>					
Parameters	symbol	unit	Variations		
Beam height	h_b	mm	$h_b - 90$	h_b	$h_b + 90$
Bay length	L_b	mm	$L_b - 1000$	L_b	$L_b + 1000$
Number of Bays	n_b	-	$n_b - 1$	n_b	$n_b + 1$

<i>Varying variables</i>					
Parameters	symbol	unit	Variations		
Column height	h_c	mm	$h_c - 90$	h_c	$h_c + 90$
Wall height	h_w	mm	$h_w - 990$	h_w	$h_w + 990$
Effective truss stiffness	k_x	kN/mm	237	338	440

Table 13: Variation of reference frames with outrigger.

Figure 44 shows the influence of changes in the number of bays. The number of bays varied with an increase and decrease in one bay. On the left side of the figure, accelerations are paired with its frequency and plotted into the ISO 10137 [1] curve. Displaying three distinct clustering groups. On the right side of the figure the top floor displacement is paired with the frequency. The figure shows three distinct groups, each of which has its own trend line. On each line, there are three more clusterings, one for each wall height. The walls are varied with an increasing and decreasing 990 mm in height.

The acceleration indicates a linear increase in performance for an increasing number of bays. The trend lines for top floor displacement show a big difference going from two to three bays, and a small increase going from three to four bays. It is unclear how the trend will continue for even further increments in the number of bays. It is possible that it will continue to decrease with increased performance.

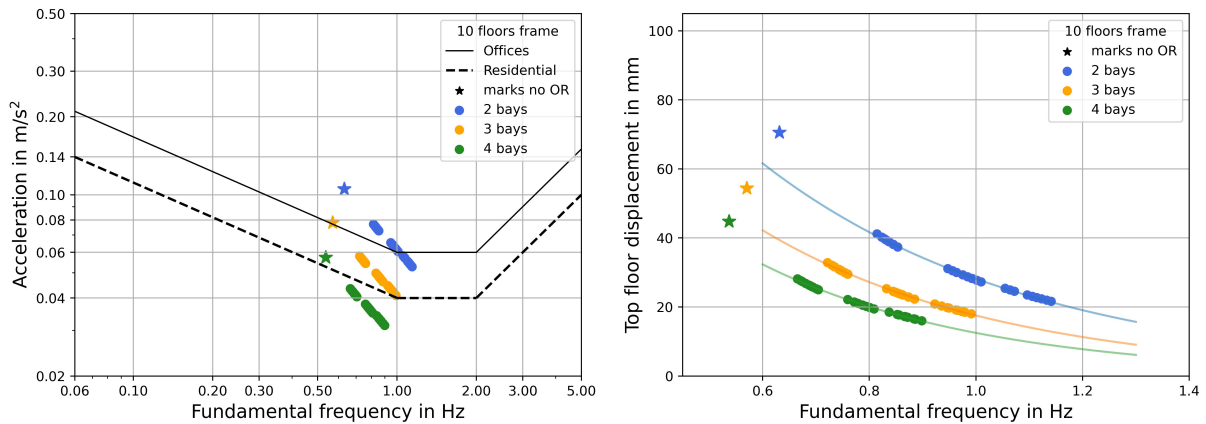


Figure 44: Influence of different number of bays

Figure 45 shows the influence of changes in the bay length. The bays are varied with an increase and decrease length of one meter. On the left side of the figure accelerations are paired with its frequency and plotted into the ISO 10137 curve. Displaying three distinct clustering groups. On the right side of the figure, the top floor displacement is paired with the frequency. The figure shows three distinct groups, each having its own trend line. On each line there are three new clusterings, one for each wall height. The walls are varied with an increasing and decreasing 990 mm in height. The trend lines show that varying the bay length gives a linear shift in performance. Decreasing the top floor displacement by approximately five millimeters for each one-meter increase in bay length. It is unclear if this trend will continue, for more than bay lengths of six, seven and eight meters.

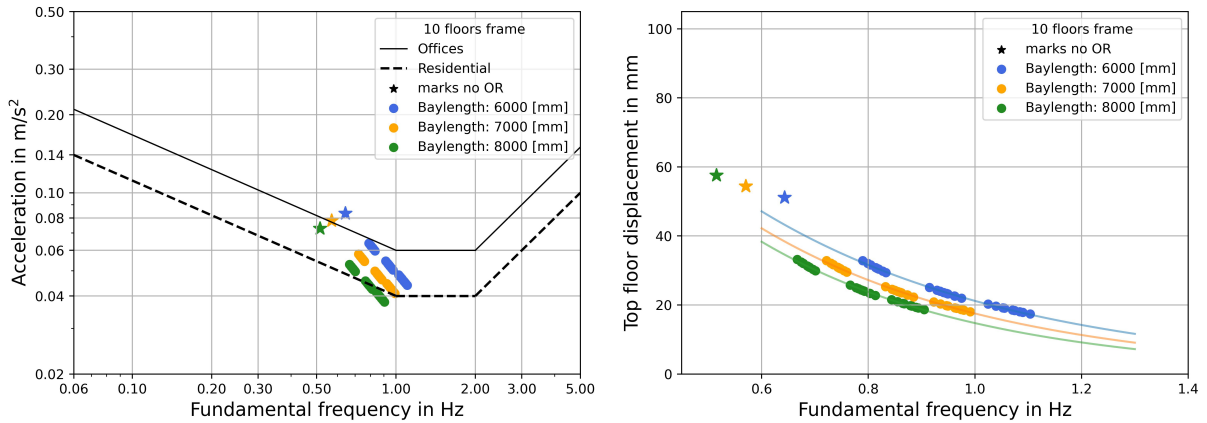


Figure 45: Influence of different bay length

For both Figure 44 and Figure 45 it is clear that varying the column- and truss height will increase the stiffness of the structure. Indicated by the increased fundamental frequency and the trend lines in both figures. The gap between column heights and truss heights are not resulting in very distinct clustering as seen with the increased wall height. The reason the column height increment is not as effective as the wall increment is because of the original wall and column size. The walls have great sizes and will therefore influence the stiffness much more than what the columns are capable of. For the increased truss height it is already shown in Section 5.2.4, that this has a decreased effect on the system stiffness.

Figure 46 shows the influence of a change in the beam height. In this figure the wall height is held constant to three meters. The beams are varied with an increased and decreased size of two lamellas of 45 mm. This will influence the rational stiffness of the beam-to-column/wall connections as these are defined by the beam height seen in Section 4.3 and Equation (17). On the left side of the figure accelerations are paired with its frequency and plotted into the ISO 10137 curve. On the right side of the figure, the top floor displacement is paired with the frequency. The plot shows three groups with similar trend lines. Both plots in the figure shows decreasing trend in acceleration and top floor displacement. The trend is concave increasing in the structural stiffness, shown with the increasing frequency.

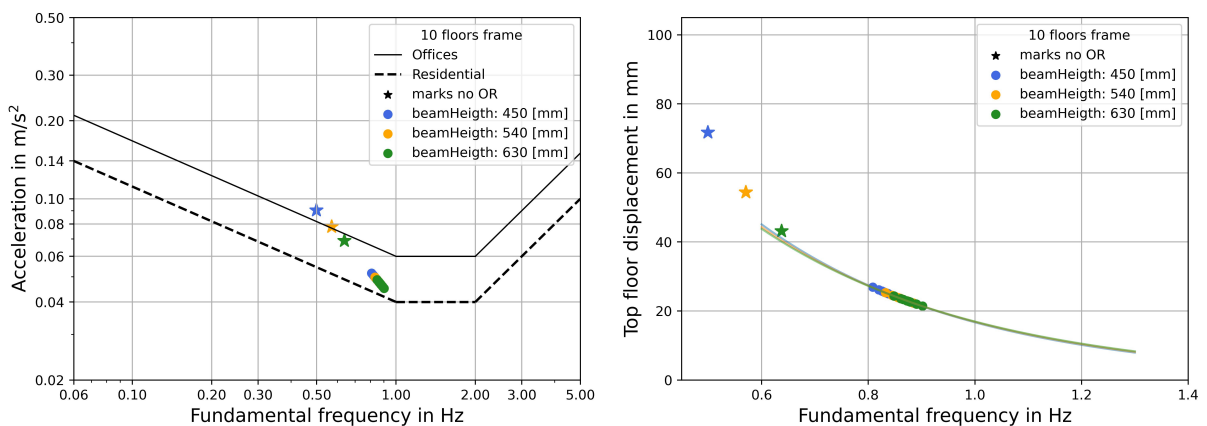


Figure 46: Influence of different beam height

5.2.6 Double outriggers

The optimal outrigger has been tested for all reference frames and is shown in Figure 47. The single outriggers shown in Figure 47 yields a 15% reduction in acceleration for the 18 floor frame, and 18% reduction in acceleration for the 16 floor frame. The reduction is present, but not as significant as for shorter frames. Hence, in this section, the reference frames are going to be tested with double outriggers. The double outrigger systems will only be tested on the reference frames with 12 floors or more. This is because the performance of one outrigger is considered insufficient in terms of acceleration for these frames. The 18 floor reference frame will not be considered in this section.

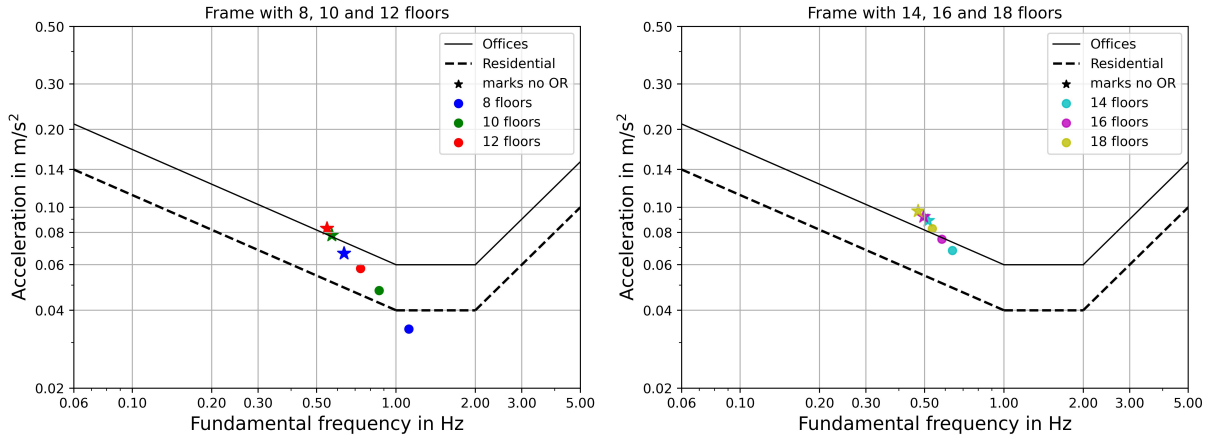


Figure 47: Performance of each reference frame with optimal single outrigger

Optimal location of two outriggers

First, the optimal location for the two outriggers was tested. Four different locations for the two outriggers are tested, and illustrated in Figure 48 and Figure 49 with a 12 floor frame:

- System 1: placing both outriggers in the center of the structure
- System 2: placing each outrigger on the 1/3 and 2/3 of the structure height
- System 3: placing each outrigger on the structure edges
- System 4: placing both outriggers in the bottom of the structure

The outrigger systems were tested in comparison with the optimal single outrigger system, developed in the previous chapters, and a frame without an outrigger system. In the next three pages, the results for 12, 14 and 16 floor frames are presented. For all frames, the best system is System 2, with respect to both top floor displacement and acceleration, where the outriggers are placed in 1/3 and 2/3 of the total height. This is also in line with the theory presented in Section 3.3.2. However, the maximum interstory drift is best for System 4. This is intuitive, as the interstory drift is largest between the ground floor and the first floor, and making the structure stiffer in the bottom section will suppress this drift. Since acceleration is the governing design criteria, System 2 is chosen as the optimal two-outrigger system.

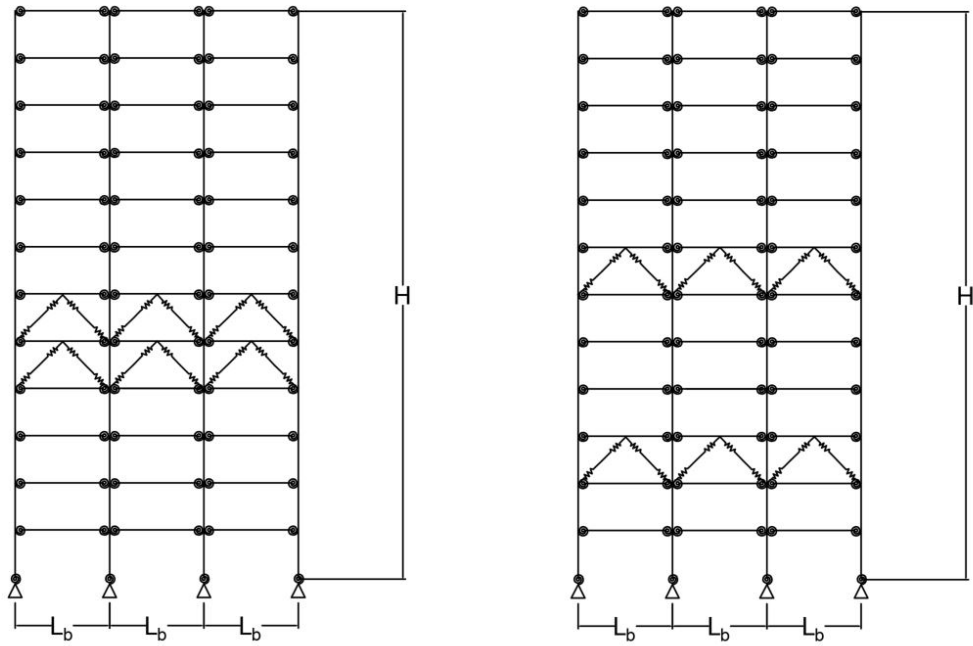


Figure 48: System 1 (left) & System 2 (right)

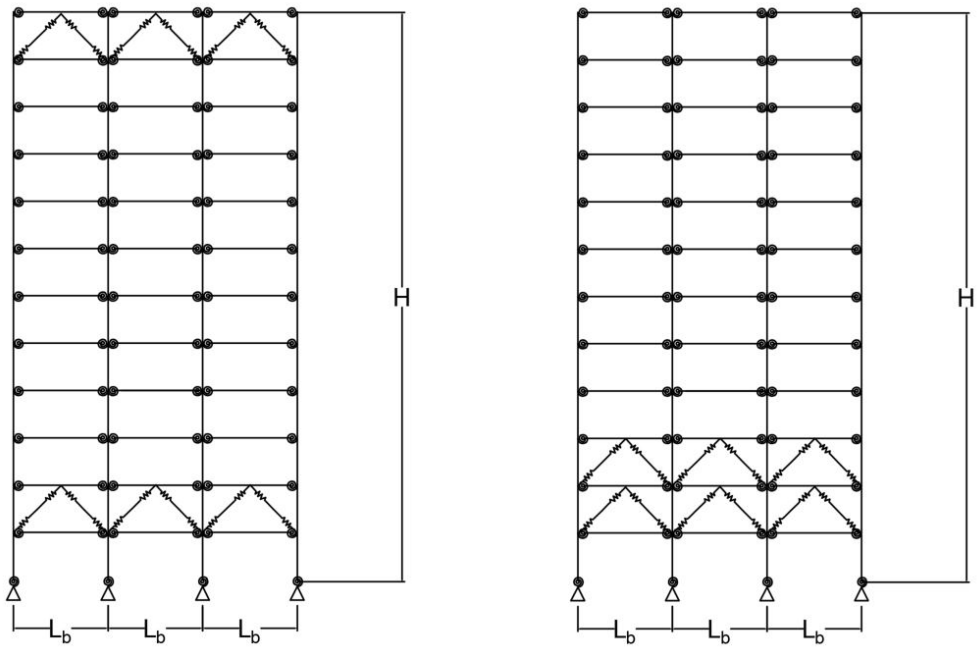


Figure 49: System 3 (left) & System 4 (right)

12 floors

No Outrigger				
Parameter	symbol	Unit	Value	reduction
Acceleration	a	m/s^2	0.0829	-
Max IDR	δ_{IDR}	mm	13.7	-
Top floor displacement	δ_{top}	mm	130.8	-
Single Optimal Outrigger				
Acceleration	a	m/s^2	0.0580	30.0 %
Max IDR	δ_{IDR}	mm	5.08	62.9 %
Top floor displacement	δ_{top}	mm	36.0	72.5 %
System 1				
Acceleration	a	m/s^2	0.0475	42.6 %
Max IDR	δ_{IDR}	mm	4.16	69.6 %
Top floor displacement	δ_{top}	mm	25.5	80.5 %
System 2				
Acceleration	a	m/s^2	0.0440	46.9 %
Max IDR	δ_{IDR}	mm	3.02	77.9 %
Top floor displacement	δ_{top}	mm	21.0	83.9 %
System 3				
Acceleration	a	m/s^2	0.0507	31.1 %
Max IDR	δ_{IDR}	mm	3.37	75.4 %
Top floor displacement	δ_{top}	mm	27.5	78.9 %
System 4				
Acceleration	a	m/s^2	0.0549	33.7 %
Max IDR	δ_{IDR}	mm	2.99	78.1 %
Top floor displacement	δ_{top}	mm	26.6	79.6 %

Table 14: Results from the double outrigger location optimization for a 12 floors frame

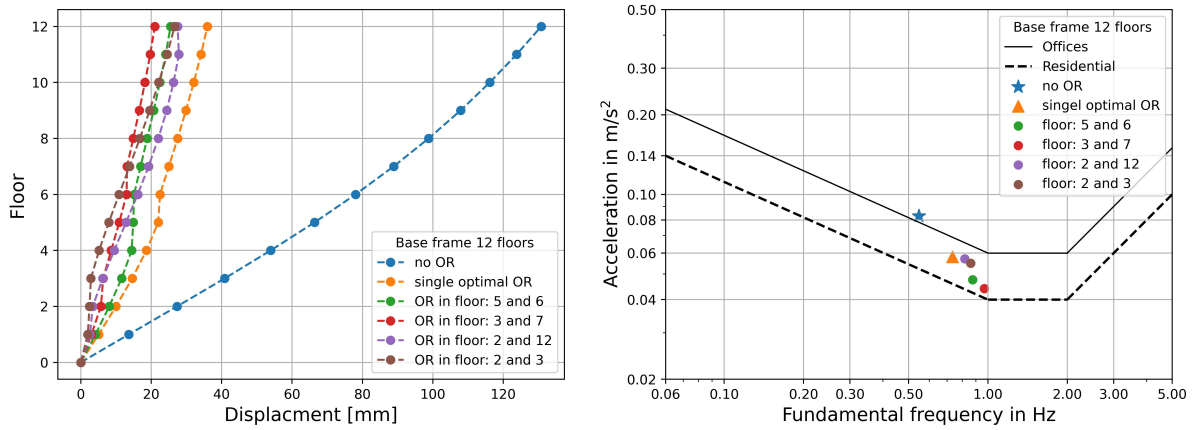


Figure 50: Different outrigger locations for the 12 floors frame

14 floors

No Outrigger				
Parameter	symbol	Unit	Value	reduction
Acceleration	a	m/s^2	0.0888	-
Max IDR	δ_{IDR}	mm	15.2	-
Top floor displacement	δ_{top}	mm	156.7	-
Single Optimal Outrigger				
Acceleration	a	m/s^2	0.0680	23.4 %
Max IDR	δ_{IDR}	mm	6.38	58.0 %
Top floor displacement	δ_{top}	mm	50.5	67.8 %
System 1				
Acceleration	a	m/s^2	0.0583	34.3 %
Max IDR	δ_{IDR}	mm	5.62	63.0 %
Top floor displacement	δ_{top}	mm	38.8	75.2 %
System 2				
Acceleration	a	m/s^2	0.0542	38.9 %
Max IDR	δ_{IDR}	mm	4.55	70.0 %
Top floor displacement	δ_{top}	mm	32.9	78.9 %
System 3				
Acceleration	a	m/s^2	0.0686	22.7 %
Max IDR	δ_{IDR}	mm	4.33	71.5 %
Top floor displacement	δ_{top}	mm	41.1	73.8 %
System 4				
Acceleration	a	m/s^2	0.0657	25.9 %
Max IDR	δ_{IDR}	mm	3.8	75.0 %
Top floor displacement	δ_{top}	mm	38.6	75.3 %

Table 15: Results from the double outrigger location optimization for a 14 floors frame

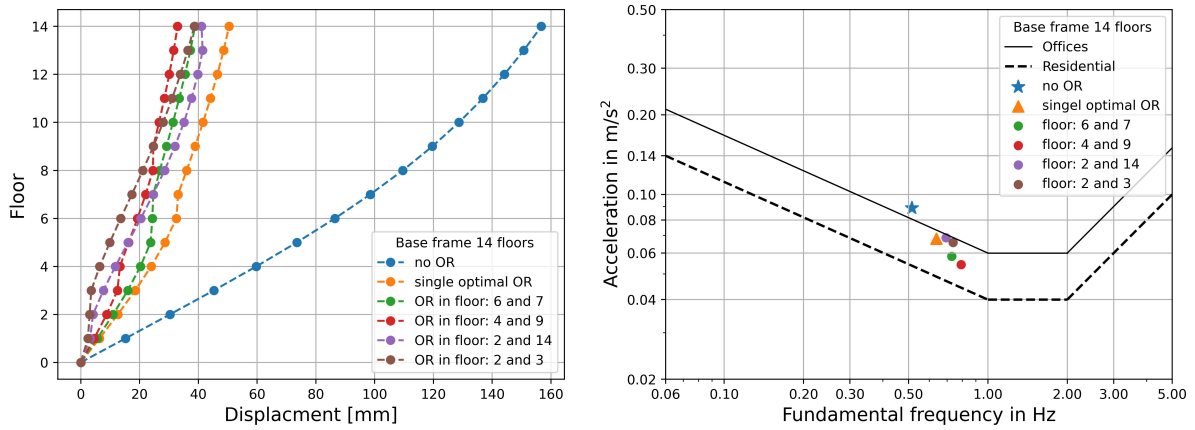


Figure 51: Different outrigger locations for the 14 floors frame

16 floors

No Outrigger				
Parameter	symbol	Unit	Value	reduction
Acceleration	a	m/s^2	0.0921	-
Max IDR	δ_{IDR}	mm	16.31	-
Top floor displacement	δ_{top}	mm	178.9	-
Single Optimal Outrigger				
Acceleration	a	m/s^2	0.0753	18.2 %
Max IDR	δ_{IDR}	mm	7.4	54.6 %
Top floor displacement	δ_{top}	mm	64.6	63.8 %
System 1				
Acceleration	a	m/s^2	0.0669	27.3 %
Max IDR	δ_{IDR}	mm	6.86	57.9 %
Top floor displacement	δ_{top}	mm	53.2	70.3 %
System 2				
Acceleration	a	m/s^2	0.0628	31.8 %
Max IDR	δ_{IDR}	mm	5.98	63.3 %
Top floor displacement	δ_{top}	mm	46.3	74.1 %
System 3				
Acceleration	a	m/s^2	0.0751	18.5 %
Max IDR	δ_{IDR}	mm	4.75	70.8 %
Top floor displacement	δ_{top}	mm	53.3	70.2 %
System 4				
Acceleration	a	m/s^2	0.0736	20.1 %
Max IDR	δ_{IDR}	mm	4.51	72.3 %
Top floor displacement	δ_{top}	mm	50.6	71.7 %

Table 16: Results from the double outrigger location optimization for a 16 floors frame

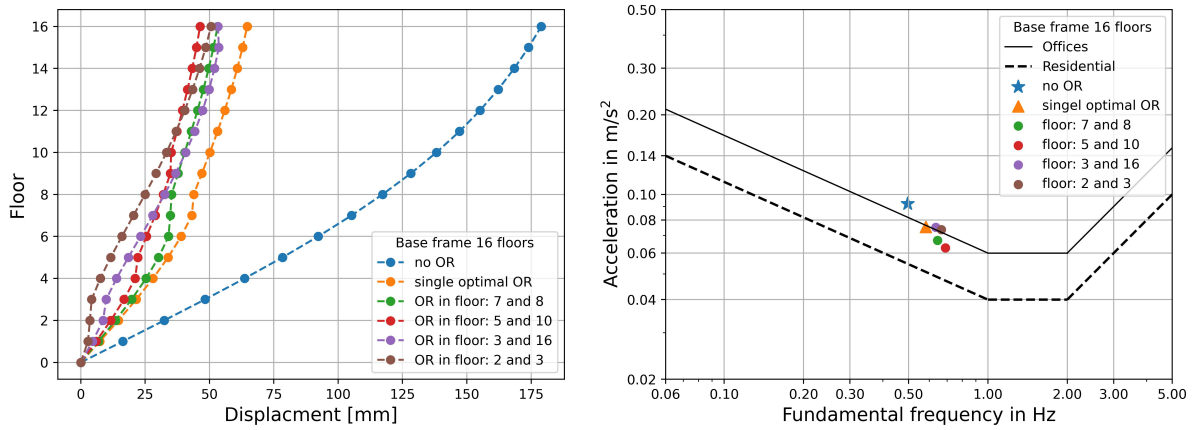


Figure 52: Different outrigger locations for the 16 floors frame

Performance of two Outriggers

With the now desired location of $1/3$ and $2/3$ of the height. The next step is to compare the performance of the single and the double optimal outrigger system. The results vary greatly depending on the frames tested. Similarly for the single outrigger systems, the performance of the double outrigger systems is better for shorter frames. The reduction in acceleration goes from 46.9% for the 12 floor frame to 38.9% for the 14 floor frame and finally to 31.8% for the 16 floor frame. All with respect to the optimal outrigger system. In comparison the reduction in acceleration for the optimal single outrigger system is 30.0%, 23.4% and 18.2% for the 12, 14 and 16 story frames, respectively.

The performance interval ranges from 17%, 15.5% and 13.6% better for the double system compared to the single outrigger system. This means that the range in performance between the two systems decreases with the increasing number of floors. Figure 53 shows that an optimal double outrigger system in the 16 floor frame yields approximately the same acceleration reduction as the single outrigger system in the 12 floor frame.

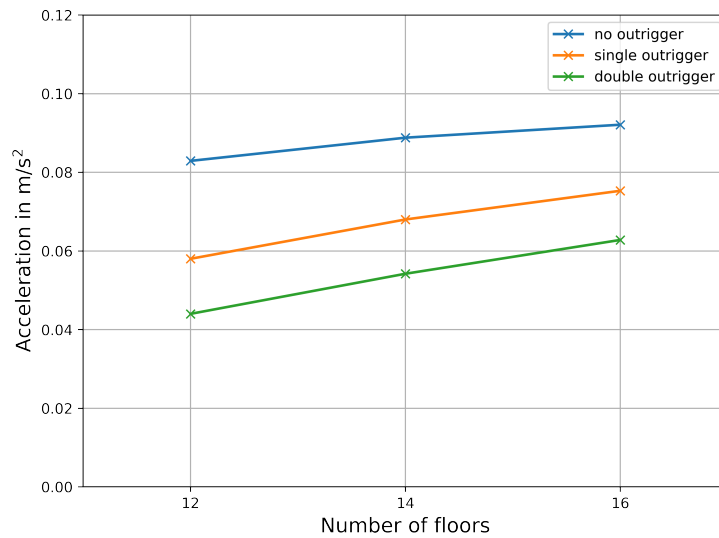


Figure 53: Accelerations for the no, single and double -outrigger systems

5.2.7 Ultimate limit state

In this section the ultimate limit state of the reference frame with an optimal single outrigger is to be elaborated. The eighth reference frames will be checked with the same ULS-procedure as the reference frames in the preliminary analysis. This thesis focuses on SLS and the potential problems high-rise buildings face. This thesis and the coherent analysis should be verified against the ULS to ensure structural safety. The full ULS-procedure is shown in Appendix D. The ultimate limit state load combination given in Section 4.1.1 and Equation (9) has been used in this analysis.

The connections are also going to be addressed in this section. The connections are an important part of timber design. Connections are often the governing component in timber design. The capacity of a connection is often significantly lower than for the member it self. It is therefore important to investigate the forces acting on the connections. This thesis will not do specific calculations for the connection capacity of each frame, but rather comment and quantify.

Check of members

The frames consists of glulam- columns, beams and truss element. The walls are made of CLT. The load bearing capacity of each element needs to be considered to evaluate the structural safety. This is done according to Eurocode (NS-EN 1995-1-1) [23] and the CLT handbook [17].

Columns

The glulam columns are mainly subjected to axial loading from the dead and live load. In addition to the lateral loading in terms of bending and shear, columns near the foundation can be subjected to substantial axial forces. It is expected that stability and stresses from axial loading will be governing.

Beams

Beams are loaded laterally from the dead and live load, this causes bending moments in the beam. The lateral loading from wind causes axial forces in the beams. The beams act as diaphragms, which transfer lateral loading to the vertical elements, thus inducing axial stresses. The beams are considered to be braced against lateral torsional buckling. The main checks for beams are assumed to be bending, bending in combination with axial forces, and shear.

Walls

The walls are located in the outermost parts of the timber framing. They transfer much of the shear forces from the wind load. It is assumed that the load bearing capacity of the crossection is substantial in both shear, axial loading and bending about strong axis. The likelihood of stability failure about the strong axis is neglectable. Thus, stability about the weak axis is the most interesting check among the ones presented in Appendix D.

Outrigger elements

All the outrigger elements are assumed to be pinned in both ends. It is assumed that they have the same boundary conditions about both the z and y- axis. Thus giving them the same buckling length about both axis. Buckling about weak axis is therefore assumed to be a governing design criteria for ULS.

Results

Figure 54 shows the results for the reference frames. The dashed line represents an utilization of 100%. This figure is divided into each respective element. The results show that the elements are mostly clustered below the utilization limit. It is however notable that some analysis for eighth floors fail in beam elements. Another take away is that for 18 floors, the columns start to fail. A more detailed version of Figure 54 is shown in Figure 55.

Out of all the 72 900 analysis only 8.85% exceeds the ULS limitations. This is a small increase from 8.7% exceeds for the frames with no outrigger. Thus a further indicator that the chosen basis frames do not have an issue with the ULS. However, in Figure 54 it shows that for frames with less than 12 floors, one might need to increase the beam height.

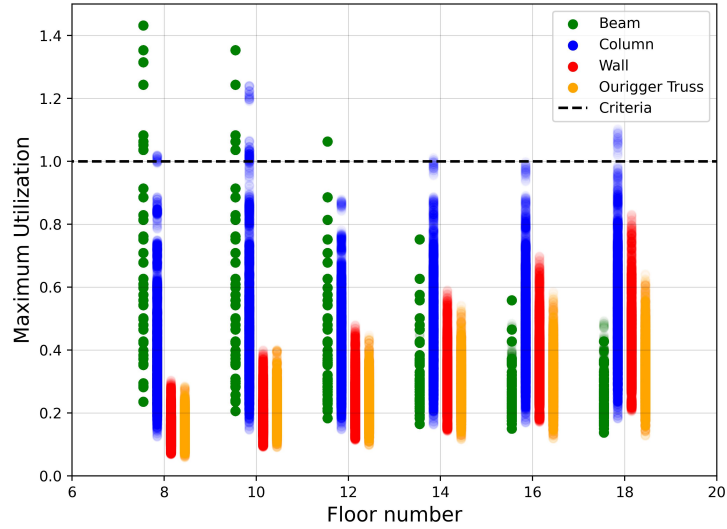


Figure 54: Ultimate limit state analysis for all frames with the optimal outrigger system

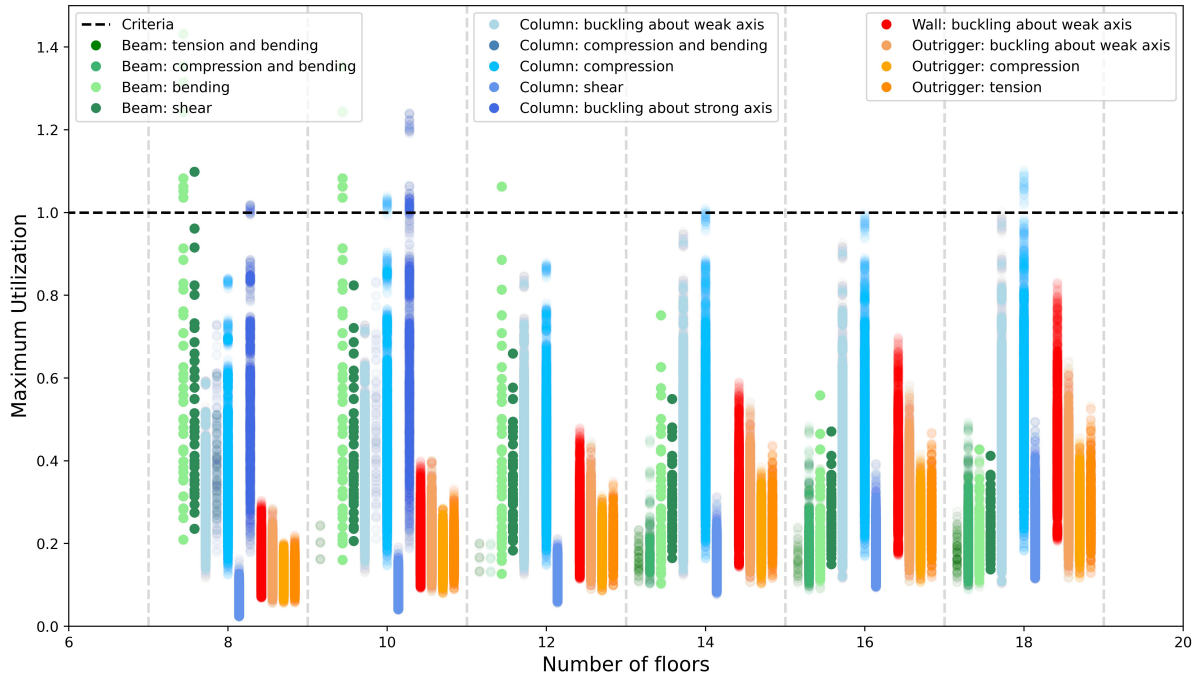


Figure 55: Detailed version of Figure 55

Connections

The connections between the beams and columns are assumed to be semi-rigid and consist of threaded rods, as shown in Figure 5. As mentioned, connections can often be the critical component in timber design, thus it is important to establish some limits for their performance. The benchmark is based on a study of ULS for semi-rigid connection performed at NTNU. The beam measures 140x450 mm and has two planes of rods. Two full scale test were performed. Each having a different placement of rods.

The beam-column connections S35-55-10 failed at 78.8 kNm and the S55-70-10 connection failed at 133.3 kNm, they can be seen in Figure 57. Both specimens failed in the column. Fracture in the panelzone due to a combination of tensile stresses perpendicular to grain and shear, caused the failure. The problem was not the connection in the beam itself, but rather the forces in the column. These findings were used as a reference. Since this ULS analysis contains many different cross sections, a formula given by associate professor Haris Stamatopoulos was used. This formula is as follows:

$$Mn = x \in [78.8, 133.3] \cdot z^2, \text{ where } z = \frac{B_h}{450} \quad (21)$$

The values 78.8 and 133.3 are the maximums for the two full scale tests. These can be assumed to be characteristic values. It is assumed that the design values are approximately 70% of the characteristic values. Thus giving the formulas:

$$Mn = x \in [55.2, 93.3] \cdot z^2, \text{ where } z = \frac{B_h}{450} \quad (22)$$

It is important to bear in mind that this analysis is based on experimental results and therefore should be considered as assumptions.

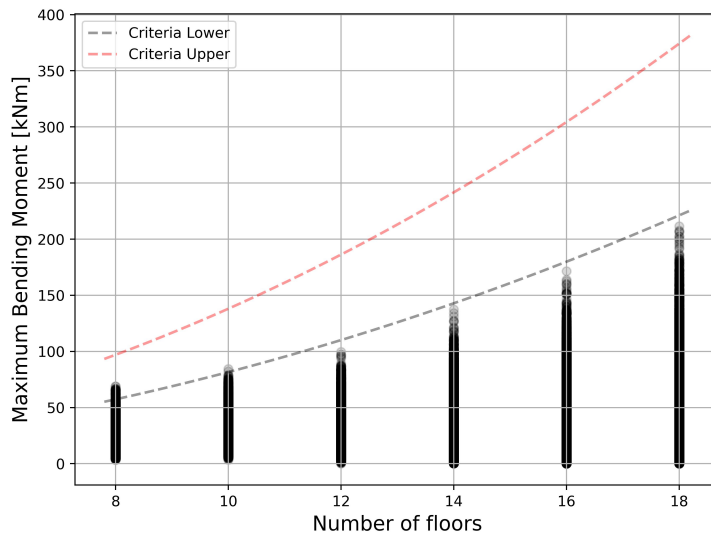


Figure 56: Shows the maximum moments from the ULS analysis

Figure 56 shows the results from the analysis in Opensees. A total of 72 900 analysis were performed. Each beam has two end moments, which in total gives 145 800 points. The dashed red line represents test S55-70-10 and the dashed black line represents test S35-55-10.

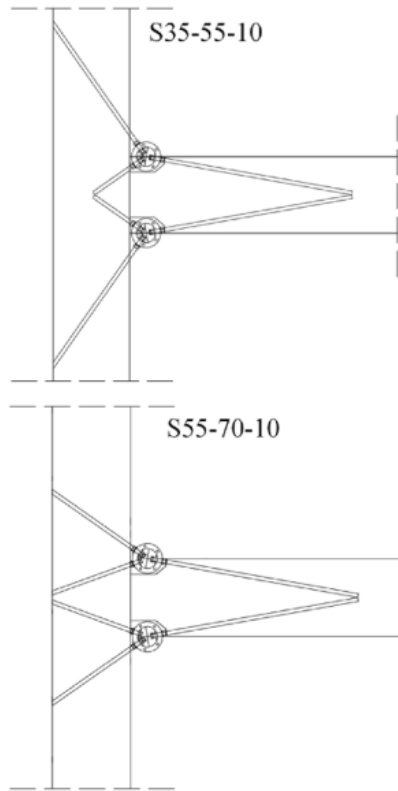


Figure 57: Two tests for placement of rods

5.2.8 Outrigger performance

In this section the influence of an outrigger system was evaluated. The evaluation was based on the acceleration of a frame with an outrigger system: acc compared to the same frame without an outrigger system: $acc0$. The same was done for the frequency: $freq$ and $freq0$, the interstory drift: Δ_{IDR} and Δ_{IDR0} , and the top floor displacement: Δ_{TFD} and Δ_{TFD0} .

Figure 58 shows the range of the ratios for the 72 900 simulations for acceleration and frequency. The figure shows the average ratios with different bands of standard deviation. It is clear that the reduction in acceleration for both the single and double outrigger systems is sharply reducing with increasing number of floors. The stiffness of the system, represented by the first structural frequency, decreases with increasing number of floors. The standard deviation of the acceleration is almost constant with increasing number of floors: $\sigma_{acc} \sim \text{constant}$, while the standard deviation of the frequency is decreasing with increasing number of floors: $\sigma_{freq} \sim f(\text{numb floors})$. Hence, it is a function of the number of floors. This is a consequence of using the same iterative values for all the reference frames. The increments for the smaller frames yields greater change in the frequency, than the same increments yields for the bigger frames. Hence, a larger spread or variance in the data. The acceleration does not suffer from this because the calculations are not calculated directly from modal analysis but rather through the methods provided by the Eurocode (NS-EN 1991-1-4) [9].

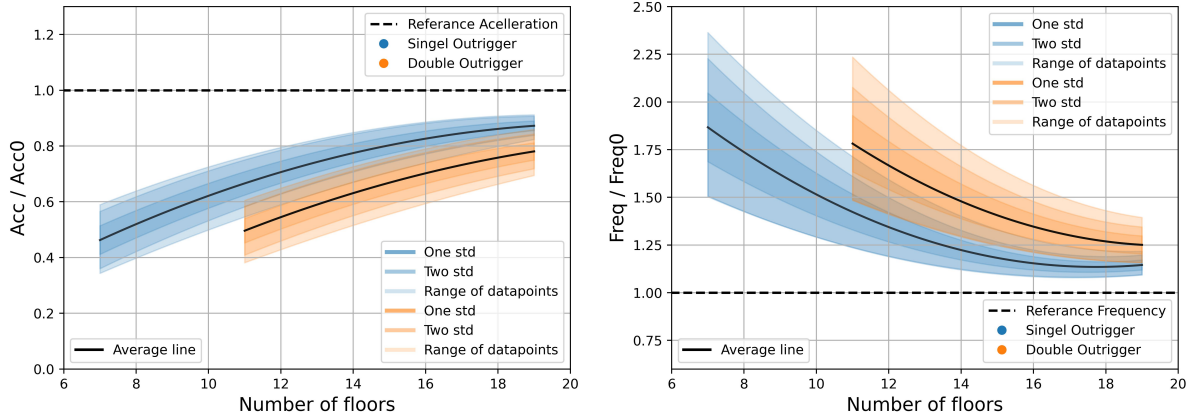


Figure 58: Outrigger influence on acceleration and frequency

The acceleration ratio average reduction is estimated as following:

One outrigger:

$$Acc_{red} = -0.0024 \cdot x^2 + 0.0883 \cdot x - 0.054 \quad (23)$$

Two outriggers:

$$Acc_{red} = -0.0018 \cdot x^2 + 0.0918 \cdot x - 0.287 \quad (24)$$

where; x = number of floors

The frequency ratio average increase is estimated as following:

One outrigger:

$$Freq_{inc} = 0.0063 \cdot x^2 - 0.2254 \cdot x + 3.134 \quad (25)$$

Two outriggers:

$$Freq_{inc} = 0.0069 \cdot x^2 - 0.2734 \cdot x + 3.954 \quad (26)$$

where; x = number of floors

Figure 59 shows the range of the ratios for the 72 900 simulations for interstory drift and top floor displacement. Similarly, with the acceleration and the frequency the effect of the outrigger is diminishing over the increasing number of floors.

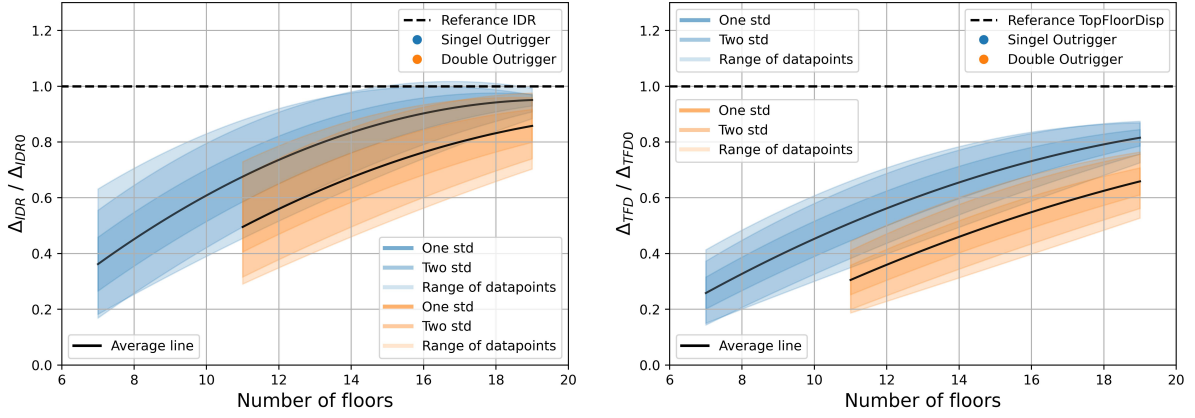


Figure 59: Outrigger influence on IDR and TFD

The inter story drift ratio average reduction is estimated as following:

One outrigger:

$$IDR_{red} = -0.0036 \cdot x^2 + 0.1446 \cdot x - 0.470 \quad (27)$$

Two outriggers:

$$IDR_{red} = -0.0027 \cdot x^2 + 0.1280 \cdot x - 0.579 \quad (28)$$

where; x = number of floors

The top floor displacement ratio average reduction is estimated as following:

One outrigger:

$$TFD_{red} = -0.0020 \cdot x^2 + 0.0996 \cdot x - 0.339 \quad (29)$$

Two outriggers:

$$TFD_{red} = -0.0014 \cdot x^2 + 0.0885 \cdot x - 0.489 \quad (30)$$

where; x = number of floors

It should be mentioned that these equations are fairly limited in their applications and serve more as a reference for what reductions a system can expect after applying the outrigger system. With the provided equations, the mean can be approximated, while the range of the standard deviations has to be measured directly from the figures.

The proposed nonlinear expressions can only be used within the range for which they are calibrated. The equations have no proven significance with extrapolation.

6 Conclusion

This paper presents a parametric study of the serviceability performance of planar moment-resisting timber frames, and with the inclusion of outrigger systems. A wide range of parameters were considered in this study: rotational stiffness of beam-to-column connections and the axial stiffness of the outrigger elements, the number of floors, number of bays and bay length, column, beam, wall and truss cross-section dimensions and spacing in-between frames. The main aim of the study was to explore the possibilities and limitations for outriggers in semi-rigid timber frames. Moreover, simple analytical equations for evaluation of the performance of the single and double optimal outriggers are developed and made available. Based on the results, the following conclusions are drawn:

- First, the optimal CLT core structure and outrigger locations, for both a single outrigger system and a double outrigger system in terms of acceleration were found. The conclusion of a single outrigger system was placing the outrigger on the floor closest to the 1/2-height of the building. The conclusion for the the double outrigger system was placing the outriggers at floors closest to the 1/3 and 2/3-height of the building. A system with an external core system is much better than a system with an internal core structure.
- Second, the optimal effective system axial stiffness was set to $330kN/mm$. The effect of axial stiffness has been shown to diminish rapidly with small increments of axial stiffness in the members.
- Third, with identical members, the chevron bracing system is proven to perform better in terms of acceleration, maximum interstory drift and top floor displacement. However, as the axial stiffness of the members of the other proposed bracing systems increases, they converge towards the optimal system in terms of equal performance.
- Fourth, the performance of the outrigger. Both the single and double outrigger systems have been presented with their potential and analytical equations for quick approximation.
- Fifth, the reduction in acceleration ranges from 50% down to 30% with the optimal outrigger systems for all tested frames.

7 Limitations and future work

7.1 Limitations

In this thesis, several hundred thousand semi-rigid frames were simulated with different types of structural properties. Through OpenSeesPy and Python, a tool has been developed to perform the analysis. However, the choices and scope of this thesis result in some limitations.

In this thesis, a finite element script in Python is developed for planar frames. The model does not take imperfections in the connections into account, and the imperfections are therefore assumed to be negligible. In addition to imperfections in connections, imperfections in members are not considered. In timber structures, the elements are prone to cracks. Cracks are present in most structural timber elements due to natural swelling and shrinkage. Since this thesis focuses on the serviceability of timber structures, it is assumed that the effect of cracks on the overall stiffness of the structure can be neglected. Thus, the developed model uses mathematically perfect members, and cracks or imperfections are not considered.

The windward width, B , is calculated under the assumption that the structure consists of numerous frames with a spacing, S , in between. This is a simplification of the calculation of the uniform wind load. The thesis only considered 2D analysis, thus neglecting oscillations in the cross-wind direction. A 2D system was chosen since collecting data for a parametric study can become computationally expensive, given that, in order to capture the influence of a parameter, various models must be developed implementing different values for the parameter, and their outcome must be analyzed. For the purpose of this investigation, it was decided that the most efficient and representative way to collect such data was to develop a 2D parametric model. The use of 2D analysis also results in only in-plane eigenmodes and lateral deformations. It does not consider out-of-plane eigenmodes or twisting.

For every floor, columns and walls are modeled with rigid boundary conditions. Thus, continuous members are generated without any joints. Therefore, the modeled frame is stiffer than an ordinary frame. Both columns and walls are assumed to have rotational stiffness independent of their member size. Future improvements should include rotational springs in the joints of the column-to-column joints.

The approximation for the rotational stiffness of the beam. The scaling of the beams with the z^2 factor may cause inaccurate stiffness. The equation for rotational stiffness in the beam-to-column connections is highly experimental. The reference value of 4500 Knm/rad for a 450mm beam and with a single plane of rods is from experiments. The formula (17) is based on the assumption that stiffness is related to both the number of planes and the z -squared ratio for height.

The approximation factor for tuning the rigid zone should be better approximated with the properties of the building. In the model developed in this theses the approximation value for the rigid zone is 100. Thus, making this part of the structure 100 times stiffer than its connecting beam. However, this factor may vary with different building properties. A wider range of approximation factors should be developed to better grasp this variety in structures.

To simplify the choice of cross-sectional dimensions, the width of the columns, beams, truss-members, and walls are kept constant at a width of 430 mm. Thus, making the stiffness only a function of the member height. This is an advantage when it comes to the parametric modelling, and the number of iterative variables is enormous. However, as consequence of this assumption one might get unrealistic beams for both the smallest and the biggest frames.

Soil structure interactions are neglected in this thesis. The foundation is assumed to not affect the boundary conditions of the structure. It is assumed that the soil provides infinite stiffness and does not undergo deformation when subjected to loading. It would be favorable to model the behavior of the soil/foundation with axial springs to account for the stiffness the soil provides. The boundary conditions for the column and walls are calculated based on a model where brackets and hold-down capacity are estimated. It is important to note that this is an assumption which, when changed, can greatly affect the outcome of the analysis.

In this thesis, the wind loading is estimated using the simplified method proposed by Eurocode. In the calculations, several simplifications were made, for instance, the determination of the size c_s and the dynamic factor c_d which were set to 1 respectively. The simplified acceleration approach using the first mode shape requires an uniform horizontal mode shape. Thus, when using an outrigger this gives a slight error because the mode shape is not truly uniform.

7.2 Future work

As highlighted in Section 7.1, the work in this thesis contains many limitations. The study has been narrowed, and in hindsight there are numerous aspects with the work that need to be investigated further. This section contains some proposals and suggestions for future work.

The main part of the study revolved around the serviceability limit state (SLS). Although the ultimate limit state (ULS) was investigated, it would be beneficial for the study to consider the capacity of the connections as well. As mentioned, connections are often the weak spot in timber design due to their complex nature. In future studies, a suggestion for connection design should be made. Furthermore, they should be verified and checked.

Semi-rigid frames are based on the implementation of connections that can be modeled as rotational springs. In this thesis, the columns and walls are modeled as continuous. In practice, this can be difficult to achieve due to the length of the members. In practice, columns and walls would have to be joined with connections along the height of the building. These connections should be studied and perhaps modeled as rotational springs. Furthermore, the boundary conditions at the base of the walls and columns should also be tested more thoroughly. In this thesis, they were not varied in terms of the rotational stiffness provided. This is likely to affect the results. The results of the analysis show that the maximum IDR occurs between the ground floor and the first floor.

More geometries and placement of the CLT walls should be included in future work. By testing the placement of the CLT-Walls one could see that the placement had a huge impact on the IDR, TFD and acceleration. In this thesis, only internal and external placement of CLT-Walls was checked. The impact and influence of CLT walls on building performance should be more thoroughly analyzed.

A future work should look for a possibility to apply shell methods to the OpenSeesPy-routine. By introducing shell elements, one can see if CLT walls can work as outriggers. A CLT wall will completely seal off the outrigger floor. This might be beneficial for the force distributions in the columns and walls as well as the shear forces. The shell elements in OpenSeesPy are yet to be developed and are therefore not something that was added to the routine. This could also be done with a different FEM program for example SAP2000.

By introducing time series data, more precise wind engineering routines could be developed and added to the OpenSeesPy-routine. This could give more precise results for both calculations of the acceleration and the wind forces. As the wind and acceleration methods are developed on non-timber materials, it could be interesting to see what impact a more precise calculation routine could provide.

References

- [1] ISO10137, 'Iso10137 braces for design for structures - serviceability of buildings and walkways against vibrations', 2007.
- [2] H. Stamatopoulos and K. A. Malo, *Wood frame solutions for free space design in urban buildings*(WOODSOL. Lund, 2017.
- [3] Alcorn, 'Embodied energy and co2 coefficients for nz building materials. centre for building performance research, victoria university, wellington', - 2003.
- [4] UN, 'Un environment and international energy agency (2017): Towards a zero-emission, efficient, and resilient buildings and construction sector. global status report 2017.', - 2017.
- [5] A. Vilguts, K. A. Malo and H. Stamatopoulos, 'Moment-resisting timber frames with semi-rigid connections', Mar. 2021.
- [6] R. Abrahamsen, 'Mjøstårnet - construction of an 81 m tall timber building', Mar. 2017. [Online]. Available: <https://ntnuopen.ntnu.no/ntnu-xmlui/handle/11250/2733575>.
- [7] Lame, *Optimization of Outrigger Structures*. Tehran, 2007.
- [8] A. Iqbal, 'Developments in tallwood and hybrid buildings and environmental impacts.', Jul. 2021. [Online]. Available: <https://doi.org/10.3390/su132111881>.
- [9] NS-EN-1991-1-4, 'Ns-en-1991-1-4 wind loads', 2005.
- [10] M. H. Ramage, H. Burrige, M. Busse-Wicher *et al.*, 'The wood from the trees: The use of timber in construction', English, *Renewable and Sustainable Energy Reviews*, vol. 68, pp. 333–359, 2017, Cited By :431. [Online]. Available: www.scopus.com.
- [11] Skullestad, 'High-rise timber buildings as a climate change mitigation measure - a comparative lca of structural system alternatives', 2016.
- [12] Sikora, 'Feasability study on further utilization of timber in china', Jul. 2018.
- [13] M. Augustin, 'Handbook 1 timber structures. leonardo da vinci pilot projects, "educational materials for designing and testing of timber structures - temtis"', Jul. 2008.
- [14] V. Fragkia, 'Wood anisotropy based on grain direction', Sep. 2020.
- [15] C. B. Ong, 'Glue-laminated timber (glulam)', English, in ser. *Wood Composites*. 2015, pp. 123–140.
- [16] *Limtreboka*. Lund, 2005.
- [17] S. Wood, *The CLT Handbook*. Stockholm, 2019.
- [18] P. Zumbrunnen, 'Pure clt - concepts and structural solutions for multi storey timber structure', Mar. 2017. [Online]. Available: https://www.forum-holzbau.com/pdf/67_IHF2017_Zumbrunnen.pdf.
- [19] Y. Tamura, *Advanced Structural Wind Engineering*. Japan: Springer, 2013.
- [20] M. Johansson, A. Linderholt, K. Jarnerö and P. Landel, 'Tall timber buildings - a preliminary study of wind-induced vibrations of a 22-storey building', English, in *WCTE 2016 - World Conference on Timber Engineering*, 2016.
- [21] P. Landel, A. Linderholt and M. Johansson, 'Dynamical properties of a large glulam truss for a tall timber building', English, in *WCTE 2018 - World Conference on Timber Engineering*, Cited By :2, 2018.
- [22] A. Feldmann, H. Huang, W. Chang *et al.*, 'Dynamic properties of tall timber structures under wind-induced vibration', en, in *World Conference on Timber Engineering (WCTE 2016)*, T. Verlag, Ed., Vienna, Austria: IMWS ITI, Vienna University of Technology, 2016, ISBN: 9783903024359.
- [23] NS-EN-1995-1-1, 'Ns-en-1995-1-1 prosjektering av trekonstruksjoner', 2004.
- [24] NS-EN-1990, 'Ns-en-1990 basics for structural design', 2002.
- [25] N.-E. 1998-1, 'Ns-en 1998-1', 2004.

-
- [26] D. Boggs, *Acceleration indexes for human comfort in tall buildings—peak or rms?*, 1997. [Online]. Available: https://www.researchgate.net/publication/240806279_Acceleration_Indexes_for_Human_Comfort_in_Tall_Buildings-Peak_or_RMS.
- [27] H. Stamatopoulos, '*design aspects of timber buildings*', *lecture notes (tkl 4212 - timber structures 2)*, Nov. 2021.
- [28] S. A and C. B, 'Tall building structures: Analysis and design. john wiley sons. inc, 1991', English, in 1991.
- [29] H.-S. Kim, L. Hye-Lym and L. You-Jin, 'Multi-objective optimization of dual-purpose outriggers in tall buildings to reduce lateral displacement and differential axial shortening', 2019.
- [30] G. Ho, *Outrigger Topology and Behaviours*. China: Advanced Steel Construction, 2016.
- [31] H.-S. Kim, L. Hye-Lym and L. You-Jin, 'Optimum location of outrigger in tall buildings using finite element analysis and gradient-based optimization method', 2020.
- [32] W. Raymond and H. M, 'Structural and construction features of the hong kong international financial center phase ii', 2003.
- [33] G. Marshall, 'Two international finance centre', 2017.
- [34] C. Hi sun, H. Goman, L. Joseph and N. Mathias, 'Outrigger design for high-rise buildings 2nd edition', 2017.
- [35] J. Paul J, 'U.s. bank center (first wisconsin bank building)', 2017.
- [36] H. Stamatopoulos, K. A. Malo and A. Vilguts, 'Moment-resisting beam-to-column timber connections with inclined threaded rods', Nov. 2021.
- [37] NS-EN-1991-1-1, 'Ns-en-1991-1-1 general actions', 2002.
- [38] M. Zhu, *Openseespy*, 2019. [Online]. Available: <https://openseespydoc.readthedocs.io/en/latest/>.

Appendix

A Python Codes

All relevant python codes used can be found in the following address:

https://github.com/hermanmb/Master__2022__Timber.

The codes can be used to reproduce the data handling, extracted features, feature selection methods and to reproduce the results of the thesis. Note that the code to reproduce the figures have not been concluded.

B Reference frames

Reference frame with 8 floors

Parameters	symbol	Unit	Value
Number of floors	n	-	8
Number of bays	n_b	-	3
Number of frames	n_f	-	6
Bay length	l_b	mm	7000
Floor height	h	mm	3500
Spacing	S	mm	5000
Column height	h_c	mm	630
Beam height	h_b	mm	450
Wall height	h_w	mm	3000
Truss height	h_t	mm	300
Column width	w_c	mm	430
Beam width	w_b	mm	430
Wall width	w_w	mm	430
Truss width	w_t	mm	430
Rotational stiffness beams	K_{rb}	kNm/rad	18000
Rotational stiffness columns	K_{rc}	kNm/rad	10000
Rotational stiffness walls	K_{rw}	kNm/rad	200 000
Base wind	V_{b0}	m/s	26
Wind load	q_w	kN/m	0.89
Dead load	g	kN/m^2	2
Live load	q_s	kN/m^2	3

Reference frame with 10 floors

Parameters	symbol	Unit	Value
Number of floors	n	-	10
Number of bays	n_b	-	3
Number of frames	n_f	-	6
Bay length	l_b	mm	7000
Floor height	h	mm	3500
Spacing	S	mm	5000
Column height	h_c	mm	630
Beam height	h_b	mm	540
Wall height	h_w	mm	3000
Truss height	h_t	mm	300
Column width	w_c	mm	430
Beam width	w_b	mm	430
Wall width	w_w	mm	430
Truss width	w_t	mm	430
Rotational stiffness beams	K_{rb}	kNm/rad	25920
Rotational stiffness columns	K_{rc}	kNm/rad	10000
Rotational stiffness walls	K_{rw}	kNm/rad	200 000
Base wind	V_{b0}	m/s	26
Wind load	q_w	kN/m	1.00
Dead load	g	kN/m^2	2
Live load	q_s	kN/m^2	3

Reference frame with 12 floors

Parameters	symbol	Unit	Value
Number of floors	n	-	12
Number of bays	n_b	-	3
Number of frames	n_f	-	6
Bay length	l_b	mm	7000
Floor height	h	mm	3500
Spacing	S	mm	5000
Column height	h_c	mm	810
Beam height	h_b	mm	630
Wall height	h_w	mm	3000
Truss height	h_t	mm	540
Column width	w_c	mm	430
Beam width	w_b	mm	430
Wall width	w_w	mm	430
Truss width	w_t	mm	430
Rotational stiffness beams	K_{rb}	kNm/rad	35280
Rotational stiffness columns	K_{rc}	kNm/rad	10000
Rotational stiffness walls	K_{rw}	kNm/rad	200 000
Base wind	V_{b0}	m/s	26
Wind load	q_w	kN/m	1.10
Dead load	g	kN/m^2	2
Live load	q_s	kN/m^2	3

Reference frame with 14 floors

Parameters	symbol	Unit	Value
Number of floors	n	-	14
Number of bays	n_b	-	3
Number of frames	n_f	-	6
Bay length	l_b	mm	7000
Floor height	h	mm	3500
Spacing	S	mm	5000
Column height	h_c	mm	810
Beam height	h_b	mm	720
Wall height	h_w	mm	3000
Truss height	h_t	mm	300
Column width	w_c	mm	430
Beam width	w_b	mm	430
Wall width	w_w	mm	430
Truss width	w_t	mm	430
Rotational stiffness beams	K_{rb}	kNm/rad	46080
Rotational stiffness columns	K_{rc}	kNm/rad	10000
Rotational stiffness walls	K_{rw}	kNm/rad	200 000
Base wind	V_{b0}	m/s	26
Wind load	q_w	kN/m	1.17
Dead load	g	kN/m^2	2
Live load	q_s	kN/m^2	3

Reference frame with 16 floors

Parameters	symbol	Unit	Value
Number of floors	n	-	16
Number of bays	n_b	-	3
Number of frames	n_f	-	6
Bay length	l_b	<i>mm</i>	7000
Floor height	h	<i>mm</i>	3500
Spacing	S	<i>mm</i>	5000
Column height	h_c	<i>mm</i>	900
Beam height	h_b	<i>mm</i>	810
Wall height	h_w	<i>mm</i>	3000
Truss height	h_t	<i>mm</i>	540
Column width	w_c	<i>mm</i>	430
Beam width	w_b	<i>mm</i>	430
Wall width	w_w	<i>mm</i>	430
Truss width	w_t	<i>mm</i>	430
Rotational stiffness beams	K_{rb}	<i>kNm/rad</i>	58320
Rotational stiffness columns	K_{rc}	<i>kNm/rad</i>	10000
Rotational stiffness walls	K_{rw}	<i>kNm/rad</i>	200 000
Base wind	V_{b0}	<i>m/s</i>	26
Wind load	q_w	<i>kN/m</i>	1.25
Dead load	g	<i>kN/m²</i>	2
Live load	q_s	<i>kN/m²</i>	3

Reference frame with 18 floors

Parameters	symbol	Unit	Value
Number of floors	n	-	18
Number of bays	n_b	-	3
Number of frames	n_f	-	6
Bay length	l_b	<i>mm</i>	7000
Floor height	h	<i>mm</i>	3500
Spacing	S	<i>mm</i>	5000
Column height	h_c	<i>mm</i>	900
Beam height	h_b	<i>mm</i>	900
Wall height	h_w	<i>mm</i>	3000
Truss height	h_t	<i>mm</i>	540
Column width	w_c	<i>mm</i>	430
Beam width	w_b	<i>mm</i>	430
Wall width	w_w	<i>mm</i>	430
Truss width	w_t	<i>mm</i>	430
Rotational stiffness beams	K_{rb}	<i>kNm/rad</i>	72000
Rotational stiffness columns	K_{rc}	<i>kNm/rad</i>	10000
Rotational stiffness walls	K_{rw}	<i>kNm/rad</i>	200 000
Base wind	V_{b0}	<i>m/s</i>	26
Wind load	q_w	<i>kN/m</i>	1.34
Dead load	g	<i>kN/m²</i>	2
Live load	q_s	<i>kN/m²</i>	3

C Axial stiffness outrigger connection

The axial stiffness of $K_x = 1000kN/mm$ in the outrigger is based on these assumptions:

Slip modulus:

$$K_{ser} = \frac{\rho_m^{1.5} \cdot d}{23} = \frac{430^{1.5} \cdot 20}{23} = 7753N/mm \quad (31)$$

Steel to timber connection (EN1995-1-1, § 7.1.(3)):

$$K_{ser} = 2 \cdot K_{ser} = 2 \cdot 7753N/mm = 15507N/mm \quad (32)$$

With a connection of 8 dowels and 8 shear planes:

$$K_{x,t} = \binom{8}{dowels} \cdot \binom{8.shear}{planes} \cdot 15507N/mm = 1000kN/mm \quad (33)$$

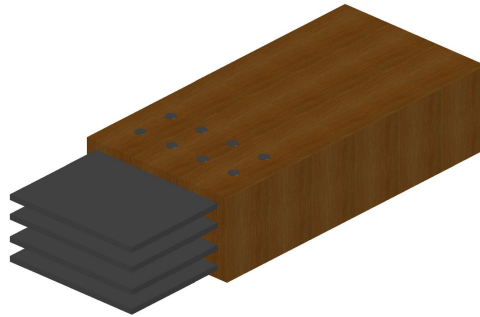


Figure 60: Connection concept

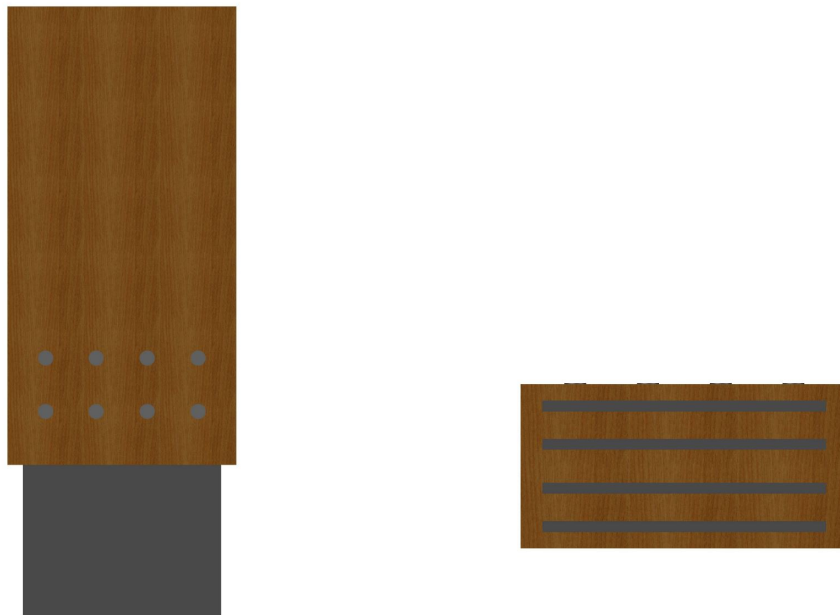


Figure 61: Connection concept; side and top view

D Ultimate limit state considerations

The frame elements should be checked according to Eurocode 5 (NS-EN 1995-1-1) [23] and the CLT-Handbook [17]. The building consists of columns, beams, walls and outrigger elements. This section contains a detailed explanation on how they are verified for ULS.

Verification of glulam members

The beams, columns and outriggers consists of glulam elements. These must be checked according to Eurocode 5. These members should be checked for:

- Axial stresses
- Bending stresses
- Combined bending and axial
- Shear
- Stability

Axial stresses

Axial forces will occur due to loads applied on the structure. These axial forces will manifest itself as tension or compression stresses. The columns at the structure foundation are likely to experience significant axial forces due to dead and live loads. Eurocode 5 (NS-EN 1995-1-1) [23] gives the following formulas for compression and tension check.

$$\sigma_{t,0,d} \leq f_{t,0,d} \quad (34)$$

$$\sigma_{c,0,d} \leq f_{c,0,d} \quad (35)$$

Bending stresses

The transverse loading of the elements will occur as bending moments, thus inducing bending stresses in the members. Both beams and columns will experience bending moments as a consequence of local lateral loads. The elements can have bending about the weak and strong axis or both. The design parameter k_m accounts for biaxial bending stresses that account for stress redistribution and inhomogeneity of the cross-sections. For rectangular members this parameter is calculated as 0.7. According to Eurocode 5 (NS-EN 1995-1-1) [23] there are two checks for bending.

$$\frac{\sigma_{m,y,d}}{f_{m,y,d}} + k_m \cdot \frac{\sigma_{m,z,d}}{f_{m,z,d}} \leq 1 \quad (36)$$

$$\frac{\sigma_{m,z,d}}{f_{m,z,d}} + k_m \cdot \frac{\sigma_{m,y,d}}{f_{m,y,d}} \leq 1 \quad (37)$$

Bending and axial stresses

The combined effect of bending and axial forces should be investigated. For combined compression and bending, the stresses in the member can be evaluated as follows:

$$\left(\frac{\sigma_{c,0,d}}{f_{c,0,d}}\right)^2 + \frac{\sigma_{m,y,d}}{f_{m,y,d}} + k_m \cdot \frac{\sigma_{m,z,d}}{f_{m,z,d}} \leq 1 \quad (38)$$

$$\left(\frac{\sigma_{c,0,d}}{f_{c,0,d}}\right)^2 + k_m \cdot \frac{\sigma_{m,y,d}}{f_{m,y,d}} + \frac{\sigma_{m,z,d}}{f_{m,z,d}} \leq 1 \quad (39)$$

If the member is subjected to tension in combination with bending moments, the stresses can be calculated in the following manner:

$$\left(\frac{\sigma_{t,0,d}}{f_{t,0,d}} + \frac{\sigma_{m,y,d}}{f_{m,y,d}} + k_m \cdot \frac{\sigma_{m,z,d}}{f_{m,z,d}} \leq 1 \right) \quad (40)$$

$$\left(\frac{\sigma_{t,0,d}}{f_{t,0,d}} + k_m \cdot \frac{\sigma_{m,y,d}}{f_{m,y,d}} + \frac{\sigma_{m,z,d}}{f_{m,z,d}} \leq 1 \right) \quad (41)$$

Stability check

The members should be checked for flexural buckling on both the weak and strong axis. Instability can be caused by axial compression and bending. The expressions for buckling are given in Eurocode 5 (NS-EN 1995-1-1) [23] as equation 6.23 and 6.24.

$$\frac{\sigma_{c,0,d}}{k_{c,y} \cdot f_{c,0,d}} + \frac{\sigma_{m,y,d}}{f_{m,y,d}} + k_m \cdot \frac{\sigma_{m,z,d}}{f_{m,z,d}} \leq 1 \quad (42)$$

$$\frac{\sigma_{c,0,d}}{k_{c,z} \cdot f_{c,0,d}} + k_m \cdot \frac{\sigma_{m,y,d}}{f_{m,y,d}} + \frac{\sigma_{m,z,d}}{f_{m,z,d}} \leq 1 \quad (43)$$

The reduction factors $k_{c,y}$ and $k_{c,z}$ is calculated as:

$$k_{c,y} = \frac{1}{k_y + \sqrt{k_y^2 - \lambda_{rel,y}^2}} \quad (44)$$

$$k_{c,z} = \frac{1}{k_z + \sqrt{k_z^2 - \lambda_{rel,z}^2}} \quad (45)$$

$$k_y = 0.5 * (1 + \beta_c(\lambda_{rel,y} - 0.3) + \lambda_{rel,y}^2) \quad (46)$$

$$k_z = 0.5 * (1 + \beta_c(\lambda_{rel,z} - 0.3) + \lambda_{rel,z}^2) \quad (47)$$

β_c is given as 0.1 for glulam.

$$\lambda_{rel,y} = \lambda_{rel,y} = \frac{\lambda_y}{\pi} \sqrt{\frac{f_{c,0,k}}{E_{0,05}}} \quad (48)$$

$$\lambda_{rel,z} = \lambda_{rel,z} = \frac{\lambda_z}{\pi} \sqrt{\frac{f_{c,0,k}}{E_{0,05}}} \quad (49)$$

For buckling to occur it is required that $\lambda_{rel,z} < 0,3$ and $\lambda_{rel,y} < 0,3$. λ_y and λ_z are the slenderness ratios of the crosssections. They are calculated as

$$\lambda_y = \sqrt{\frac{L_{eff,y}}{i_y}} \quad (50)$$

$$\lambda_z = \sqrt{\frac{L_{eff,z}}{i_z}} \quad (51)$$

The buckling lengths $L_{eff,y}$ and $L_{eff,z}$ are dependent on the buckling shape of the column. For out of plane buckling the column is considered to buckle as if it is pinned in both ends. Resulting in a buckling factor equal to 1 and a buckling length $L_{eff,z}$ equal to the column height. The buckling length about strong axis requires a more complex calculation. This factor was roughly set to 0.8. This is a simplification, the factor is based on discussion with Phd candidate osama abdelfattah hegeir.

CLT

The walls consist of CLT elements. These can be designed according to the CLT-handbook. Shear forces and lateral loads are assumed not to be a concern. The strong axis is located in the direction of the wind. Thus, providing the element with bug bending and shear capacity. As

The shear forces and bending moments caused by the lateral loads will not be problematic for the walls, since they are located with their strongest axis with respect to shear and bending in this direction. The bending moments caused by the lateral loads should not be of any concern. The shear walls are checked for stability, hence buckling out of plane.

Stability

The CLT-handbook is used as a guideline for stability checks of the CLT members. This stability verification can be done in line with Eurocode 5. The walls are mainly subjected to axial forces from the dead and live load. This causes axial stresses.

$$\frac{\sigma_{c,x,d}}{k_{c,y} \cdot f_{c,0,xlay,d}} + \frac{\sigma_{m,y,d}}{f_{m,xlay,d}} \leq 1 \quad (52)$$

$$\frac{N_d}{k_{c,y} \cdot A_{x,net} \cdot f_{c,0,xlay,d}} + \frac{M_{y,d}}{W_{x,net} \cdot f_{m,xlay,d}} \leq 1 \quad (53)$$

The reduction factor $k_{c,y}$ is calculated in the same way as for glulam. Thus:

$$k_{c,y} = \frac{1}{k_z + \sqrt{k_z^2 - \lambda_{rel,z}^2}} \quad (54)$$

with k_y as:

$$k_y = 0.5 * (1 + \beta_c(\lambda_{rel,y} - 0.3) + \lambda_{rel,y}^2) \quad (55)$$

The relative slenderness factor is determined by

$$\lambda_{rel,y} = \frac{\lambda_y}{\pi} \sqrt{\frac{f_{c,0,xlay,k}}{E_{0,05}}} \quad (56)$$

where:

$$\lambda = \frac{L_{ref}}{i_{x,ef}} \quad (57)$$

$$L_{ref} = \beta \cdot L \quad (58)$$

The walls are assumed to be pinned for out of plane buckling, thus giving a β factor equal to 1.0. $i_{x,ef}$ is the slenderness radius and can be calculated accordingly.

$$i_{x,ef} = \sqrt{\frac{I_{x,ef}}{A_{net}}} \quad (59)$$

The factor $I_{x,ef}$ is calculated using the Gamma method. A_{Net} is the net area of the CLT wall, the area of the lamellas in the strong direction.

E Wind load calculation

This part of the Appendix explains the routine for calculation of wind loads. It consists of an example calculation for a 10-floor reference frame. This is done according to the Eurocode (NS-EN 1991-1-4) [9]. The example calculation is performed in the same manner and procedure as in the Pythonscript, located in Appendix A, under the name WindFunction. Table F shows the data for the reference frame of 10 floors.

Reference frame with 10 floors

Parameters	symbol	Unit	Value
Number of floors	n	-	10
Number of bays	n_b	-	3
Number of frames	n_f	-	6
Bay length	l_b	mm	7000
Floor height	h	mm	3500
Spacing	S	mm	5000
Column height	h_c	mm	630
Beam height	h_b	mm	540
Wall height	h_w	mm	3000
Truss height	h_t	mm	300
Column width	w_c	mm	430
Beam width	w_b	mm	430
Wall width	w_w	mm	430
Truss width	w_t	mm	430
Rotational stiffness beams	K_{rb}	kNm/rad	25920
Rotational stiffness columns	K_{rc}	kNm/rad	10000
Rotational stiffness walls	K_{rw}	kNm/rad	200 000
Base wind	V_{b0}	m/s	26
Wind load	q_w	kN/m	1.00
Dead load	g	kN/m ²	2
Live load	q_s	kN/m ²	3

Wind Velocity

$$v_m(z) = c_r(z) \cdot c_0(z) \cdot v_b \quad (60)$$

c_r = roughness factor : It is a function of the building height z

c_0 = orography factor : Norwegian National Annex states $c_0 = 1.0$

v_b = standard wind velocity at reference height of 10m

$$v_b = c_{prob} \cdot c_{dir} \cdot c_{season} \cdot v_{b,0} \quad (61)$$

c_{dir} = direction factor : Norwegian National Annex States $c_{dir} = 1,0$

c_{season} = season factor : Norwegian National Annex States $c_{season} = 1,0$

c_{prob} = probability factor: Can be taken as $c_{prob} = 1,0$

$v_{b,0}$ = fundamental wind velocity for Trondheim : $v_{b,0} = 26$ m/s

$$v_b = 1 \cdot 1 \cdot 1 \cdot 26m/s = 26m/s \quad (62)$$

$$c_r(z) = k_r \cdot \ln\left(\frac{z}{z_0}\right) \quad (63)$$

k_r and z_0 depend on the terrain category. The terrain category describes the topology of the area surrounding the structure. In these calculations, it is assumed that the location is Trondheim and that the terrain category is 4. To fulfill terraincategory 4 at least 15% of the surface area must be covered with buildings and their average height exceeds 15 m (NS-EN 1991-1-4) [9].

$k_r = 0.24$ for terraincategory = 4
 $z_0 = 1$ for terraincategory = 4
 $z_{min} = 16$ for terraincategory = 4

$$c_r(z) = 0.24 \cdot \ln(z) \tag{64}$$

Pressure Zones

When calculating the final wind load according to the Eurocode (NS-EN 1991-1-4) [9], the shape of the profile of the velocity pressure areas is dependent on the height and width of the building. Figure shows the zones 62. There are three categories. This structure falls into the middle category. Note that in the Eurocode the width of the building is indicated as b , the depth of the building is indicated as d , and the height of the building is indicated as h . The authors of this thesis have used B as a symbol of the width of the building, D as a symbol of the depth of the building, and H for the total height of the building and. These symbols will be used in the further calculations.

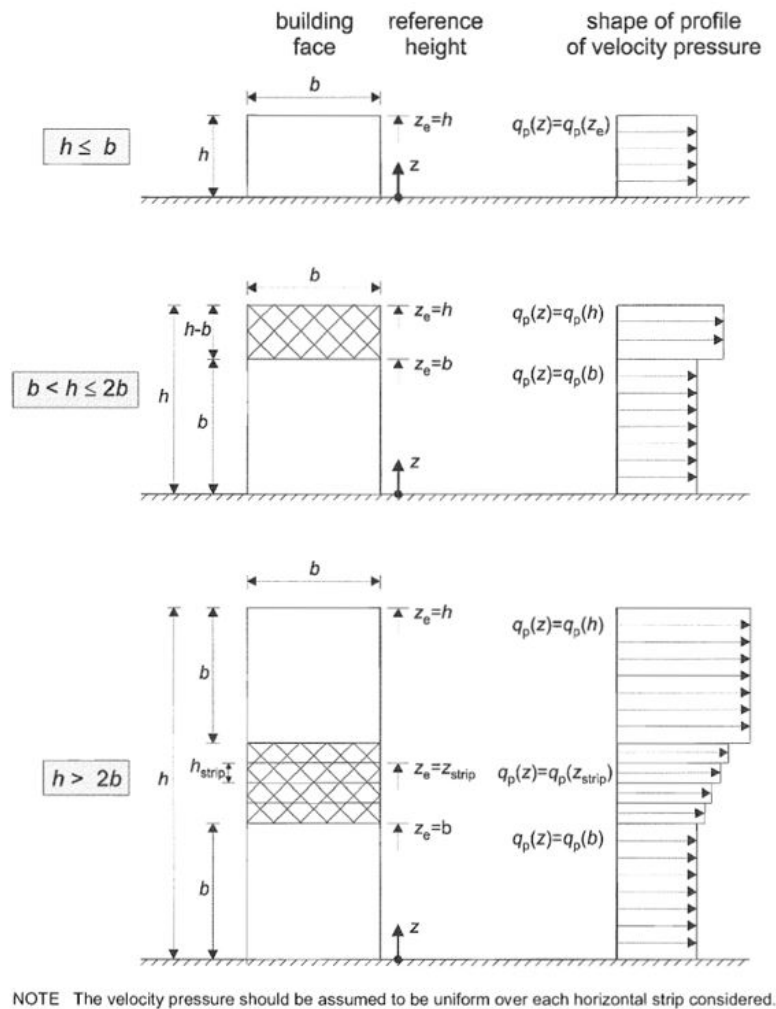


Figure 62: Figure 7.4 NS-EN-1991-1-4 - WindZones

$$H = h \cdot n = 3.5m \cdot 10 = 35m \quad (65)$$

$$B = \frac{S \cdot (n_f - 1)}{1000} = \frac{5000mm \cdot 5}{1000} = 25m \quad (66)$$

$$B < H < 2B \Rightarrow 25m < 35m < 50m \quad (67)$$

There are two zones for this structure. The zone nearest the base will be called zone 1 and the zone at the top is zone 2. The next step is to calculate the peak velocity pressure for each of the two zones.

Peak Wind Pressure

According to Eurocode (NS-EN 1991-1-4) [9], the peak wind velocity pressure is calculated as:

$$q_p(z) = (1 + 7 \cdot I_v(z)) \cdot \frac{1}{2} \cdot \rho \cdot v_m^2 \quad (68)$$

$I_v(z)$ = Turbulence intensity

ρ = air density: $\rho = 1.25kg/m^3$

v_m = mean wind velocity : see Equation (60)

$$I_v = \frac{k_l}{c_0 \cdot \ln \frac{z}{z_0}} \quad (69)$$

k_l = turbulence factor: Taken as 1

c_0 = orography factor : Norwegian National Annex states $c_0 = 1.0$

Now, the peak wind pressure can be calculated for each zone.

Zone 1

$z_1 = B = 25$ m

$$v_m(B) = c_r(B) \cdot c_0(B) \cdot v_B = 0.24 \cdot \ln(25) \cdot 1 \cdot 26m/s = 20.09m/s \quad (C.1)$$

$$I_v = \frac{k_l}{c_0 \cdot \ln \frac{B}{z_0}} = \frac{1}{\ln(28)} = 0.3107 \quad (70)$$

$$q_p(z_1) = q_p(D) = (1 + 7 \cdot 0.3107) \cdot \frac{1}{2} \cdot 1.25kg/m^3 \cdot (20.09m/s)^2 = \underline{0.8005kN/m^2} \quad (71)$$

Zone 2

$z = H = 35$ m

$$v_m(H) = c_r(H) \cdot c_0(H) \cdot v_b = 0.24 \cdot \ln(35) \cdot 1 \cdot 26m/s = 22.19m/s \quad (C.1)$$

$$I_v = \frac{k_l}{c_0 \cdot \ln \frac{z}{z_0}} = \frac{1}{\ln(28)} = 0.2813 \quad (72)$$

$$q_p(z_1) = q_p(b) = (1 + 7 \cdot 0.2812) \cdot \frac{1}{2} \cdot 1.25kg/m^3 \cdot (20.8m/s)^2 = \underline{0.9133kN/m^2} \quad (73)$$

Wind pressure

The end goal is to calculate the forces of the wind pressure in each of the two zones. First, the total wind pressure must be obtained for each zone. Note that the values of c_{pe} and c_{pi} are absolute values.

Pressure:

$$w_e = q_p(z_e) \cdot (c_{pe} + c_{pi}) \quad (74)$$

q_p = peak wind pressure

c_{pe} = Windward pressure

c_{pi} = leeward pressure

The values of the external pressure coefficients can be taken from Table 4.1 in (NS-EN 1991-1-4) [9]. Figure 64 illustrates the different pressure zones for a rectangular building. Zone D and E are the windward and leeward zones, respectively. The pressure coefficient c_{pe} is calculated by interpolation for each of these zones. For the 10-floor reference frame, interpolation gives:

Zone D - Windward pressure:

$$C_{pe} = 0.8000$$

Zone E - Leeward Pressure:

$$C_{pe} = -0.5333$$

Zone 1

$$w_e = q_p(z_e) \cdot (c_{pe} + c_{pi}) = 0.8005kN/m^2 \cdot (0.8000 + 0.5333) = \underline{1.0673kN/m^2} \quad (75)$$

Zone 2

$$w_e = q_p(z_e) \cdot (c_{pe} + c_{pi}) = 0.9133 \cdot (0.8000 + 0.5333) = \underline{1.2177kN/m^2} \quad (76)$$

Values of external pressure coefficient for vertical walls of rectangular plan buildings
(EN1991-1-4, Tab.:4.1)

ZONE	A		B		C		D		E	
	$c_{pe,10}$	$c_{pe,1}$	$c_{pe,10}$	$c_{pe,1}$	$c_{pe,10}$	$c_{pe,1}$	$c_{pe,10}$	$c_{pe,1}$	$c_{pe,10}$	$c_{pe,1}$
5	-1.2	-1.4	-0.8	-1.1	-0.5		+0.8	+1.0	-0.7	
1	-1.2	-1.4	-0.8	-1.1	-0.5		+0.8	+1.0	-0.5	
≤ 0.25	-1.2	-1.4	-0.8	-1.1	-0.5		+0.7	+1.0	-0.3	

Note: Values for $c_{pe,1}$ are intended for the design of small elements and fixings with an element of $1m^2$ or less such as cladding elements and roofing elements. Values for $c_{pe,10}$ may be used for the design of the overall load bearing structure of buildings. The external pressure coefficient $c_{pe,1}$ and $c_{pe,10}$ is using for loaded area of $1m^2$ and $10m^2$ respectively.

Figure 63: Table 4.1 NS-EN-1991-1-4

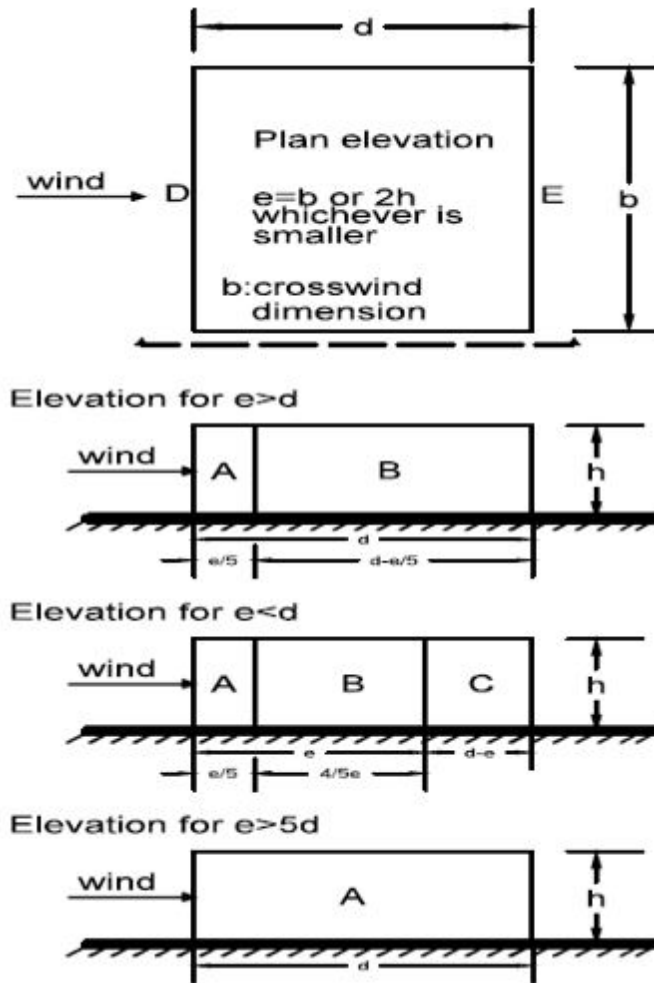


Figure 64: Figure 7.5 NS-EN-1991-1-4

Wind forces

Forces created by wind pressure can now be calculated for each zone. Note that since the pressure coefficients c_{pe} on the leeward and windward side are obtained simultaneously, it is necessary to implement a lack of correlation coefficient. This lack of correlation coefficient c_{cor} is included in the calculation of forces.

The lack of correlation between these sides was therefore taken into account in the calculation of forces.

Forces:

$$F_w = c_s \cdot c_d \cdot \sum (w_e) \cdot A_{ref} \cdot l_c \quad (77)$$

A_{ref} = Area of the facade of the building for the reference zone

c_s = Size factor: $c_s = 1$ (simplification)

c_d = Dynamic factor: $c_d = 1$ (simplification)

c_{cor} = Lack of correlation coefficient: Interpolation between $c_{cor} = 0.85$ for $H/D = 1$ and $c_{cor} = 1$ for $H/D = 5$. Thus, giving $l_c = 0.875$

A line load can be calculated for each of the two zones. This can be used to calculate the final uniform line load with the use of base moments and shear.

Zone 1

$$F_w = 1 \cdot 1 + \cdot 1.0673kN/m^2 \cdot 25m \cdot 35m \cdot 0.875 = 817kN \quad (78)$$

The lateral line load for zone 1 is:

$$f_1 = \frac{827}{35} = \underline{23.35kN/m} \quad (79)$$

Zone 2

$$F_w = 1 \cdot 1 + \cdot 1.1987 \cdot 35 \cdot 30 \cdot 0.875 = 932N \quad (80)$$

The lateral line load for zone 2 is:

$$f_2 = \frac{932}{35} = \underline{26.64kN/m} \quad (81)$$

Calculation of final uniform windload

The final uniform wind load is calculated by calculating the base moment and base shear created by the two line loads for zone 1 and zone 2. An approximate line load for the base shear is calculated. Then the moment due to this line load is calculated. A modifying factor is calculated based on the relation between the actual base moment and the base moment created by the average line load due to base shear. The final average line load is the average line load from the shear multiplied with this modifying factor.

V_b = Shear force at base

M_b = Moment at base

f_{vb} = Lineload calculated from shear force at base

$M_{f_{vb}}$ = Moment at base calculated from lineload f_{vb}

C_{mod} = Modifying factor

$$V_b = f_1 \cdot h_1 + f_2 \cdot h_2 = 23.35 \cdot 25 + \cdot 26.64 \cdot 10 = 850.1kN \quad (82)$$

f_1 = Line load zone 1

f_2 = Line load zone 2

h_1 = Height of zone 1

h_2 = Height of zone 2

$$M_b = f_1 \cdot h_1 \cdot \frac{h_1}{2} + f_2 \cdot h_2 \cdot (h_1 + \frac{h_2}{2}) = 23.35 \cdot 25 \cdot 12.5 + 26.64 \cdot 10 \cdot 30 = 15287kNm \quad (83)$$

$$f_{vb} = \frac{V_b}{h} = \frac{850.1kN}{35m} = 24.29kN/m \quad (84)$$

$$M_{f_{vb}} = f_{vb} \cdot \frac{h^2}{2} = 24.29kN/m \cdot \frac{(35m)^2}{2} = 14876kNm \quad (85)$$

$$C_{mod} = \frac{M_b}{M_{f_{vb}}} = \frac{15287kNm}{14876kNm} = 1.0276 \quad (86)$$

The final average lineload can then be calculated:

$$f = \frac{f_{vb} \cdot C_{mod}}{B} = \frac{24.29kN/m \cdot 1.0276}{25m} = \underline{0.998kN/m} \approx \underline{1.00kN/m} \quad (87)$$

F Acceleration calculation

This part of the appendix explains the routine for calculation of wind-induced acceleration. It consists of an example calculation for a 10-floor reference frame. This is done according to the Eurocode (NS-EN 1991-1-4) [9]. The example calculation is performed in the same manner and procedure as in the Pythonscript, located in Appendix A, under the name AccelFunction. Table F shows the data for a reference frame of 10 floors.

Reference frame with 10 floors

Parameters	symbol	Unit	Value
Number of floors	n	-	10
Number of bays	n_b	-	3
Number of frames	n_f	-	6
Bay length	l_b	mm	7000
Floor height	h	mm	3500
Spacing	S	mm	5000
Column height	h_c	mm	630
Beam height	h_b	mm	540
Wall height	h_w	mm	3000
Truss height	h_t	mm	300
Column width	w_c	mm	430
Beam width	w_b	mm	430
Wall width	w_w	mm	430
Truss width	w_t	mm	430
Rotational stiffness beams	K_{rb}	kNm/rad	25920
Rotational stiffness columns	K_{rc}	kNm/rad	10000
Rotational stiffness walls	K_{rw}	kNm/rad	200 000
Base wind	V_{b0}	m/s	26
Wind load	q_w	kN/m	1.00
Dead load	g	kN/m ²	2
Live load	q_s	kN/m ²	3

Acceleration

H = total height: H = 35 m

B = cross wind dimesion: B = 25 m

D = parallel to the wind dimension of the building: D = 21 m

$$v_m(z) = c_r(z) \cdot c_0(z) \cdot v_b \quad (88)$$

c_r = roughness factor : It is a function of the building height z

c_0 = orography factor : Norwegian National Annex states $c_0 = 1.0$

v_b = standard wind velocity at reference height of 10m

$$v_b = c_{prob} \cdot c_{dir} \cdot c_{season} \cdot v_{b,0} \quad (89)$$

c_{dir} = direction factor : Norwegian National Annex States $c_{dir} = 1,0$

c_{season} = season factor : Norwegian National Annex States $c_{season} = 1,0$

c_{prob} = porbability factor: Can be taken as $c_{prob} = 0,73$

$v_{b,0}$ = fundamental wind velocity for Trondheim : $v_{b,0} = 26$ m/s

$$v_b = 1 \cdot 1 \cdot 1 \cdot 26m/s = 26m/s \quad (90)$$

$$c_r(z) = k_r \cdot \ln\left(\frac{z}{z_0}\right) \quad (91)$$

k_r and z_0 depend on the terrain category. The terrain category describes the topology of the area surrounding the structure. In these calculations, it is assumed that the location is Trondheim and that the terraincategory is 4. To fulfill terraincategory 4 at least 15% of the surface area must be covered with buildings and their average height exceeds 15 m (NS-EN 1991-1-4) [9].

$k_r = 0.24$ for terraincategory = 4
 $z_0 = 1$ for terraincategory = 4
 $z_{min} = 16$ for terraincategory = 4

$$c_r(z) = 0.24 \cdot \ln(z) \quad (92)$$

Peak Wind Pressure

According to the Eurocode [9], the peak wind velocity pressure is calculated as:

$$q_p(z) = (1 + 7 \cdot I_v(z)) \cdot \frac{1}{2} \cdot \rho \cdot v_m^2 \quad (93)$$

$I_v(z)$ = Turbulence intensity
 ρ = air density: $\rho = 1.25 \text{ kg/m}^3$
 v_m = mean wind velocity : see Equation (88)

$$I_v = \frac{k_l}{c_0 \cdot \ln \frac{z}{z_0}} \quad (94)$$

k_l = turbulence factor: Taken as 1
 c_0 = orography factor : Norwegian National Annex states $c_0 = 1.0$
 $r = 0$ as the radius of building edges
 $Z_t = 200$ as recommended in the Eurocode
 $L_t = 300$ as recommended in the Eurocode
 $Z_0 = 1$

$freq = 0.57$
 ξ = damping: $\xi = 0.019$
 $mass = 1551987 \text{ kg}$
 $eigenvector = [1.00, 0.9144, 0.8240, 0.7309, 0.6325, 0.53, 0.4244, 0.3169, 0.2090, 0.1030, 0]$

Normalized mode shape at the point of interest $\phi = 0.9144$.

In the calculation of K_x , a simplified approach has been used. The method of fitting a the polynom: $(z/h)^\delta$ to the fundamental mode shape $\phi_1(z)$. The value of interest is the exponent: δ . The equation is presented below:

$$\phi_1(z) = \frac{z^\delta}{h} \quad (95)$$

$$\delta = \text{findingBestExponent}(eigenVector, numFloor) = 0.932423 \quad (96)$$

This function provides a method to fit the polynom: $(z/h)^\delta$ to the fundamental mode shape $\phi_1(z)$

$$Z_s = \max(0.6 \cdot H, Z_{min}) = 21.0 \quad (97)$$

$$K_x = \frac{(2 \cdot \delta + 1) \cdot (\delta + 1) \cdot (\log(Z_s/Z_0) + 0.5) - 1}{(\delta + 1)^2 \cdot \log(Z_s/Z_0)} = 1.474001 \quad (98)$$

The building mass is modeled using the quasi-load combination shown in Equation (11) in combination with the structural properties shown below:

$$\text{Total Mass} = \text{Quasi load} \cdot \text{Spacing} \cdot \text{Number of floors} \cdot \text{Number of bays} \cdot \text{Bay length} = 1551987kg$$

$$V_b = V_{b0} \cdot C_{dir} \cdot C_{season} \cdot C_{prop} = 18.98 \quad (99)$$

$$C_{r(z_s)} = Kr \cdot (\log(\max(Z_{min}, Z_s)/Z_0)) = 0.73068538 \quad (100)$$

$$V_{m(z_s)} = V_b \cdot C_{r(z_s)} = 13.8684086 \quad (101)$$

$$I_{V(z_s)} = K_l / (C_0 \cdot \log(\max(Z_{min}, Z_s)/Z_0)) = 0.32845873 \quad (102)$$

$$\alpha = 0.67 + 0.05 \cdot \log(Z_0) = 0.67 \quad (103)$$

$$L(Z_s) = Lt \cdot \frac{\max(Z_{min}, Z_s)^\alpha}{200} = 66.27017 \quad (104)$$

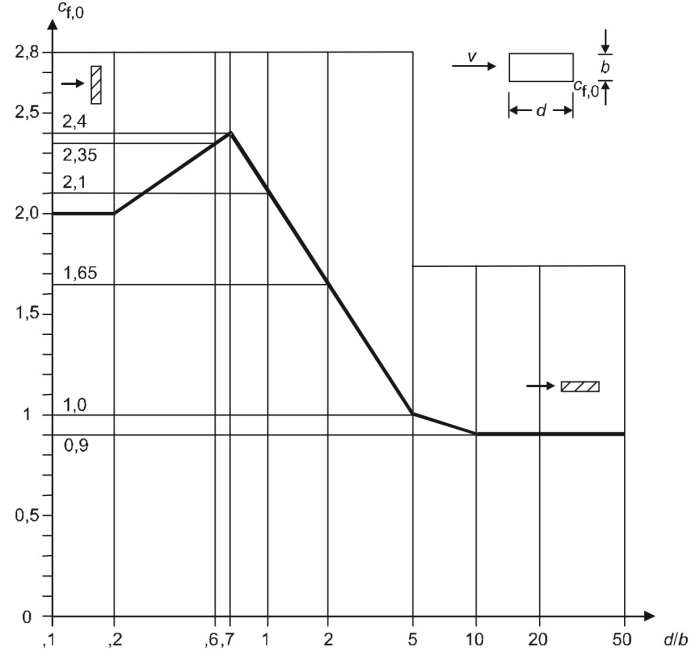


Figure 65: Figure 7.23 NS-EN-1991-1-4

$$x = D / B = 0.84$$

$$C_{f0} = f(x) = 2.26$$

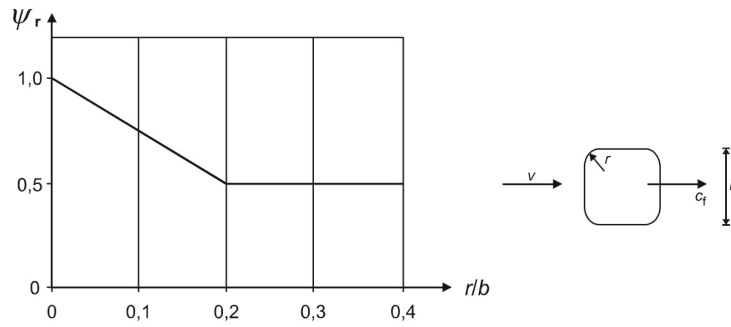


Figure 66: Figure 7.24 NS-EN-1991-1-4

$$r / B = 0$$

$$\psi_r = 1$$

No.	Position of the structure, wind normal to the plane of the page	Effective slenderness λ
1		<p>For polygonal, rectangular and sharp edged sections and lattice structures:</p> <p>for $\ell \ge 50$ m, $\lambda = 1,4 \ell/b$ or $\lambda = 70$, whichever is smaller</p>
2		<p>for $\ell < 15$ m, $\lambda = 2 \ell/b$ or $\lambda = 70$, whichever is smaller</p> <p>For circular cylinders:</p> <p>for $\ell \ge 50$, $\lambda = 0,7 \ell/b$ or $\lambda = 70$, whichever is smaller</p> <p>for $\ell < 15$ m, $\lambda = \ell/b$ or $\lambda = 70$, whichever is smaller</p>
3		<p>For intermediate values of ℓ, linear interpolation should be used</p>
4		<p>for $\ell \ge 50$ m, $\lambda = 0,7 \ell/b$ or $\lambda = 70$, whichever is larger</p> <p>for $\ell < 15$ m, $\lambda = \ell/b$ or $\lambda = 70$, whichever is larger</p> <p>For intermediate values of ℓ, linear interpolation should be used</p>

Figure 67: Figure 7.24 NS-EN-1991-1-4

$$\lambda = f(H) = 2.32$$

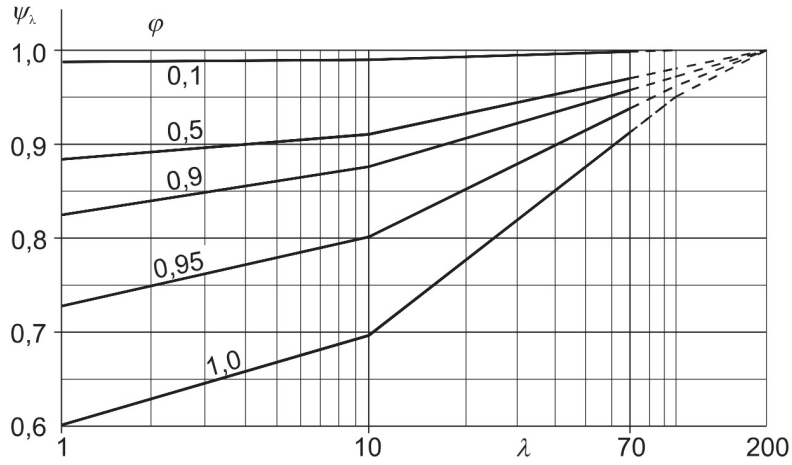


Figure 68: Figure 7.24 NS-EN-1991-1-4

$$\begin{aligned}\varphi &= 1 \\ \psi_\lambda &= f(\lambda) = 0.61466666\end{aligned}$$

$$C_f = C_{f0} \cdot \psi_r \cdot \psi_\lambda = 1.3891466 \quad (105)$$

$$b = ((1 + 0.9 \cdot ((B + H)/L(Z_s))^{0.63})^{-1})^{0.5} = 0.736136142 \quad (106)$$

$$f_L = freq \cdot L(Z_s)/V_{mzs} = 2.726071287 \quad (107)$$

$$S_L = 6.8 \cdot \frac{f_L}{(1 + 10.2 \cdot f_L)^{5/3}} = 0.0684819 \quad (108)$$

$$m_e = (\text{Total Mass})/H = 44342 \quad (109)$$

$$\xi_a = \frac{C_f \cdot \rho \cdot V_{m(zs)} \cdot B}{2 \cdot freq \cdot (m_e)} = 0.01189950 \quad (110)$$

$$\xi_s = 2\pi \cdot \frac{\xi}{(1 + \xi^2)^{-0.5}} = 0.119402 \quad (111)$$

$$\xi_L = \xi_a + \xi_s = 0.1313015 \quad (112)$$

$$\eta_h = 4.6 \cdot H \cdot f_L/L(Z_s) = 6.62285122 \quad (113)$$

$$\eta_b = 4.6 \cdot B \cdot f_L/L(Z_s) = 4.7306080 \quad (114)$$

$$R_h = \frac{1}{\eta_h} - \frac{1}{(2 \cdot \eta_h^2)} \cdot (1 - \exp(-2 \cdot \eta_h)) = 0.13959304 \quad (115)$$

$$R_b = \frac{1}{\eta_b} - \frac{1}{(2 * \eta_b^2)} \cdot (1 - \exp(-2 \cdot \eta_b)) = 0.18904833 \quad (116)$$

$$R = ((\pi^2) \cdot S_L \cdot R_h \cdot R_b / (2 \cdot \xi_L))^{0.5} = 0.2606192 \quad (117)$$

$$\sigma_p = \frac{C_f \cdot \rho \cdot B \cdot I_{v(zs)} \cdot V_{m(zs)}^2}{m_e} \cdot R \cdot K_x \cdot \phi = 0.0217249 \quad (118)$$

$$K_p = \max[((2 \cdot \log(freq \cdot 600))^{0.5}) + \frac{0.6}{(2 \cdot \log(freq \cdot 600))^{0.5}}, 3] = 3.59195 \quad (119)$$

$$C_s C_d = \frac{1 + 2 \cdot K_p \cdot I_{V(zs)} \cdot (b^2 + R^2)^{0.5}}{1 + 7 \cdot I_{V(zs)}} = 0.861614 \quad (120)$$

$$\text{acceleration: } a = K_p \cdot \sigma_p = 0.078035 \quad (121)$$

